The United Nations University

GEOTHERMAL TRAINING PROGRAMME
Orkustofnun, Grensásvegur 9,
IS-108 Reykjavík, Iceland

Reports 2002
Number 1

# A RESERVOIR STUDY OF OLKARIA EAST GEOTHERMAL SYSTEM, KENYA

**M.Sc. Thesis**
Department of Civil and Environmental Engineering,
University of Iceland

by

**Cornel Otieno Ofwona**
Kenya Electricity Generating Co., Ltd.
Olkaria Geothermal Project
P.O. Box 785, Naivasha
KENYA

United Nations University,
Geothermal Training Programme
Reykjavík, Iceland
Report 1 - 2002
Published in September 2002

ISBN 9979-68-098-9

This M.Sc. thesis has also been published in June 2002 by the
Department of Civil and Environmental Engineering,
University of Iceland

## INTRODUCTION

The Geothermal Training Programme of the United Nations University (UNU) has operated in Iceland since 1979 with six months annual courses for professionals from developing countries. The aim is to assist developing countries with significant geothermal potential to build up groups of specialists that cover most aspects of geothermal exploration and development. During 1979-2002, 279 scientists and engineers from 39 countries have completed the six months courses. They have come from Asia (44%), Africa (26%), Central America (14%), and Central and Eastern Europe (16%). There is a steady flow of requests from all over the world for the six months training and we can only meet a portion of the requests. Most of the trainees are awarded UNU Fellowships financed by the UNU and the Government of Iceland.

Candidates for the six months specialized training must have at least a B.Sc. degree and a minimum of one year practical experience in geothermal work in their home countries prior to the training. Many of our trainees have already completed their M.Sc. or Ph.D. degrees when they come to Iceland, but several excellent students who have only B.Sc. degrees have made requests to come again to Iceland for a higher academic degree. In 1999, it was decided to start admitting one or two outstanding UNU Fellows per year to continue their studies and study for M.Sc. degrees in geothermal science or engineering in co-operation with the University of Iceland. An agreement to this effect was signed with the University of Iceland. The six months studies at the UNU Geothermal Training Programme form a part of the graduate programme.

It is a pleasure to introduce the second UNU Fellow to complete the M.Sc. studies at the University of Iceland under the co-operation agreement. Mr. Cornel O. Ofwona, reservoir engineer of the Kenya Electricity Generating Co. Ltd., completed the six months specialized training at the UNU Geothermal Training Programme in October 1996. His research report was entitled “Analysis of injection and tracer tests data from the Olkaria-East geothermal field, Kenya”. After working for five more years as a reservoir engineer at Olkaria, he came back to Iceland and enrolled for the M.Sc. studies at the Faculty of Engineering of the University of Iceland in January 2001. He defended his M.Sc. thesis presented here, entitled ”A reservoir study of the Olkaria East geothermal system, Kenya”, in June 2002. His studies in Iceland were financed by a fellowship from the Government of Iceland through the UNU Geothermal Training Programme. We congratulate him on his achievements and wish him all the best for the future. We thank the Faculty of Engineering of the University of Iceland for the co-operation, and his supervisors for their dedication.

With warmest wishes from Iceland,

Ingvar B. Fridleifsson, director,
United Nations University
Geothermal Training

## DEDICATION

This work is dedicated to the beloved members of my family who passed away within the duration I was doing this study. To my father John who encouraged me to learn Science subjects from my tender age, to my dear wife Brenda who gave me the support and used to endure my long absence from home and to my beloved grandfather Rafael who imparted in me the wisdom on how to live with other people and face the challenges of life. Even though they are physically gone, without their inspiration, I would never have managed to realize this dream.

## ACKNOWLEDGEMENTS

This work was sponsored by the Government of Iceland, through the United Nations University (Geothermal Training Programme). The Olkaria data was provided by Kenya Electricity Generating Company Ltd. who also granted me a one and a half year study leave.

I would like to express my heart-felt gratitude to Dr. Ingvar Birgir Fridleifsson who saw the wisdom of proposing me for consideration for this study. Thanks to Prof. Jónas Elíasson, my main advisor for his very good teaching and support. Great appreciation to my second supervisor and teacher, Mr. Grímur Björnsson, who taught me how to model with the TOUGH simulator and spent so many of his weekends guiding me in this work. I appreciate the warmth and friendship that existed between me and the staff at Orkustofnun and with the teachers I interacted with during my study at the University of Iceland.

Thanks to the management of Kenya Electricity Generating Company Ltd. for granting me the study leave and to Mr. Godwin Mwawongo who worked tirelessly to ensure that I got every data I needed from Olkaria. My gratitude also goes to Mr. Lúdvík S. Georgsson and Mrs. Gudrún Bjarnadóttir for their effort to ensure that I could stay comfortably in Iceland.

## ABSTRACT

The conceptual model of the Eastern Olkaria geothermal system comprising of Olkaria Northeast and Olkaria East fields has been reviewed. The 3-D natural state model developed by Bodvarsson and Pruess (1987), has been updated to include the natural state thermodynamic conditions of all the wells drilled to date, with special emphasis to Olkaria Central wells. Both lumped parameter and distributed parameter models have been used to study the reservoir response to 20 years of production at Olkaria East field and some performance prediction for the next 20 years has been done.

Based on these studies, the following is concluded:

- That Olkaria East reservoir is an open system with a good pressure support and can be approximated by a simple first order differential equation whereby the recharge can be modelled as a direct proportion of pressure drawdown. In the natural state, the hydrology is controlled by convection.
- Three upflow zones seem to exist in the Eastern Olkaria geothermal system with two in the Northeast field and one in the East field.
- In the natural state, the Eastern geothermal system can be simulated by a recharge of 320 kg/s of 1290 kJ/kg water and the Western system by 245 kg/s of 1200 kJ/kg water. Steam amounting to 128 kg/s is lost along the Ololbutot fault and Olkaria Central zones resulting in cold temperatures deep down in the wells.
- Pressure drawdown in the Olkaria East field is localised within the producing zones. The deep reservoir still appears to be intact and can be exploited further to boost up the generating capacity of the field.
- A reasonable preliminary match to the history data is achieved from a coarse grid by lumping together many wells within a specified grid block and producing the sum out of one well. With this match, it is predicted that mean enthalpies will fall to about 1700–1800 kJ/kg in the next 20 years if production is maintained at the same rate and pressure drawdown will eventually stabilize as the fluid recharge rates equalize the production rates. However, a better prediction would be obtained from an extended grid producing from deeper aquifers.

**TABLE OF CONTENTS**

Page



## LIST OF FIGURES

**LIST OF TABLES** Page



**LIST OF FIGURES IN APPENDICES**

Page

Page

## 1.0 INTRODUCTION

Electricity generation from geothermal energy in Kenya is set to increase ten fold in the next 15 to 20 years from the current 58 MWe. This has been necessitated by the bad weather pattern that has persisted in the last few years and has rendered hydro-electric power generation, from which Kenya gets its 70% of electricity quite unreliable. To meet this demand, steam production from proven geothermal reservoirs like those within the Olkaria geothermal system will have to be increased as this will be easier and less costly than to bank on the unexplored prospects. This will call for a more elaborate and advanced reservoir engineering work so as to ensure optimum exploitation. This study was borne out of the need to acquire these advanced skills that will enable us solve some complex reservoir management problems that might arise.

Olkaria geothermal system has now been under exploitation for twenty years and a lot of reservoir data has been collected. It is therefore reasonable to use these data for a study of this magnitude. In this work, I will review the conceptual model of the eastern part of the greater geothermal system that covers Olkaria East and Northeast fields. I will then perform some lumped convective and exploitation calculations, update the existing 3-D natural state model of the whole Olkaria system that was developed by Bodvarsson and Pruess (1987) and finally attempt to build a coarse numerical exploitation model of the Olkaria East field.

This thesis is submitted to the University of Iceland for a Master of Science degree in Environmental Engineering. It is evaluated as 30 units of 60, which are claimed for the curriculum. I earned 15 of the other 30 units in summer 1996 when I was a student at the United Nations University, Geothermal Training Program, Iceland. The remaining 15 units were covered as course work at the University of Iceland.

Numerical (computer) simulation of the data was done by use of TOUGH2 software in conjunction with other in-house computer programs developed at Orkustofnun, the National Energy Authority of Iceland.

## 2.0 THE OLKARIA GEOTHERMAL SYSTEM

### 2.1 Location and geological setting

Olkaria geothermal system is located in the East African Rift Valley to the south of Lake Naivasha and 120 km northwest of Nairobi. This geothermal system, covering an area more than 120 km$^2$, is associated with a volcano that is one of the several volcanic centres situated within the Central Kenyan Rift amongst which include Longonot, Eburru, Suswa and Menengai, (Figure 1).

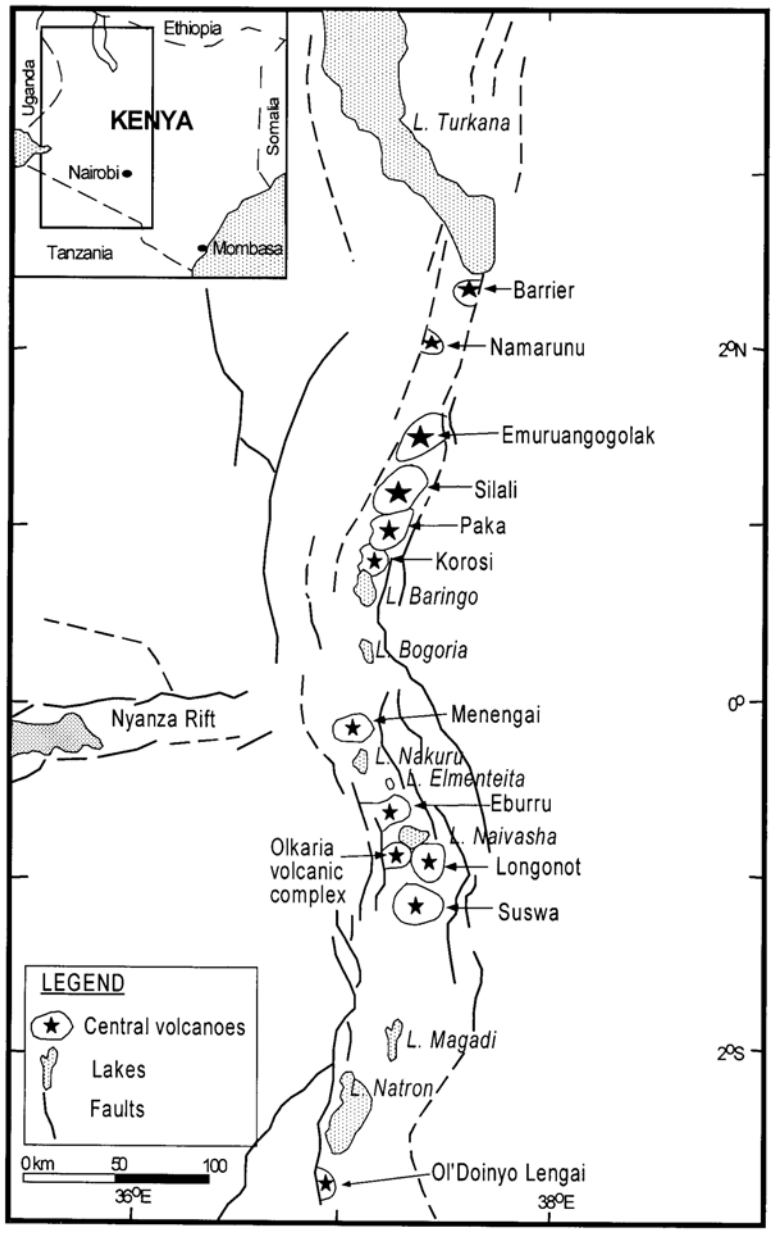


Figure 1: Location of Olkaria geothermal system within the Kenya Rift Valley (From Muchemi, 1999)

## 2.2 A brief history of the development

Exploration of this geothermal resource was initiated by the United Nations and the Government of Kenya in 1956 and has been continuous since 1970. The early exploration work involved drilling of two wells OW-X1 and OW-X2 both of which are located in the northern part of the prospect (Figure 2). OW-X1 was drilled to 502 m and OW-X2 to 942 m. Although they encountered high temperatures, they failed to discharge and work was stopped in 1959 (KPC, 1981).

In 1970, Olkaria Geothermal Project was initiated and was jointly financed by UNDP and the Kenya Government. During the same year, further exploration work consisting of geological mapping and geophysical and geochemical surveys as well as more investigations on the two exploration wells began. In 1972, well OW-X2 was coaxed into production through a small diameter pipe at atmospheric pressure and continuously produced for a year before being shut-in. Glover (1972) gave an estimation of the natural heat loss from the geothermal system to be close to 400 MWt with 90 % of this coming from steam discharge through surface vents. On the basis of the success in producing from well OW-X2 and the results of surface exploration, a technical review meeting was held in December 1972 and a recommendation made to drill four more exploration wells.

Drilling started in 1973 with well OW-1 located to the southeast of the greater Olkaria system. This well was drilled to a depth of 1003 m and did not discharge on its own due to low temperature and permeability. The temperature measured at 1000 m was 126°C and the water rest level was 618 m below the wellhead. The well was stimulated into production by air-lift, but it could not sustain production. Following this unsuccessful result with well OW-1, it was decided to move about 3.5 km to the northeast of this well for drilling of well OW-2.

Drilling of well OW-2 gave positive results. It was drilled to 1350 m and encountered a 240°C steam zone at 650 m. Maximum temperature recorded was 280°C at the bottom. Discharge at atmospheric pressure gave 70 – 75 % steam and total flow rate was 9 kg/s at a pressure of 6 bar-abs. It is due to the success in this well that further appraisal and production drilling were done in the vicinity culminating in the 1976 feasibility study for utilisation of geothermal steam for generation of electricity at Olkaria (SWECO and VIRKIR, 1976). The study indicated that development of the geothermal resource was attractive and the authorities decided to construct a 30 MWe power plant of two 15 MWe units with possible extension by addition of a third 15 MWe unit (Svanbjörnsson et. al., 1983). The first unit was brought on line in July 1981, the second in December 1982 and the third in April 1985.

Since then, the geothermal field has been producing steam for generation of 45 MWe in the area currently called Olkaria East field. Further exploration drilling in the northeast and west of this field has led to demarcation of two more fields in which two more power stations are being constructed and each will produce 64 MWe. Generally, Olkaria geothermal system is now divided into East field, Northeast field, Central field, West field, Northwest field, Southeast field and Domes field (Figure 2). The total number of wells drilled to date is 102 and exploration drilling is now focussed in Olkaria Domes field and production drilling in Olkaria West field. Ormat Inc. is now developing Olkaria West field and they commissioned their first 13 MWe Binary cycle unit in August 2000. In this study, I will combine Olkaria East and Northeast fields and call it Olkaria East geothermal system, and will be my study area.

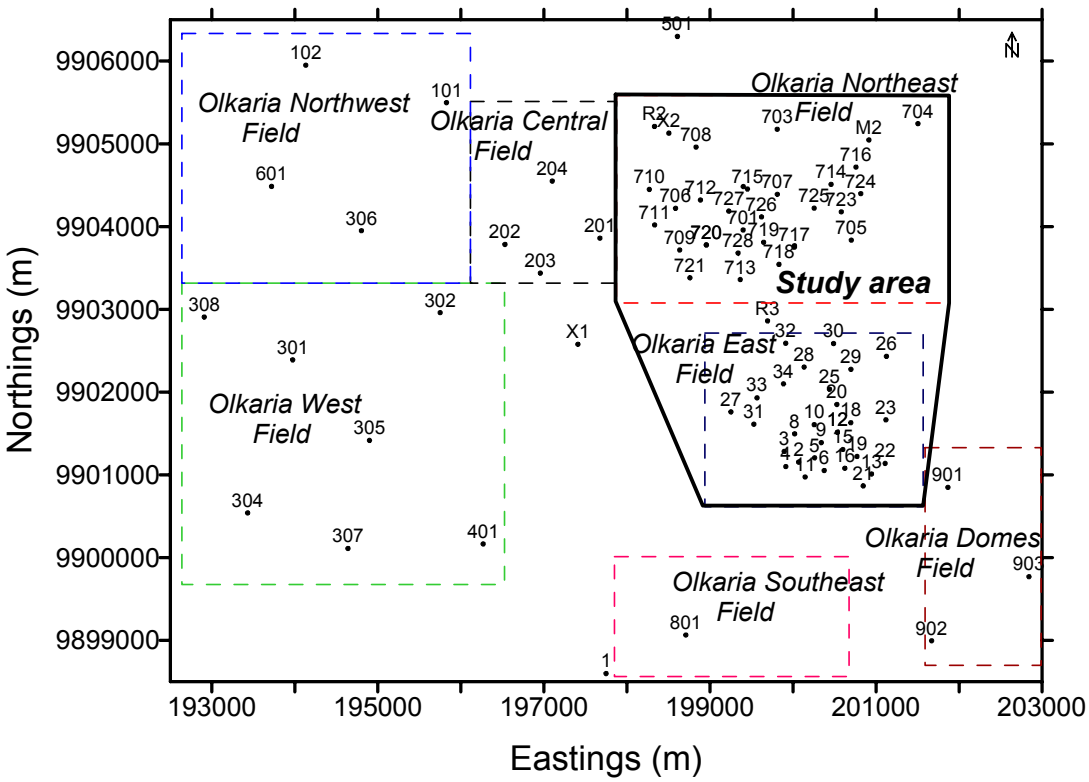


Figure 2: Location of the geothermal fields, drilled wells and the study area (the dots represent wells)

### 2.3 Geological overview

Olkaria geology has been studied by many workers (Naylor, 1972; Clark et. al., 1990; Brown, 1984; Odongo, 1993; Muchemi, 1999; etc) and various views have been expressed but what seems to be a general consensus is that the geothermal field is a remnant of an old caldera complex which has subsequently been cut by N-S normal rifting faults that have provided loci for later eruptions of rhyolitic and pumice domes. Eruptions associated with Olkaria volcano and Ololbutot fault zone (Figure 3) produced rhyolitic and obsidian flows and then eruptions from Longonot and Suswa volcanoes (Figure 1) ejected pyroclastic ash that has blanketed much of the area. NW, NNW, N-S, NNE and NE trending faults and ring structure are observed in the geothermal complex (Muchemi, 1999; Odongo, 1993). The most prominent structures are the NE trending Olkaria fault, N-S trending Ololbutot fault, Olkaria fracture, the Ring fracture, Suswa fault and Gorge Farm fault.

Subsurface stratigraphy of Olkaria wells shows that from the surface (which is at an average elevation of 2000 m a.s.l.) to about 1400 m a.s.l., the rocks consist of Quaternary comendites and pantellerites with an extensive cover of pyroclastics. Below these, the dominant rocks are trachytes with basalt flows and tuffs that mainly occur as thin intercalations (Figure 4). The rock stratigraphy is essentially horizontal (Muchemi, 1999; Brown, 1984).

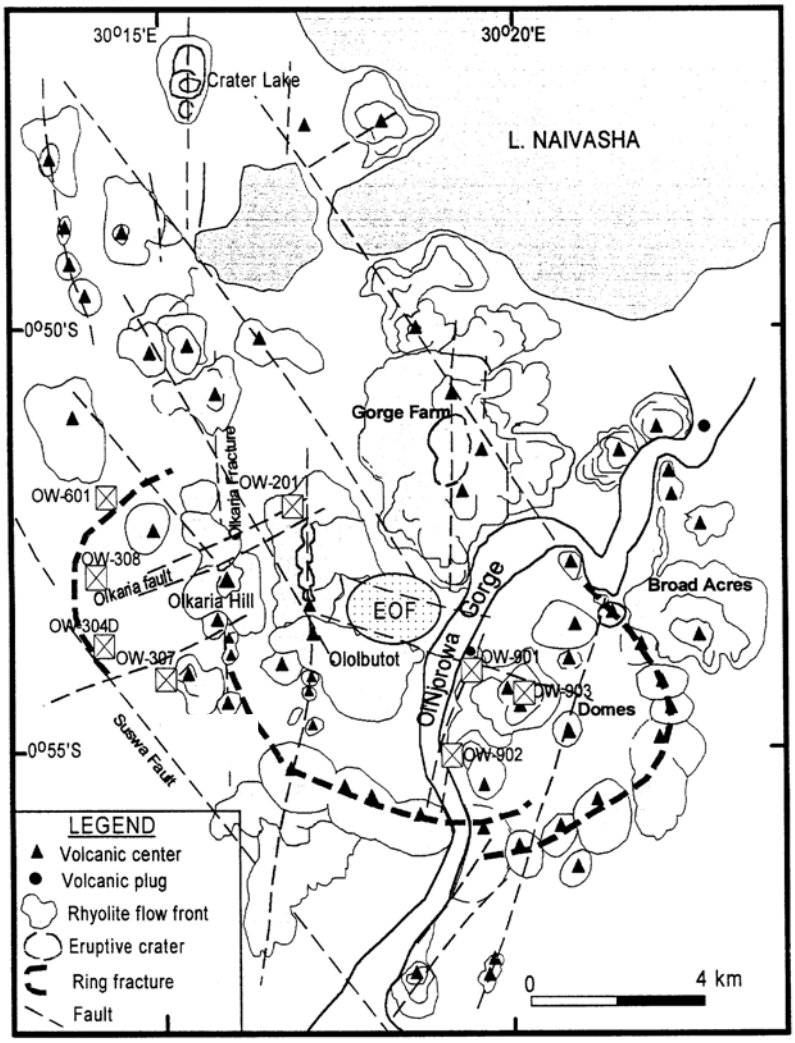


Figure 3: Geological structural map of Olkaria geothermal system (from Muchemi, 1999)

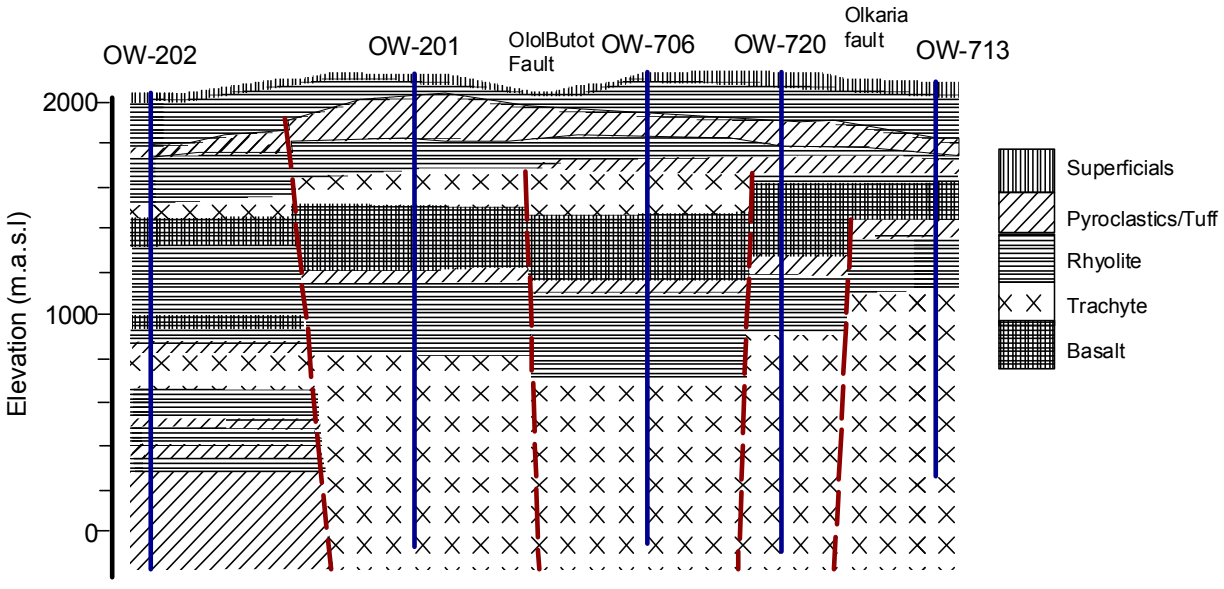


Figure 4: General subsurface stratigraphy of Olkaria reservoir

Rocks down to 1400 m a.s.l. are nearly impermeable and act as caprock to the system. Below this depth permeability is encountered at the fractures, lava contacts and porous pyroclastic beds and tuffs. A look at well productivity indicates that wells located close to known or inferred faults produce highest mass flows hence indicating the importance of vertical permeability.

Clay mineral analysis on cores and cuttings from wells OW-501 and OW-703 indicated the presence of smectite, carbonates and kaolinite. The presence of these minerals has been interpreted to indicate influx of cool low pH bicarbonate fluids into the reservoir from the north (Leach and Muchemi, 1987). Other hydrothermal minerals found in this field include zeolites, epidotes, pyrite, magnetite, haematite, calcite, quartz, adularia, chlorites, and illite.

## 2.4 Geophysical overview

It is observed from resistivity measurements that low anomalies within the Olkaria geothermal system are controlled by linear structures in the NE-SW and NW-SE directions (Muchemi, 1999). The geothermal resource is defined by less than 15 Ω m resistivity anomaly at 1000 m a.s.l. and occur at the intersection of these structures (Figure 5). High resistivity regions within or bounding these low resistivity anomalies coincide with NE and NW trending faults and are interpreted to be conduits channelling cold water recharging the system. It is inferred from MT data that deep low resistivity occurs at a depth of 4 - 5 km and is thought to define the heat source.

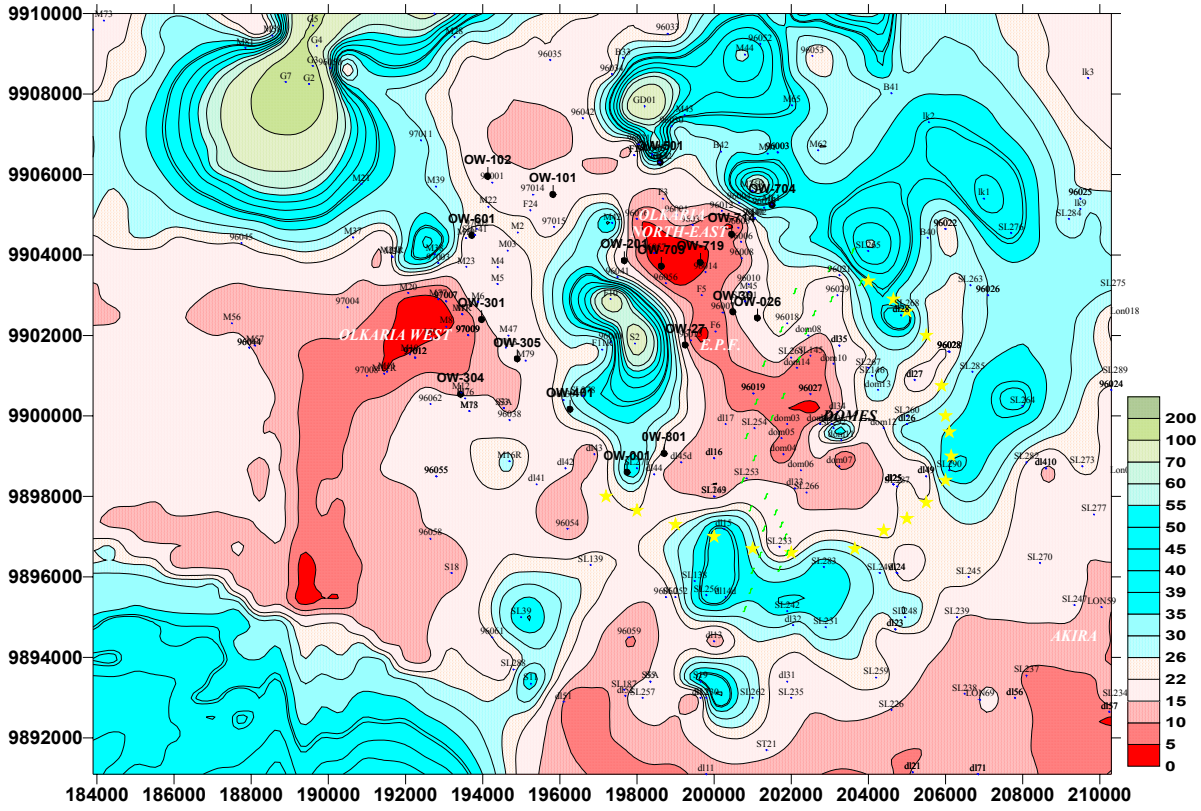


Figure 5: Integrated TEM and DC Schlumberger resistivity (Ω m) at 1000 m a.s.l. (source – Kenya Electricity Generating Company Ltd.)

Seismic monitoring of micro-earthquakes within the Olkaria geothermal system (Simiyu and Malin, 2000) has shown that shallow, high frequency events associated with movement of hot geothermal fluids, occur at the intersection of NE-SW and NW-SE trending faults. Deep, low frequency events, which have been associated with movement of cold water far from areas of strong heat source, occur away from these zones (Figure 6).

Studies of shear wave attenuation beneath Olkaria geothermal field (Simiyu, 1998) indicate deep attenuating bodies below Olkaria hill, Gorge Farm volcanic centre and Domes area at about 7 to 18 km depth. These bodies coincide with zones of deep low resistivity and positive magnetic anomaly and have been interpreted to be zones of molten magmatic bodies that provide heat source for the Olkaria geothermal system. From magnetic studies, these bodies are approximated to be at temperatures above 575°C.

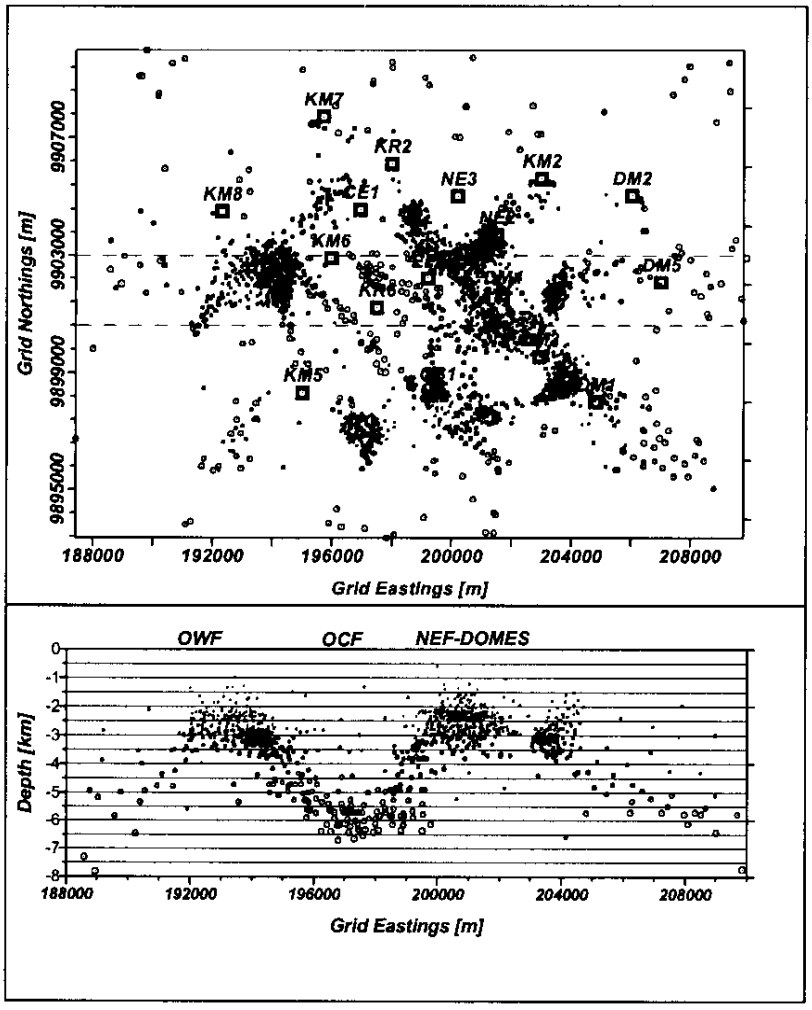


Figure 6: Location of micro-earthquakes in the Olkaria geothermal system (from Simiyu and Malin, 2000)

## 2.5 Geochemical overview

The waters discharged by wells in the Olkaria geothermal system (before exploitation) vary depending on which field the well is located. Wells in Olkaria Northeast field discharge neutral sodium chloride waters with chloride concentrations in the range of 400 – 600 ppm and bicarbonate concentrations < 1000 ppm. Wells in Olkaria West field discharge mainly

sodium bicarbonate waters with concentrations about 10,000 ppm and chloride concentrations ranging from 50 – 200 ppm while wells in Olkaria Central field discharge a mixture of sodium chloride and sodium bicarbonate waters. Olkaria Domes wells discharge mixed sodium bicarbonate-chloride-sulphate waters with mean chloride concentrations of 180 – 270 ppm and Olkaria East wells discharge sodium chloride waters with chloride concentrations in the range of 200 – 350 ppm (Muchemi, 1999).

Average temperatures calculated from silica geothermometer indicate 230 – 260°C for Olkaria East field, 265 – 270°C for Olkaria Northeast field, 186 – 259°C for Olkaria Central field and 232 – 242°C for Olkaria Domes field. K/Na ratio gives 230 – 260°C for Olkaria East field, 260 – 290°C for Olkaria Northeast field and 230 – 260°C for Olkaria West field. Calculated temperature declines towards northwest and east directions from areas around OW-701, OW-707, OW-726, OW-714, and OW-727 in Olkaria Northeast and to the south and southwest directions from areas around OW-305 and OW-301 in Olkaria West (Wambugu, 1996). The reservoir $CO_2$ concentrations vary from > 10,000 ppm in Olkaria West field to < 10 ppm in Olkaria East field.

## 3.0 CONCEPTUAL RESERVOIR MODEL

### 3.1 Fluid and heat flow in hydrothermal systems

The most basic features in a hydrothermal system are aquifers containing channels of hot fluid, paths for cold water recharge and heat source. Heat source, in most cases, is always intrusive magmatic bodies and cold water recharge originates as meteoric waters from ground surface and percolates down through faults and fissures to considerable depths where it is heated to high temperatures. The heated water rises through other faults and its place taken by incoming meteoric water. Heat is transferred from the heat source by conduction through the rocks and by convection due to fluid movements.

In cold groundwater systems there is no variation in fluid density and flow is driven solely by pressure gradient between two points. The discharge is obtained according to Darcy's law (Bear, 1979),

$$q = \frac{k\rho g}{\mu}\frac{d}{dl}\left(\frac{P}{\rho_w g} + z\right) \tag{3.1}$$

However, in hydrothermal systems, due to buoyancy forces generated as a result of decrease in density when the cold meteoric water is heated at great depths, fluid flow may occur even against the direction of decreasing pressure gradient.

A convective cell is formed between the upflow zone $\rightarrow$ cap rock $\rightarrow$ outflow zone $\rightarrow$ downflow zone $\rightarrow$ upflow zone. The flow characteristics within this cell are functions of Rayleigh number, Ra, given by (Kjaran and Eliasson, 1983):

$$Ra = \frac{g\beta\rho_w c_w kh\Delta T}{\nu_w \lambda} \tag{3.2}$$

This gives the ratio of the buoyant forces to viscous resistance (in this case the viscosity of the of the fluid and the viscous drag of the rock matrix on fluids). For a horizontally fully saturated aquifer, convection will set in when Ra $\cong 4\pi^2$ (in geothermal reservoirs, Ra = 100 to 1000).

This would imply that for convection to be maintained in a hydrothermal system, permeability has to be greater than some value for a given reservoir state. This condition can be expressed as:

$$k > \frac{4\pi^2 \nu_w \lambda}{g\beta\rho_w c_w \Delta T h} \tag{3.3}$$

We therefore see that, before exploitation, the initial fluid distribution in the hydrothermal reservoir is controlled by dynamic balance of mass and heat. Once exploitation begins, flow of fluid is controlled by the pressure gradient generated due to well discharge and flow to and from the wells will also be much greater than flow in the natural state.

The part of a geothermal system exploitable for hot water and steam is no doubt related to its upflow zone. In this zone, especially in liquid dominated systems, due to the high pressures deep in the reservoir, water exists as liquid at some temperature. As the water rises due to

variations in density, its pressure falls and at some point when saturation pressure is reached, it will begin to boil and continue flowing up as steam and water mixture. Above the saturation point, temperature is obtained by the saturation relation:

$$T = T_{sat}(P) \tag{3.4}$$

Below the saturation point temperature is nearly constant and pressure gradient is equal to the local hydrostatic gradient plus the dynamic gradient. The dynamic gradient, however, is very small and can be neglected and so the pressure relation is given by:

$$\frac{dP}{dz} = \rho_w g \tag{3.5}$$

Equation 3.5 can be utilised to generate boiling point depth curve (BPD) for saturation conditions by solving numerically the following equation (Arason and Björnsson, 1994).

$$P(z) = P_0 + g\int_{z_0}^{z} \rho_{sat}\, dz \tag{3.6}$$

Discharge emanating from the upflow zone flows away laterally with almost no convection and can be treated in the same way as flow in cold groundwater. If the reservoir is liquid dominated and the wells exhibit hydrostatic pressure gradient, we can calculate fluid potentials in the flow domain and find the areal potential distribution. The result of doing this will be to show areas of high potential that will indicate hot upflow zones and areas of low potential that will indicate downflow zones for cooled water, leakage or discharge zones. The fluid potential at a point in the flow domain is defined as mechanical energy per unit mass and is given by:

$$\Phi = gh \tag{3.7}$$

where $h$ is the hydraulic head given by

$$h = z + \frac{P}{\rho_w g} \tag{3.8}$$

Since $g$ is a constant, calculating hydraulic head is as good as calculating the fluid potential.

### 3.2 Temperature and pressures in the Olkaria geothermal system

Formation temperature and initial pressures serve as the base for conceptual and numerical models and should be carefully analysed in order to get a good realistic model. Temperatures and pressures as measured from the wells are often affected by inter zonal flow within the wells, cooling of the formation during drilling, and cooling due to boiling during well discharge. Shallow cold groundwater may also leak through the casing annulus and cool the well. Temperature recovery after drilling can be estimated by Albright and Horner methods assuming that conduction is the major mode of heating. The resulting data can then be used to estimate the formation pressure (Arason and Björnsson, 1994). However, it is not possible to apply these methods when there is boiling in the well. In this case, it is necessary to check

the temperature and pressure logs for boiling conditions in comparison with boiling point for depth curve and the enthalpy of the discharged fluid.

An attempt was made to estimate the formation temperature and pressures for all available wells in Olkaria. BOILCURV computer program for generating boiling point with depth curves and PREDYP program for calculating pressure in a static water column when the temperature is known (Arason and Björnsson, 1994) were used where appropriate. The estimated formation temperature and initial pressures are shown together with the measured data in Appendix A. This data was so much and its analysis took a very long time. It can be observed that temperature and pressures obtained from wells in Olkaria East field follow the boiling point with depth curve. Similarly, temperature and pressures from wells located in the upflow zones of Olkaria Northeast and West also follow the boiling point with depth curve. Wells outside these upflow zones show either isothermal temperatures at depth below the casing shoe, indicating inter zonal flow or reversed temperatures suggesting counter flow of hot outflow and cold inflow from shallow and deep aquifers, respectively.

Areal temperature distributions (Figures 7 to 9) show hottest zones in Northeast field, West field and in the north around well OW-101. Coldest zones are in NE around well OW-704, in the NW around well OW-102, in the south and SW around wells OW-307 and well OW-801 and in the Olkaria Central field.

Figures 10 and 11 show vertical cross-sections of temperature in the E-W and N-S directions. From the E-W section, we observe hot plumes in Olkaria West and Northeast fields separated by a cold temperature zone in Olkaria Central field. Some cooler down flow zone seem to occur within the hot plume in Olkaria Northeast. From the N-S section, we generally observe a wide zone of hot plume covering both Olkaria Northeast and Olkaria East fields with a cooler down flow zone between the two fields. Temperatures fall further south.

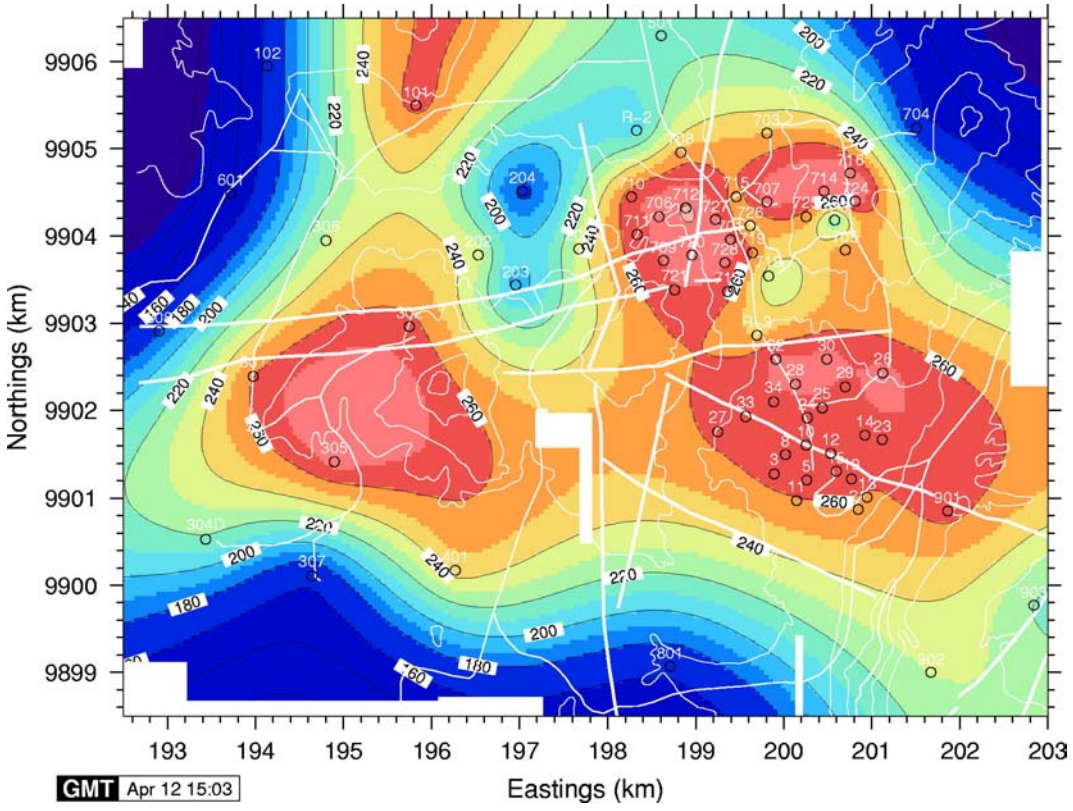


Figure 7: Temperature distribution at 1000 m a.s.l.

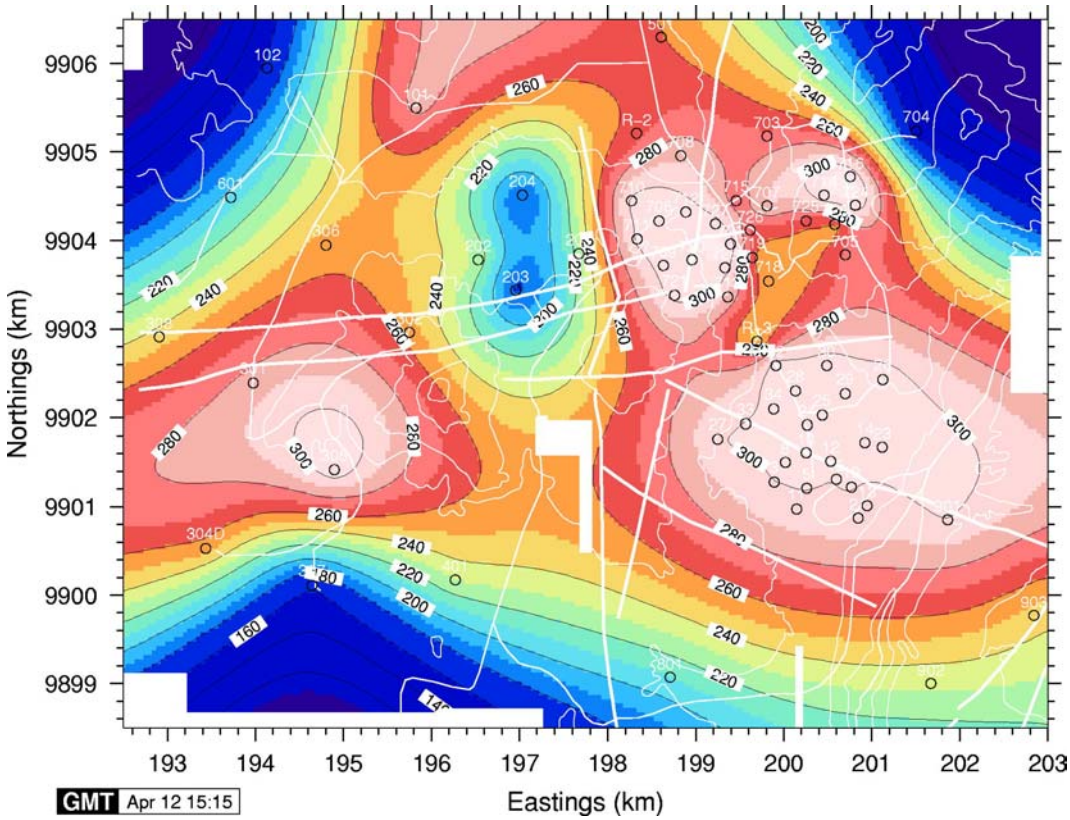


Figure 8: Temperature distribution at 500 m a.s.l.

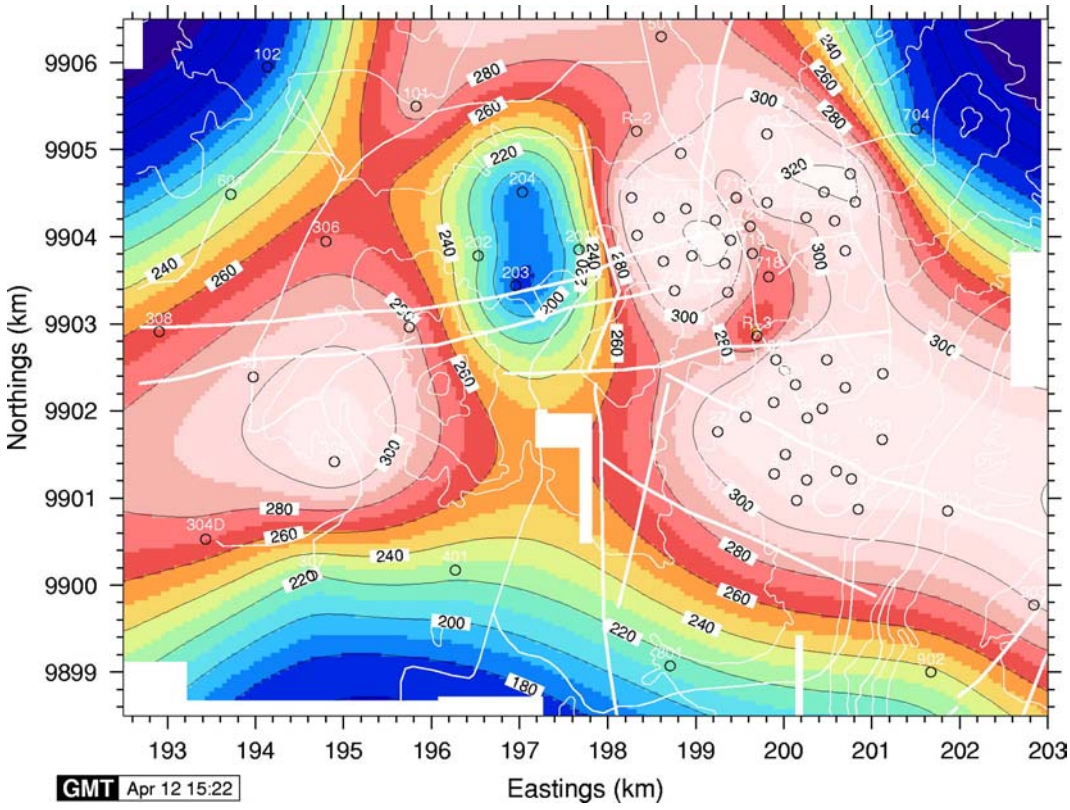


Figure 9: Temperature distribution at 250 m a.s.l.

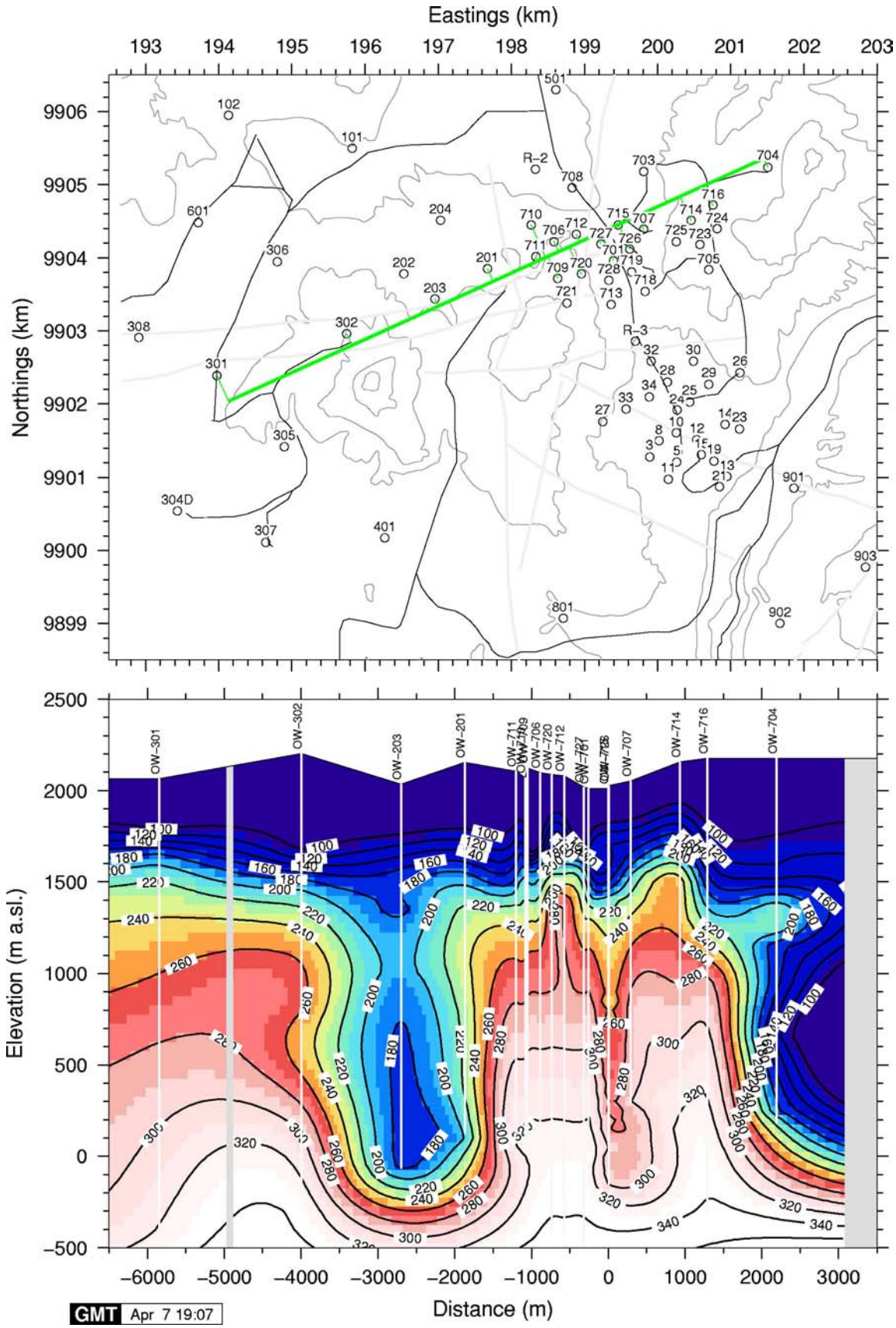


Figure 10: A general E-W temperature cross section

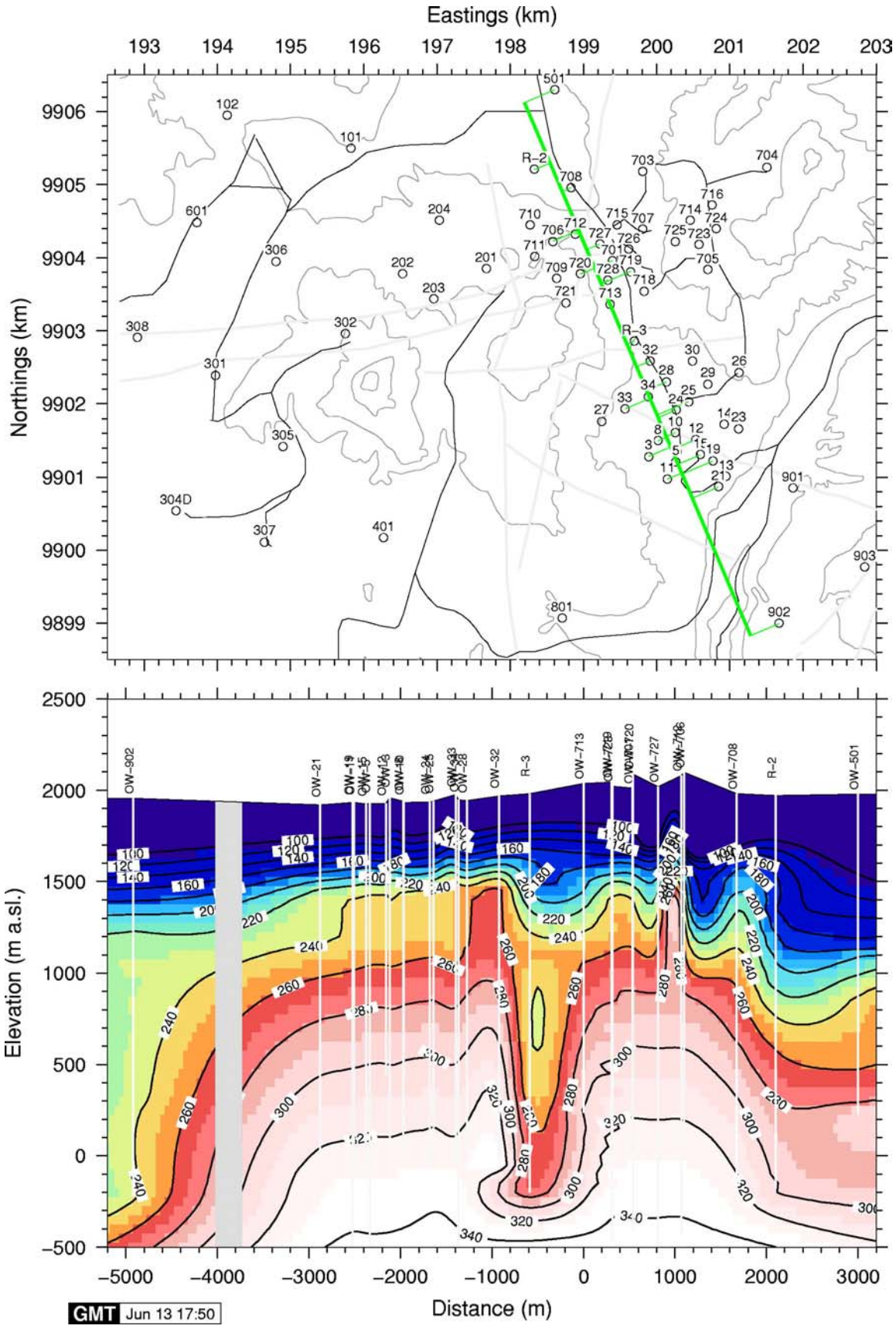


Figure 11: A general N-S temperature cross section

Figure 12 shows pressure distribution at 1000 m a.s.l. Low pressure zones are in the central and northwest corner and high pressure zones occur in the eastern and western sides. The low pressure zone in the central coincides with the low temperature and high resistivity zone and is also a zone of high steam loss from fumaroles. The high pressure zones coincide with upflow zones recharging the system.

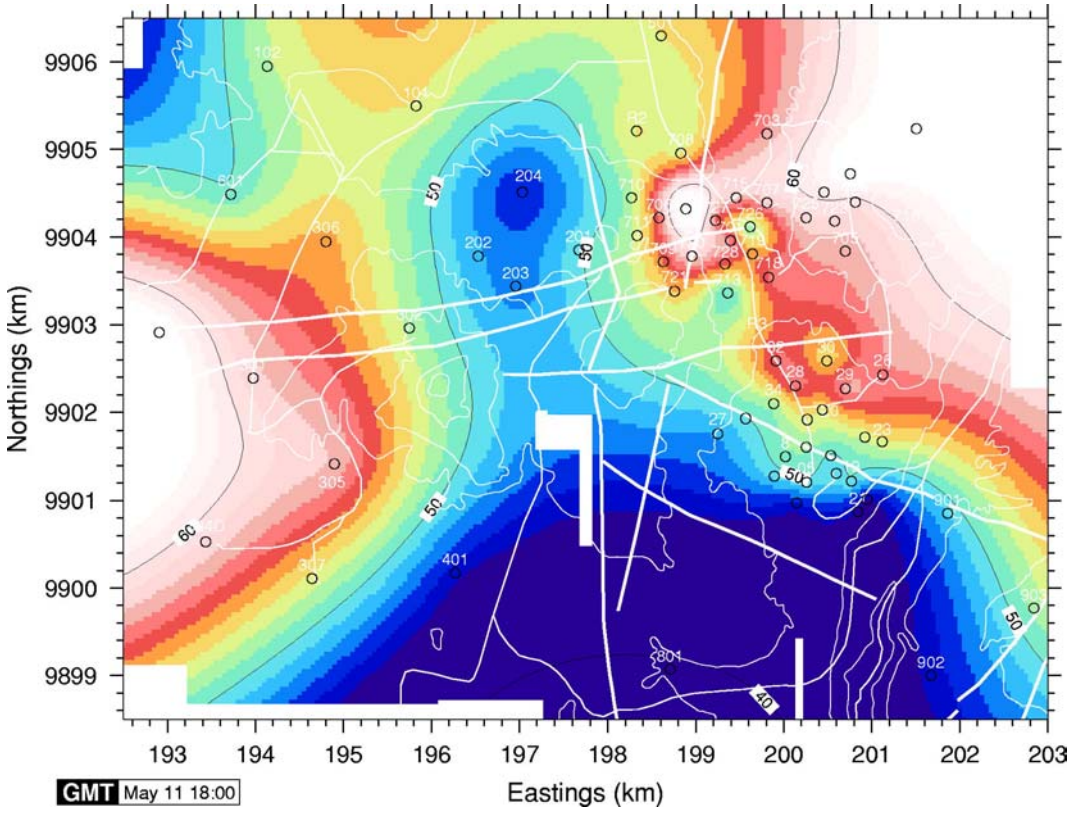


Figure 12: Pressure distribution at 1000 m a.s.l.

### 3.3 Well Characteristics

The casing design for the Olkaria wells consists of 20" diameter surface casing to a depth of 30 - 40 m, 13 3/8" diameter anchor casing to 260 – 350 m depth, 9 5/8" diameter production casing to 500 – 800 m depth and then 7" diameter slotted liners in the production hole (Figure 13).

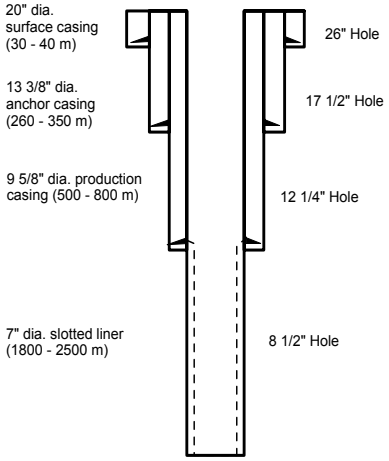


Figure 13: Casing design for Olkaria wells

Most of the early wells drilled in the Olkaria East field intercepted low formation permeabilities in the range of 4 milli-darcy in the liquid zone and 7.5 milli-darcy in the steam zone (Bodvarsson and Pruess, 1984). Wells drilled later towards the north and generally in the Olkaria Northeast field have better permeabilities and are also better producers.

Well productivity is affected both by inflow performance and wellbore performance. Inflow performance is the ability of the geothermal fluid to flow through the feed zone when there is a pressure drop between the reservoir and the well. It is greatly influenced by formation permeability. To a greater extent, Olkaria wells have low productivity because of the low permeabilities. Wellbore performance describes the contribution the casing design has on the pressure behaviour when fluid moves from the feed zone to the wellhead. It depends on the fluid temperature and reservoir pressure, well diameter and well depth. Since pressures and temperatures are unique properties of a particular reservoir, the only factor that can be optimised in wellbore performance is casing size. It has been shown for Svartsengi and the Geysers geothermal fields that increased casing sizes minimize wellbore effects leading to better well productivities (Kjaran and Eliasson, 1983). There is need to do studies on wellbore performance for Olkaria wells to investigate the effects and benefits of larger casing design. The data was not available to do this during this study.

Figure 14 below is a N-S cross-section indicating location of feed zones in the wells. Most of the feed zones are intercepted at contact points between successive rock strata. Shallow feed zones in most of the wells produce steam.

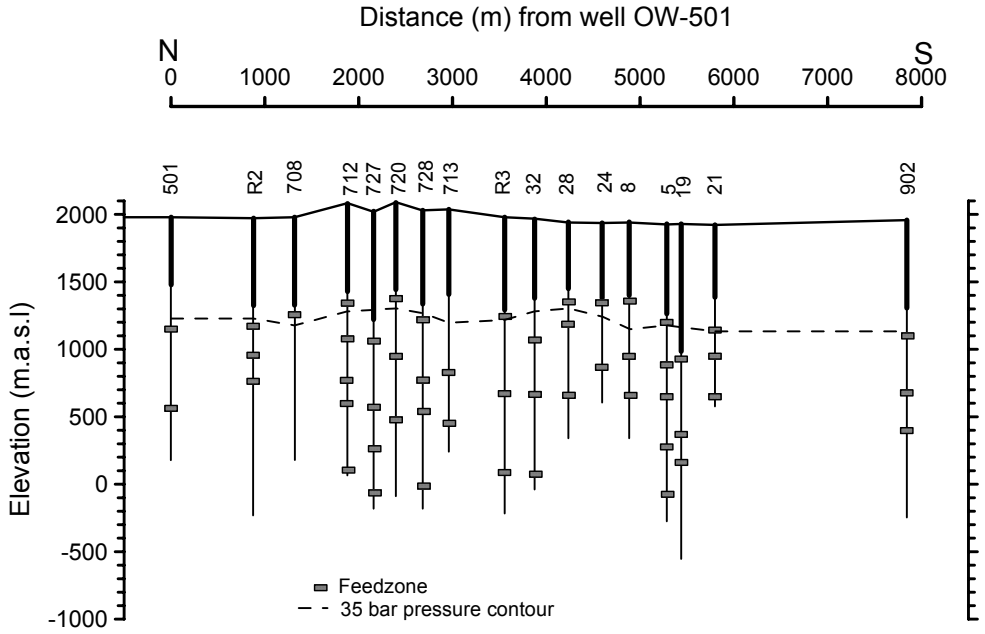


Figure 14: A N-S cross-section showing feed zones and 35 bar pressure contour

### 3.4 Pressure potentials and flow pattern in the Olkaria geothermal system

Figures 15 – 17 show pressure potentials in the initial state in the Olkaria reservoir. High potentials occur in the western field and the eastern fields with a low potential between them. The low pressure potential extends to the south and indicates an area of rapid heat and mass sink (downflow or fluid and heat loss). High potential areas indicate zones of fluid and heat inflow/upflow. The arrows point to the possible direction of flow. Data analysis was done by using the formulas from section 3.1.

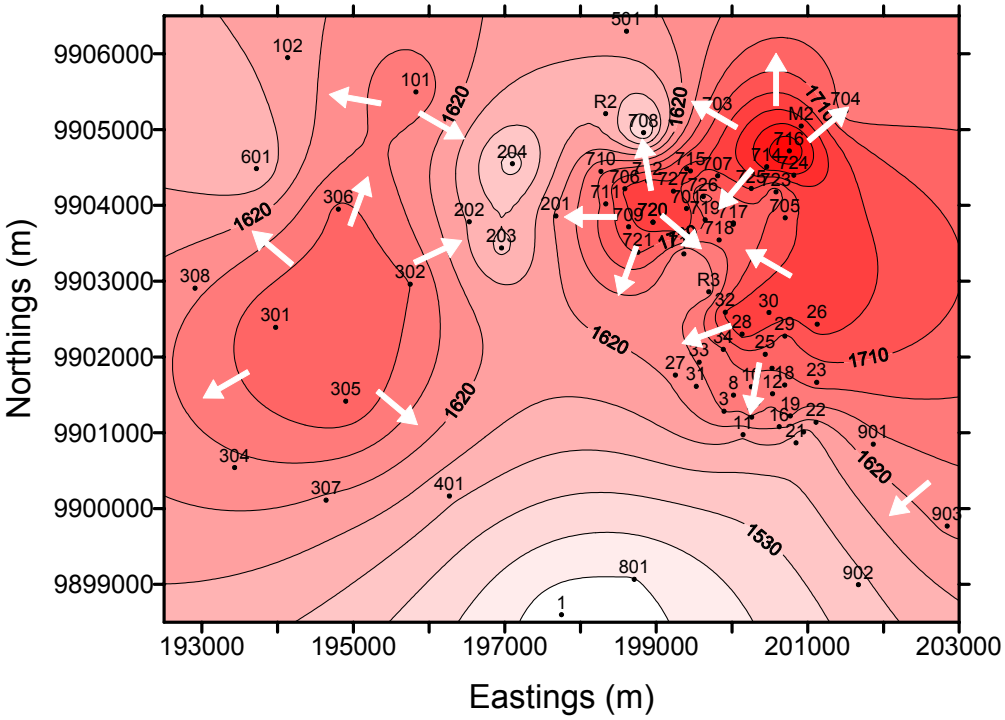


Figure 15: Pressure potential (m) at 1000 m a.s.l. and flow directions

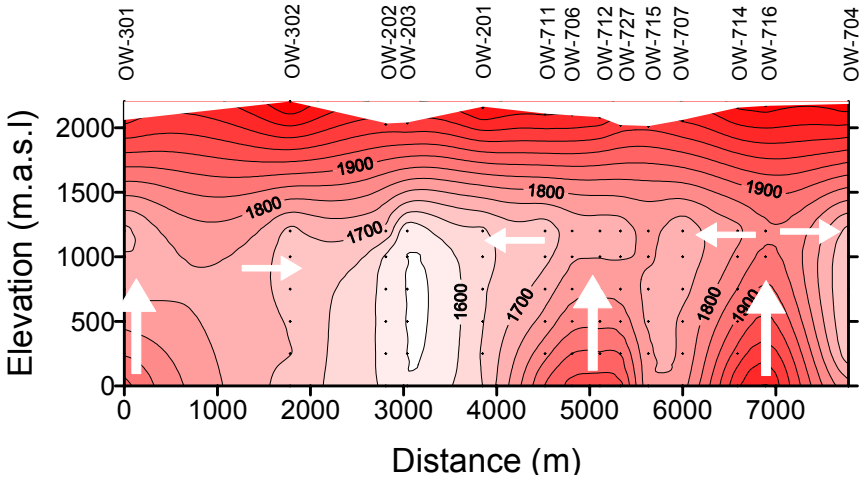


Figure 16: A W-E cross-section of pressure potential

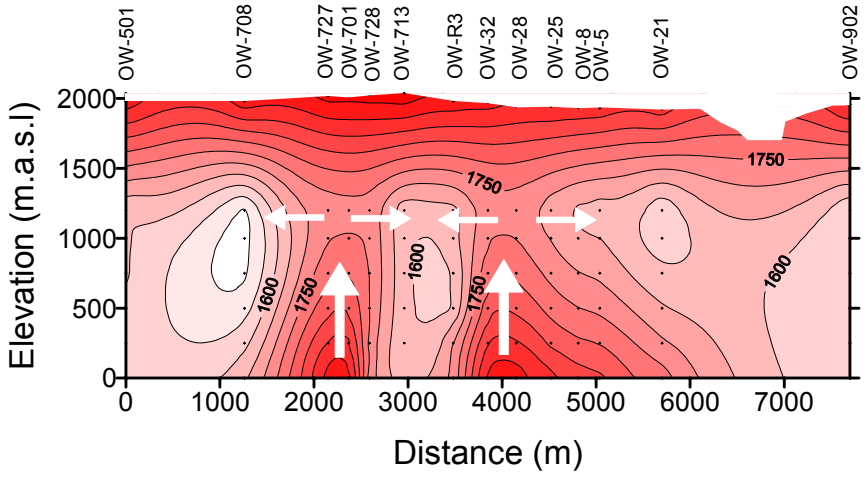


Figure 17: A N-S cross-section of pressure potential

### 3.5 Conceptual reservoir model

#### 3.5.1 Previous conceptual models

Conceptual model of the Olkaria geothermal system has been reviewed several times over the years as more information is acquired from surface studies and deep drilling. The first model (Figure 18) was proposed by Sweco and Virkir (1976). In their model, the geothermal reservoir was visualised as boiling water overlain by a 50 – 150 m thick steam zone capped by tuffaceous caprock. Water originating from the surface penetrated down to 1600 m b.s.l. where on heating by heat flux from the underlying hot bedrock, it acquired a temperature of 320°C. This 320°C water then boiled off as it rises up to give a two-phase mixture of steam and water. The rising steam condensed below the cap rock and the condensate fell back ending in a convective circle.

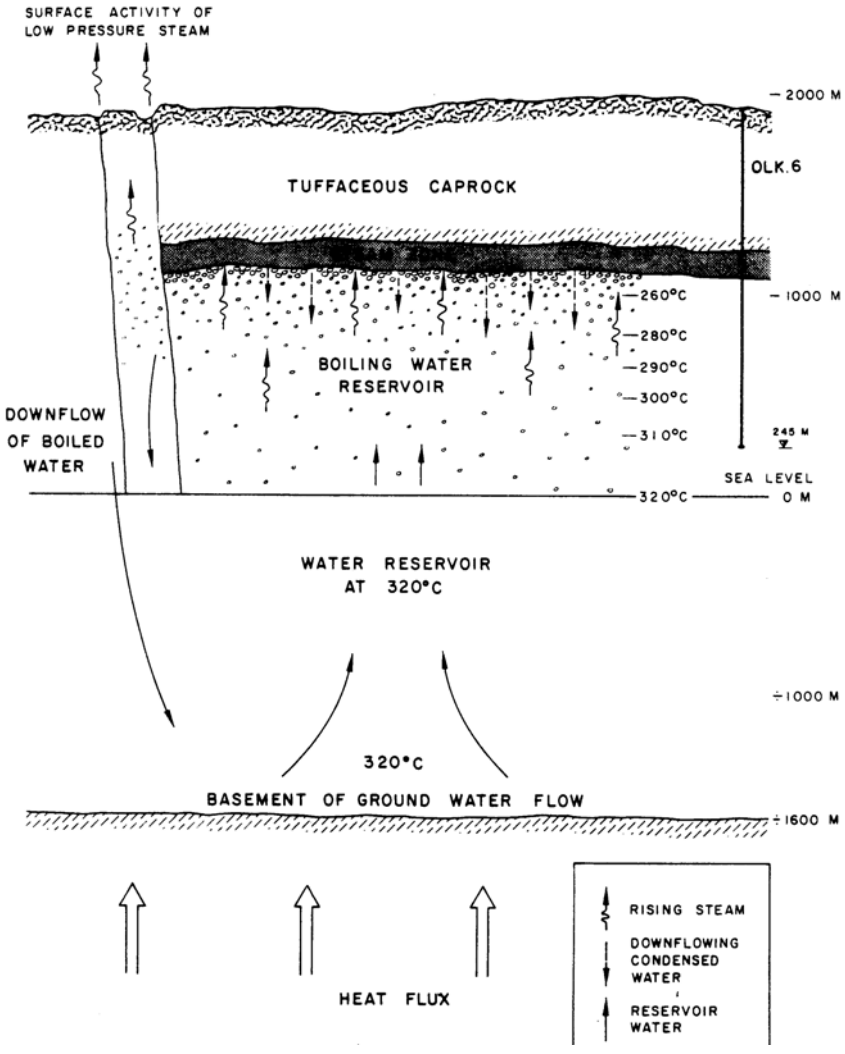


Figure 18: 1976 conceptual model of Olkaria geothermal reservoir (from Sweco and Virkir, 1976)

In the model by Bodvarsson et al., (1987), fluid recharge to the Olkaria East reservoir was proposed to come from an upflow zone in the north close to OW-716. The steam zone (50 – 150 m thick) thinned towards the north and thickened to the south. The cap rock was proposed to be at 500 – 700 m depth. Another upflow zone was proposed to be in Olkaria West. The waters discharged from these areas were different with Olkaria West discharging

sodium bicarbonate waters and Olkaria Northeast and East discharging sodium chloride waters. Fluid discharged from the two upflow zones flowed along Olkaria fault from east and west to converge and flow to the south along Ololbutot fault with extensive steam loss along this fault. Part of the discharge from the Olkaria West upflow moved to the north along the Olkaria fracture.

The latest review of the conceptual model is contained in Muchemi, (1999). The views expressed in the previous models have remained more or less the same and just refined and strengthened with additional information that has been acquired. Interpretation of MT and magnetic data together with surface geology has indicated that there is a highly differentiated magma chamber beneath the Olkaria geothermal system. Shallow heat sources occur along N-S, NW, NE striking faults and the ring fracture. Fluid movement is controlled by NW-SE and NE-SW faults and overall productivity of the fields and individual wells are correlated to the intersection of these faults, in the vicinity of the heat source. In addition to the two upflow zones proposed in the earlier models, a possible third upflow zone is proposed to be in the Olkaria Domes field. Fluid chemistry and reservoir temperatures seem to suggest that Olkaria West, Olkaria Central, Olkaria Northeast/Olkaria East and Olkaria Domes are in separate systems.

### 3.5.2 Revised conceptual model

In this section, I now present a possible slight revision to the current conceptual reservoir model (Figure 19). The two distinct hydrothermal systems of Western and Eastern Olkaria are clearly separated by the low pressure potential and temperature zone of Olkaria Central. In the Eastern part, it seems possible that there are two upflow zones in Olkaria Northeast field and one upflow zone in Olkaria East field. A downflow zone extending from OW-723 through OW-R3/713 in a NE-SW direction seems to be separating Olkaria Northeast and Olkaria East fields. Olkaria East field is one big upflow zone that is possibly centred around OW-28, 30 and 32. From this zone, fluids move mainly to the south with extensive boiling occurring to develop steam zone below the cap rock. There is a possibility of a N-S fluid movement into the downflow zone.

The two upflow zones in Olkaria Northeast are centred around wells OW-714, 716 and around wells OW-706, 720, 709, 728 and 701. A downflow zone extending from OW-717/718 through OW-708 in a NW-SE direction separates them. Extensive boiling also occurs in these two upflow zones to form steam caps below the cap rock. The other upflow zones occur around wells OW-301/305 area and well OW-101 area. OW-901 could be an extension of Olkaria East and from only three wells now drilled in Olkaria Domes, it is still not possible to delineate a separate upflow zone for this field.

These observations are supported by distribution of high fluid potentials, high temperature distributions as well as shallow micro-earthquake clusters and low resistivity distribution around these zones. Calculated temperatures from geothermometers also point to support these observations.

Cold water recharge into the reservoir seems to occur from all the directions. No clear marked hydrological boundaries can be observed from reservoir data or otherwise, in the Olkaria system. Olkaria Central seems to be a heat sink zone where there is tremendous cooling of the hot rising waters that come from the upflow zones. This cooling is evident from large steam discharge along Ololbutot fault and altered grounds in Olkaria Central field. Figure 19 gives a possible presentation of a conceptual model of the Eastern Olkaria system.

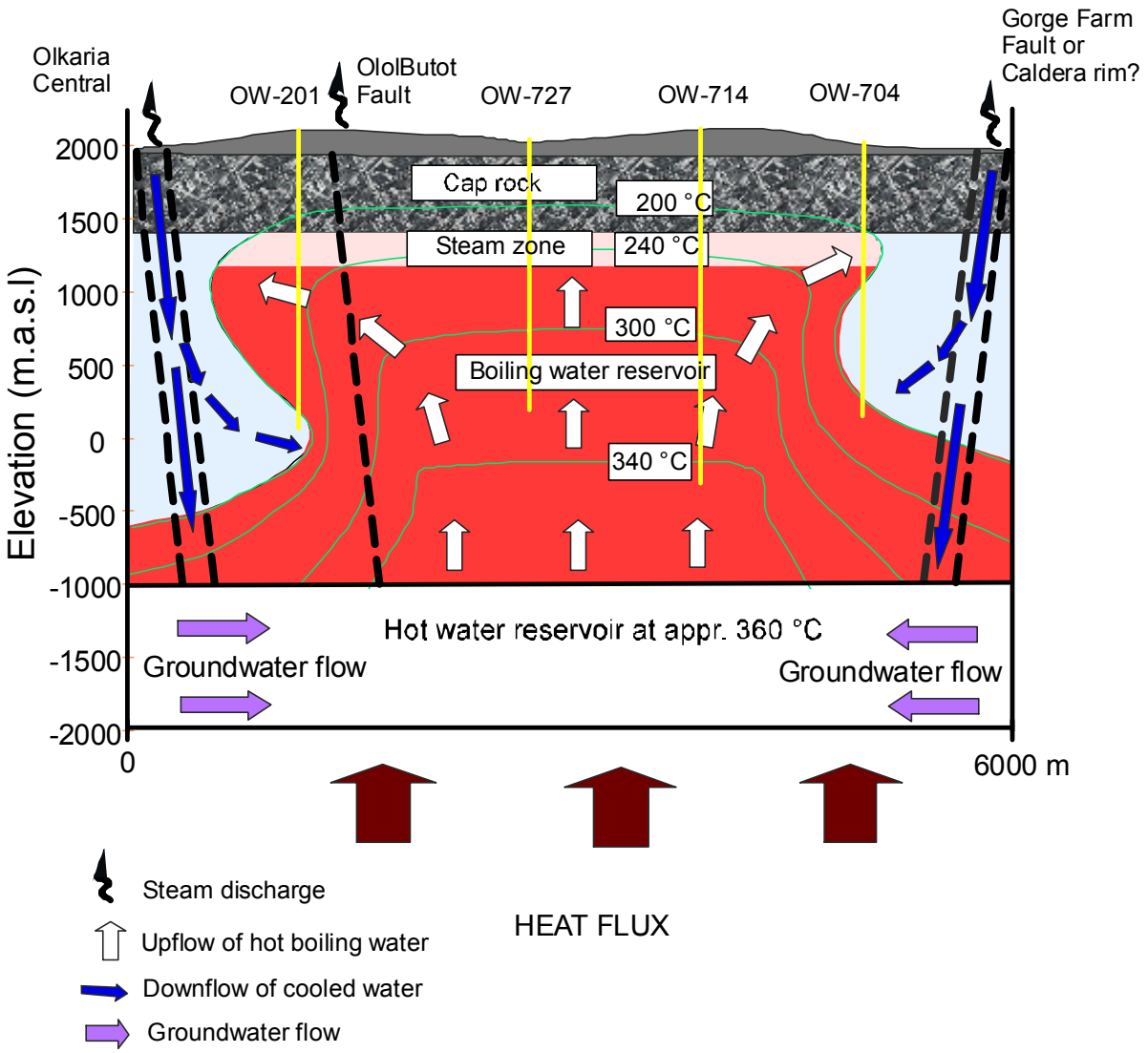


Figure 19: A revised conceptual model of the Eastern Olkaria system (section from east to west)

### 3.6 Hydrological model

The regional groundwater flow in the Olkaria area is southwards from Lake Naivasha in the north (KPC, 1981). The Lake Naivasha catchments area includes the neighbouring escarpments of the Rift Valley. In the Eastern geothermal system, deep inflow of cooler recharge fluid into the reservoir seems to occur along the Gorge Farm fault in the northeast and along the fracture zone in Olkaria Central between Ololbutot fault and Olkaria hill. In the northern part, the regional groundwater flow seems likely to encroach into the geothermal system and mixes with hot water flowing from the upflow zone. This is supported by the occurrence of smectite, illite and chlorite-illite in the northern wells OW-501 and OW-703 and by their down hole temperature profiles and discharge behaviour. In general, the most likely hydrological setting are geothermal convective systems in three almost separate sections with segments of rapid downflow in-between them. Outflow through steam vents and compensating inflow are through active faults through the caprock.

## 4.0 LUMPED RESERVOIR MODEL

In lumped-parameter (material and energy balance) models, the reservoir is considered as a single unit categorized by changes in a single set of variables. The model ignores any internal structure in the reservoir and the parameters to be determined are estimated from the averaged field history rather than from individual well information. The result of this is to match or forecast the gross behaviour of the reservoir.

Normally, a lumped-parameter model only links the mass withdrawal to the changes in the production zone of the reservoir. It forecasts only the features of the production zone and if important processes occur outside this zone, the utility of the model is reduced (Grant et al., 1982). However, it is quite simple and offers a first step in evaluation of the collected data to indicate a rough direction of events.

### 4.1 Lumped convective model

In this study, I will use a lumped convective model by Eliasson, 1973, and Kjaran and Eliasson, 1983, to estimate heat and mass flows in the upflow zones observed in the conceptual model.

Darcy's law for flow in the convective cell can be written as:

$$\oint \frac{g}{K} U ds + \oint \rho g . ds + \oint \frac{\partial p}{\partial x} ds = 0 \qquad (4.1)$$

The first term is due to energy dissipation in the flow, the second due to buoyancy effects in the convection (density difference between the upflow and downflow) and the third term is due to the pressure gradient and must be equal to zero for the closed integration path.

The first term can be approximated by:

$$\oint \frac{g}{K} U ds = \frac{g}{K} \frac{u}{1-\varepsilon} l \qquad (4.2)$$

where $u$ is the mass flux in the upflow and $\varepsilon$ is the energy dissipation factor and must be much smaller than 0.5. The second term is approximated by:

$$\oint \rho g ds = g l \Delta\rho \qquad (4.3)$$

where $\Delta\rho$ is the density difference between the downflow and upflow. Equating 4.2 and 4.3 and with $A$ as the upflow area, the upflow can be estimated from the following equation:

$$W_{up} = KA(1-\varepsilon)\Delta\rho \qquad (4.4)$$

The total natural heat loss is then obtained by:

$$H_{loss} = W_{up} C_w (T_{up} - T_{down}) \qquad (4.5)$$

This heat is lost through steam vents, surface springs and by conduction through the caprock.

Figure 20 below is a simple vertical lumped convective model of Olkaria Northeast field. It depicts hot water flowing up from the two perceived upflow zones in the conceptual model and out into the Olkaria Central area and well OW-704 area. Cooled water enters the convective cells at depths beneath these outflow areas. In the middle of the two convective systems, there is some mixing of fluids from the two upflow zones with steam condensate and possibly shallow groundwater leaking through the cap rock. Steam leakages through the faults occur at the surface and cold meteoric water also flows down through the faults. If the upflow areas are estimated as the extent of 1800 m pressure potential at 1000 m a.s.l. (Figures 15 and 16), then the upflow rates can be estimated as flows:

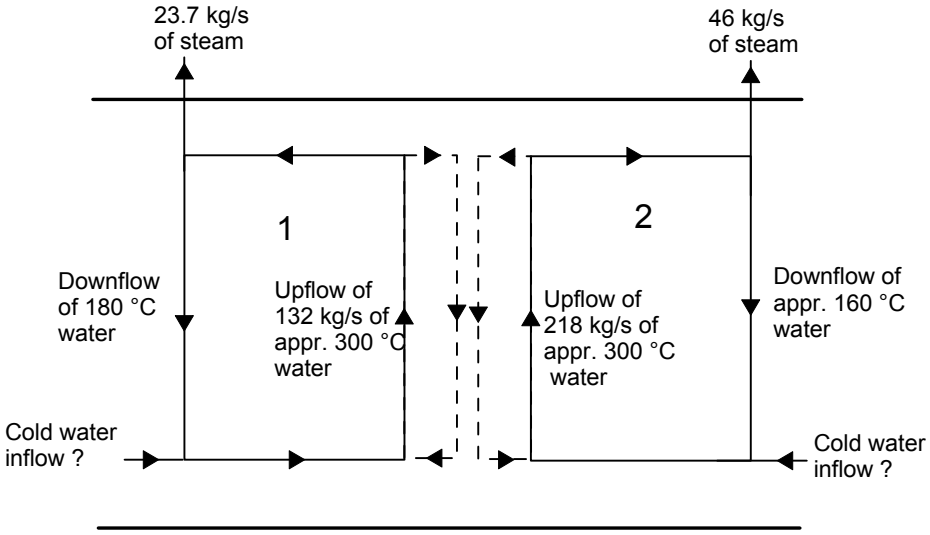


Figure 20: A convective model of Olkaria Northeast reservoir

Average transmissivity obtained from interference tests done in Olkaria Northeast field (Ofwona, 2000) is 20 darcy-meter and transmissivity in the Olkaria fault as estimated from numerical model (Bodvarsson, 1993) is 200 darcy-meter. Assuming a reservoir thickness of 1000 m, average permeability is obtained to be 18 milli-darcy. If we assume that the upflow water is 300°C, then the hydraulic conductivity is calculated as $K$ = (18 x $10^{-15}$ $m^2$ x 9.81 $m/s^2$)/0.127 x $10^{-6}$ $m^2/s$ = 1.4 x $10^{-6}$ m/s. For cell 1, $\Delta\rho$ = 900 – 712 = 188 $kg/m^3$, $A$ = 1 x $10^6$ $m^2$ and for cell 2 $\Delta\rho$ = 920 – 712 = 208 $kg/m^3$, $A$ = 1.5 x $10^6$ $m^2$. Using Equation 4.4, upflow rate in cell 1 = 132 kg/s and in cell 2 = 218.4 kg/s. Heat flow from cell 1 is then 132 kg/s x 4.2 kJ/kg°C x 120°C = 66.5 MWt and from cell 2 equals to 128.4 MWt. If this is solely lost by steam vents to the surface, amount of steam expelled will be equal to about 70 kg/s.

### 4.2 Lumped exploitation model

An overall material balance for a producing geothermal reservoir is given by the expression

$$M_n = M_o - M_p + M_i + M_r \qquad (4.6)$$

It states that the mass of fluids in the reservoir now equals to what was originally in place, less what has been produced, plus what has been injected and what has recharged the reservoir from the external source. A fall in reservoir pressure can be measured and related to the mass of fluid produced.

The conservation of mass equation for a basic reservoir model with discharge and recharge, with fluid withdrawal from the reservoir and reservoir recharge from an external source, can be written as (Grant et. al., 1982):

$$S_m \frac{dP}{dt} + W - W_r = 0 \tag{4.7}$$

If the reservoir contains boiling water overlain by a steam or vapour dominated zone, like the case of Olkaria East field, then because of the high compressibility of the vapour zone, pressure in this zone may be considered constant. Analysis of drawdown data can be treated as in unconfined reservoir case with fluid withdrawal assumed to be mainly from the water zone with the upper compressible region remaining undisturbed. Pressure in the liquid zone can be assumed to be in hydrostatic equilibrium. If the reservoir pressure falls by an amount $\Delta P$, a fall in water level of an amount $\Delta P / \rho_w g$ results. Total volume loss is given as,

$$\Delta V = \frac{A\phi\Delta P}{\rho_w g} \tag{4.8}$$

and

$$\frac{dP}{dt} = \frac{\rho_w g q}{A\phi} \tag{4.9}$$

giving

$$S_m = \frac{A\phi}{g} \tag{4.10}$$

The recharge rate is approximated by:

$$W_r = \alpha_r \Delta P \tag{4.11}$$

Here $\alpha_r$ is lumped recharge coefficient that incorporates the effects of permeability and thickness of the matrix through which recharging fluid traverses. Equation 4.7 can then be written as:

$$W = \alpha_r \Delta P - S_m \frac{dP}{dt} \tag{4.12}$$

Solution to this equation for a constant production rate starting at time $t = 0$ is given by:

$$\Delta P = \frac{W}{\alpha_r}\left(1 - e^{-t/\xi}\right) \tag{4.13}$$

where

$$\xi = \frac{S_m}{\alpha_r} \tag{4.14}$$

is the response time constant for the system. For short times (t << $\xi$), recharge is negligible and pressure will decline almost linearly with time:

$$\Delta P = \frac{Wt}{S_m} \tag{4.15}$$

At steady state, i.e. large discharge times much greater than the time constant (t >> $\xi$), the pressure will stabilise at a value determined by a balance with the recharge:

$$\Delta P = \frac{W}{\alpha_r} \tag{4.16}$$

For variable discharge rates, we define a unit response function for the reservoir as:

$$\Delta P = \int_0^t W(\tau) f(t-\tau) d\tau \tag{4.17}$$

where $f$ is the instantaneous unit response function for the reservoir. Another response function can be defined as:

$$F(\tau) = \int_0^t f(\tau) d\tau \tag{4.18}$$

which in this case is given by:

$$F(\tau) = \frac{1}{\alpha_r}(1 - e^{-t/\xi}) \tag{4.19}$$

The solution for variable discharge rate is then given by:

$$\Delta P(t) = \sum_i (W_i - W_{i-1}) F(t - t_{i-1}) \tag{4.20}$$

As we have seen above, for an unconfined liquid dominated reservoir, production of fluid will result in a fall in reservoir liquid level. The original liquid in place is given by

$$M_o = Ah\phi\rho \tag{4.21}$$

and drawdown equation without recharge or water influx can be expressed from Equation 4.8 by:

$$\Delta h = \frac{M_p}{A\phi\rho} \tag{4.22}$$

This implies that a graph of drawdown (whether water level or pressure) with cumulative mass production should be a straight line if there is no water influx. These ideas are applied in chapter 6.

## 5.0 NUMERICAL MODEL

### 5.1 Theoretical background

#### 5.1.1 General partial differential equations for flow in two-phase geothermal reservoirs

In geothermal reservoirs, mass is carried through the medium by the percolation of fluid through the system of pores and fractures while heat is transferred by convection, conduction (diffusion) and dispersion. The process of heat transfer alters the density of the fluid, thus creating buoyancy forces that alter the course of the flow. Flow without heat transfer is a linear process and all velocities and fluid pressures are determinable from the boundary values. No streamlines are created within the fluid and the flow is entirely dependent on the external pressure conditions.

Flow with heat transfer is a non-linear process depending both on pressure and temperature at the boundary. Streamlines may be created within the fluid and if there is no flow through the boundaries, internal flow can occur. Due to the non-linearity of these processes, the equations describing flow in geothermal systems can only be solved by numerical methods since no analytical solutions exist.

The partial differential equations governing two-phase flow of water and steam in geothermal systems can be written for conservation of mass, momentum and energy with the necessary constitutive relationships and equation of state. Assuming a homogeneous isotropic media and neglecting solute transport, chemical reactions, kinetic energy, viscous dissipation and potential, these equations take the following forms:

Conservation of mass

For a rock matrix saturated with steam and water mixture, a fraction of the pore space is filled with each phase. The fraction of pore space filled with water is $S_w$ and the remainder, 1- $S_w$, is occupied by steam. A unit reservoir volume then contains in its pore space a mass $\phi S_w \rho_w$ of water and a mass $\phi(1-S_w)\rho_s$ of steam, giving a total fluid mass per unit volume of $\phi S_w \rho_w + \phi(1-S_w)\rho_s$. Both liquid and vapour phases can move independently through the medium and hence there are separate mass flux densities for the individual phases. The conservation of mass equation for the case where there is a source (or sink) term is therefore written as:

$$\frac{\partial}{\partial t}\left(\phi\rho_w S_w + \phi\rho_s(1-S_w)\right) + div(\rho_w q_w + \rho_s q_s) = Q_M \qquad (5.1)$$

Conservation of energy

The total energy contained in a unit volume of the reservoir is the sum of energy contained in the rock, $(1-\phi)\rho_r U_r$, and that contained in the two-phase fluid, $\phi S_w \rho_w U_w + \phi(1-S_w)U_s\rho_s$. Energy is transported through the reservoir by convection and conduction. The convective flux is given by $\rho_w q_w h_w + \rho_s q_s h_s$ and the conductive-dispersive flux by $\lambda\nabla T$. The equation for conservation of energy can therefore be written as (White and Kissling, 1992):

$$\frac{\partial}{\partial t}\left(\phi\rho_w S_w U_w + \phi\rho_s(1-S_w)U_s + (1-\phi)\rho_r U_r\right) + div(\rho_w q_w h_w + \rho_s q_s h_s - \lambda\nabla T) = Q_E \qquad (5.2)$$

Conservation of momentum

When two phases occupy the same pore volume, each reduces the flow of the other below what it would be if it fully saturated the medium. The resulting permeability reduction factors are called relative permeabilities and are functions of water saturation. For two-phase flow of steam and water, Darcy's law takes the form:

$$q_w = -k\frac{k_{rw}}{\mu_w}(\nabla P - \rho_w g) \tag{5.3}$$

$$q_s = -k\frac{k_{rs}}{\mu_s}(\nabla P - \rho_s g) \tag{5.4}$$

Constitutive relations

A single-phase reservoir contains at any time a distribution of pressure and temperature and a two-phase reservoir contains pressure-temperature and saturation. These primary thermodynamic variables must be supplemented with constitutive equations that express secondary variables and parameters as functions of a set of the primary variables of interest. The existence of steam and water in contact means that the pressure and temperature are related by the saturation curve and due to capillarity effects, the vapour pressure of the water phase will be lowered. The constitutive relations therefore, are:

$$P = P_{sat}(T) \text{ or } T = T_{sat}(\mathrm{P}) \tag{5.5}$$

$$P_{cap}\,(S_w) = P - P_w \tag{5.6}$$

Various empirical functions of relative permeabilities and capillary pressures are available from various authors and are documented Grant et al., 1982; Kjaran and Eliasson, 1983; and Pruess et al., 1999; among others. The coupling of pressure and temperature through the saturation relation means that the mass and energy conservation equations are strongly coupled (Grant et. al., 1982) making the thermodynamic properties (density, viscosity, enthalpy and internal energy) be functions of a single variable (pressure or temperature) hence simplifying the task of solving the equations.

The solutions to these equations are obtained numerically by use of either finite difference or finite elements method. The former is the widely used method by geothermal modellers.

### 5.1.2 Finite difference formulations

Aquifer discretization is done in both space and time. The region of interest is divided into blocks or volume elements (Figure 21) using the Cartesian coordinate system. The aquifer and fluid properties are assumed to be constant throughout the element, but are allowed to differ between different elements. In this way, a non-homogeneous aquifer is approximated as a collection of different homogeneous regions. Elements are node centred and boundaries separating the elements are located at an equal distance from each node. The discretized flux is expressed in terms of averages over parameters for elements i and j.

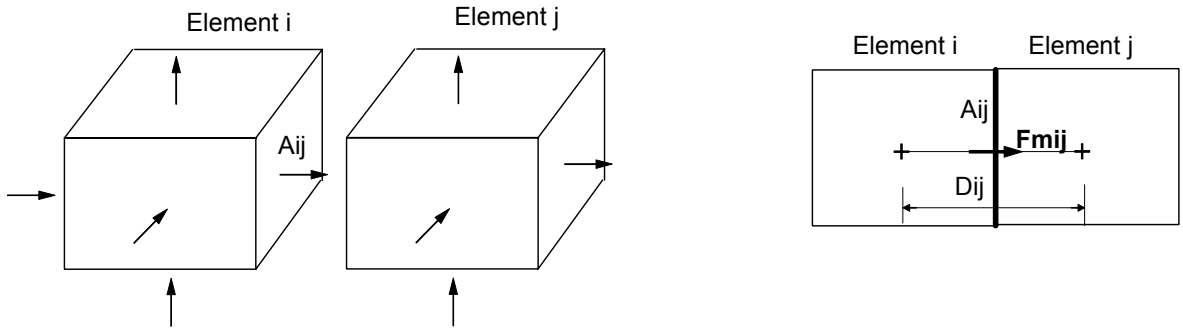


Figure 21: Volume elements

Time is discretized as a first order finite difference and the flux and mass/energy accumulation terms are evaluated at the new time level; $t^{n+1} = t^n + \Delta t$ to obtain the numerical stability needed for an efficient calculation of multiphase flow (Pruess et. al., 1999). In this way, the fluxes are expressed in terms of the unknown thermodynamic parameters at the time step $t^{n+1}$, so that these unknowns are only implicitly defined in the resulting equations. Time discretization of equations 5.1 and 5.2 results in the following set of coupled non-linear algebraic equations (Yang et. al., 1991):

Mass balance

$$V_i\left(M_{mi}^{n+1} - M_{mi}^{n}\right) + \sum_j A_{ij} F_{mij}^{n+1} \Delta t_{n+1} - \left(Q_{mi}^{n+1} \Delta t_{n+1}\right) = 0 \tag{5.7}$$

Energy balance

$$V_i\left(M_{ei}^{n+1} - M_{ei}^{n}\right) + \sum_j A_{ij} F_{eij}^{n+1} \Delta t_{n+1} - \left(Q_{ei}^{n+1} \Delta t_{n+1}\right) = 0 \tag{5.8}$$

where,

$$M_{mi}^{n+1} = \phi_i \left(\rho_w S_w + \rho_s (1 - S_w)\right)_i^{n+1} \tag{5.9}$$

$$M_{ei}^{n+1} = \phi_i \left(\rho_w S_w U_w + \rho_s (1 - S_w) U_s\right)_i^{n+1} + (1 - \phi_i) \rho_r C_{ri} T_i^{n+1} \tag{5.10}$$

and

$$U_r = C_r T \tag{5.11}$$

The mass flux consists of both liquid (water) and vapour (steam) phases and can be written as:

$$F_{mij}^{n+1} = F_{mijw}^{n+1} + F_{mijs}^{n+1} \tag{5.12}$$

and in terms of Darcy's law as:

$$F_{mijw}^{n+1} = -\left(\rho_w \frac{k k_{rw}}{\mu_w}\right)_{ij}^{n+1} \left[\frac{P_j^{n+1} - P_i^{n+1}}{D_{ij}} - \rho_{wij}^{n+1} g_{ij}\right] \tag{5.13}$$

$$F_{mijs}^{n+1} = -\left( \rho_s \frac{kk_{rs}}{\mu_s} \right)_{ij}^{n+1} \left[ \frac{P_j^{n+1} - P_i^{n+1}}{D_{ij}} - \rho_{sij}^{n+1} g_{ij} \right] \tag{5.14}$$

The energy flux is written as:

$$F_{eij}^{n+1} = h_{wij}^{n+1} F_{mijw}^{n+1} + h_{sij}^{n+1} F_{mijs}^{n+1} - \lambda_{ij}^{n+1} \frac{T_j^{n+1} - T_i^{n+1}}{D_{ij}} \tag{5.15}$$

The weighted interface densities are linear averages and are written as:

$$\rho_{wij} = \frac{1}{2}(\rho_{wi}^{n+1} + \rho_{wj}^{n+1}) \tag{5.16}$$

$$\rho_{sij} = \frac{1}{2}(\rho_{si}^{n+1} + \rho_{sj}^{n+1}) \tag{5.17}$$

Permeability is harmonically averaged and is obtained from:

$$\frac{D_{ij}}{k_{ij}} = \left( \frac{d_i}{k_i} + \frac{d_j}{k_j} \right) \tag{5.18}$$

Interface mobility and enthalpies are evaluated from (Yang et. al., 1991):

$$\left( \rho_w \frac{k_{rw}}{\mu_w} \right)_{ij}^{n+1} = \left( \rho_w \frac{k_{rw}}{\mu_w} \right)_i^{n+1} \tag{5.19}$$

and

$$h_{wij}^{n+1} = h_{wi}^{n+1} \tag{5.20}$$

for

$$\frac{P_j^{n+1} - P_i^{n+1}}{D_{ij}} - \rho_{wij}^{n+1} g_{ij} < 0 \tag{5.21}$$

$$\left( \rho_s \frac{k_{rs}}{\mu_s} \right)_{ij}^{n+1} = \left( \rho_s \frac{k_{rs}}{\mu_s} \right)_i^{n+1} \tag{5.22}$$

and

$$h_{sij}^{n+1} = h_{si}^{n+1} \tag{5.23}$$

for

$$\frac{P_j^{n+1} - P_i^{n+1}}{D_{ij}} - \rho_{sij}^{n+1} g_{ij} < 0 \tag{5.24}$$

$$h_{wij}^{n+1} = h_{wj}^{n+1} \tag{5.25}$$

for

$$\frac{P_j^{n+1} - P_i^{n+1}}{D_{ij}} - \rho_{wij}^{n+1} g_{ij} > 0 \tag{5.26}$$

$$h_{sij}^{n+1} = h_{sj}^{n+1} \tag{5.27}$$

for

$$\frac{P_j^{n+1} - P_i^{n+1}}{D_{ij}} - \rho_{sij}^{n+1} g_{ij} > 0 \tag{5.28}$$

### 5.1.3 Solutions to the discretized equations

Equation 5.7 and 5.8 can be written in residual forms as:

$$R_{2i-1} = V_i\left(M_{mi}^{n+1} - M_{mi}^{n}\right) + \sum_j A_{ij} F_{mij}^{n+1} \Delta t_{n+1} - \left(Q_{mi}^{n+1} \Delta t_{n+1}\right) = 0 \tag{5.29}$$

$$R_{2i} = V_i\left(M_{ei}^{n+1} - M_{ei}^{n}\right) + \sum_j A_{ij} F_{eij}^{n+1} \Delta t_{n+1} - \left(Q_{ei}^{n+1} \Delta t_{n+1}\right) = 0 \tag{5.30}$$

These equations are applied for each volume (block) element $V_i$, for all the blocks in the reservoir. The unknowns are the independent primary variables, pressure and temperature (or saturation) in the *i*th block at the end of (n + 1)th time step (that is, $P_i^{n+1}$, $T_i^{n+1}$ (or $S_i^{n+1}$)). The secondary parameters $\rho_w$, $\rho_s$, $U_w$, $U_s$, $\mu_w$, and $\mu_s$ are calculated from the primary variables by use of Steam Table data.

Equations 5.29 and 5.30 can be solved by Newton's iteration method (Appendix D) or more rigorous and fast converging iterative methods such as conjugate gradient, pre-conditioned conjugate gradient, Bi-Conjugate Gradient Stabilized etc (Moridis and Karsten, 1998;). To obtain the approximate solutions, the residuals are minimized or reduced to a preset convergence tolerance after a number of iterations otherwise the time step is reduced and a new iteration is started. Because of the large number of numerical computations involved, computer softwares have been developed to solve these equations. TOUGH is one of the widely used for geothermal applications and has been used for modelling Olkaria reservoir before. It will therefore form the basis of my numerical modelling study.

TOUGH (acronym for Transport Of Unsaturated Groundwater and Heat) was developed at Lawrence Berkeley Laboratory. It is a general-purpose software which can handle a wide variety of flow problems in the field of geothermal reservoir engineering, nuclear waste

isolation, environmental assessment and remediation, and unsaturated and saturated zone hydrology. It is a commercially available software and the details of its architecture is documented in Pruess et al., (1999).

### 5.2 Previous numerical simulation work in Olkaria

Several numerical simulation studies have been carried out in Olkaria from 1980 to 1993. These include Bodvarsson, 1980; Bodvarsson and Pruess, 1981; Bodvarsson et al., 1982; Bodvarsson et al., 1987, Bodvarsson and Pruess, 1987 and Bodvarsson, 1993. In the 1980 study, a simple vertical model was employed to study the effects of vertical permeability on the production capacity. The objective was to evaluate if fluid production should be limited to the steam zone or if the long-term reservoir performance would improve with combined production from both steam zone and underlying boiling reservoir. The main conclusion was that excessive production from the steam zone would cause localized boiling and pressure decline, thus limiting the productive life of the system and production from the underlying liquid dominated zone would lead to a counter flow of steam and liquid, resulting in optimal depletion of the reservoir.

The 1981 studies dealt with the effects of horizontal and vertical permeability and the importance of areal extent of the production area. The simulation neglected the steam zone and considered only a 550 m thick water dominated zone. The results showed that a long-term production of 45 MWe was possible at Olkaria.

In the 1984 work (Bodvarsson et. al., 1987), a detailed three-dimensional well by well model was developed for the Olkaria East field using the numerical code MULKOM. The model was calibrated against 6.5 years of production history and investigated various reservoir development schemes to study the effects of different well spacing on well deliverabilities, power production of 45 MWe and 105 MWe and the effects of injection on well performance and reservoir depletion. The results showed that an optimum density of 11 wells per square kilometre was the most suitable and that an area of 2 $km^2$ was appropriate for production of 45 MWe for 30 years but 9.5 $km^2$ would be required for production of 105 MWe. It also showed that injection would help in sustaining steam flow rates from wells.

In the 1987 model (Bodvarsson and Pruess, 1987), a detailed 3-Dimensional natural state model of the entire Olkaria geothermal field was developed. The results indicated that two major upflow zones, in Olkaria Northeast and West feed the geothermal system at a total recharge rate of 600 kg/s with the one in Olkaria West being 350 kg/s and the one in Northeast being 250 kg/s. The fluids from the two upflow zones mix near well OW-201 and discharge mostly southwards along the Ololbutot fault (260.5 kg/s) with a smaller discharge to the north along the Olkaria fracture zone (175.1 kg/s). Heat amounting to 400 $MW_t$ is lost from the system with most of it through steam fumaroles. The Olkaria East wells are fed by about 50 kg/s from the Northeast upflow zone and the average permeabilities of the major faults and fractures were estimated to be hundreds of milli-darcies.

In the 1993 model (Bodvarsson, 1993), the aim was to investigate the generating capacity of Olkaria Northeast geothermal reservoir, effects of reinjection both on individual wells and the entire reservoir performance and the degree of interference that might occur between the Olkaria Northeast and East reservoirs. The model was run in TOUGH and the results concluded that the Northeast reservoir was capable of 64 MWe and probably more power production for 30 years and that due to its relatively high permeabilities and temperatures compared to the East field, it would have modest pressure and flow rate declines, especially if

reinjection is employed. Interference between the East and Northeast reservoirs would also be minimal.

### 5.3 Present work

Between the year 1987 and 2000, 9 wells have been drilled and are producing in the East field, 5 wells drilled and tested in the West field, 3 in Central field, 1 in Southeast field, 25 in Northeast field and 3 in the Domes field. Most of the new wells drilled in the Northeast field were included in the model by Bodvarsson (1993). In the present work, just for study purposes, I will make use of the existing 3-D natural state numerical grid developed by Bodvarsson and Pruess (1987), and attempt to recalibrate it with the data from all the new wells that were not drilled by then. I will then try to match the production history data with the updated model.

#### 5.3.1 An update to the existing 3-D natural state model of the entire Olkaria system

The objectives of natural state modelling is to help in validating the conceptual model and to quantify the natural mass and heat flow within the hydrothermal system as well as to provide the initial thermodynamic conditions for exploitation modelling. It involves setting up of a model with an approximate permeability structure based on the conceptual model. A numerical grid of the system is used during the computer simulation runs to match the observed (or measured) thermodynamic field conditions such as temperature and pressure distributions. The simulation of the model should be carried out over a long period of time approximating to the development of the geothermal system over geologic time. Iterations are performed by adjusting parameters such as permeability distribution, mass and heat flow into and out of the system and boundary conditions on lateral as well as top and bottom boundaries until the calculated results match the observed data.

Figure 22 shows the grid used by Bodvarsson and Pruess (1987), to model 3-D natural state of the entire Olkaria geothermal system and which is also used in this work. It covers an area of 110 $km^2$ and is partitioned into 128 blocks. In the vertical dimension, the model assumes an impermeable caprock of 700 m thickness beneath which underlies a permeable reservoir of 850 m total thickness that is further partitioned into three layers so as to give a total of 384 grid blocks. When this model was developed, the existing wells drilled by then were between 900 m to 1600 m depth (1100 m a.s.l. to 400 m a.s.l.) and so this covered them pretty well. However, wells drilled later on have been deeper and have intercepted deeper aquifers.

Initial and Boundary conditions

In order to obtain a solution to the governing equations, hydrodynamic and thermal boundary conditions must be specified. These conditions can be deduced from a thorough examination of hydrologic and thermodynamic data and from data obtained by geologic, geophysical and geochemical investigations.

The major hydrogeologic features of the Olkaria system include Olkaria fracture, Olkaria fault, Suswa fault, Gorge farm fault and Ololbutot fault (Figure 3). In the model of Bodvarsson and Pruess (1987), the hydrothermal system is recharged by two major upflow zones located near the western and eastern ends of the Olkaria fault. The fluid from the upflow zones move along the Olkaria fault as they undergo conductive cooling as well as cooling by steam loss to the surface and converge in Olkaria Central zone. Major outflow with substantial steam loss and cooling occurs towards the south along the Ololbutot fault and

towards the north along Olkaria fracture zone. The reservoir is assumed to be bounded in the east and west by no flow boundaries (very low permeability) and in the north and south by constant pressure boundaries of 45 bars at 1075 m a.s.l. and 28 bars at 1075 m a.s.l., respectively. The main model parameters are summarized in Table 1.

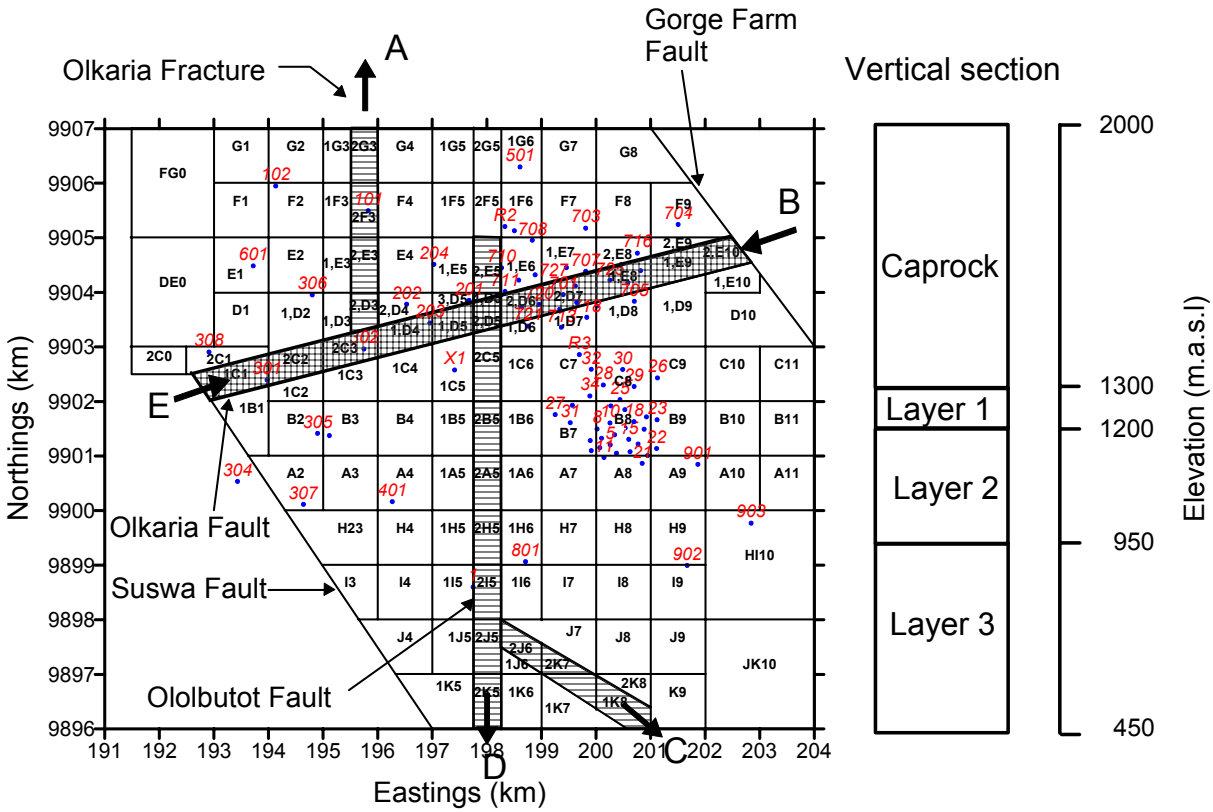


Figure 22: Grid used in the current 3-D numerical model

Model update

Appendix B1 shows graphs detailing pressures and temperatures calculated by the recalibrated model (this work) and those from the 1987 model in relation to the estimated formation temperatures. We can observe that the 1987 model matches the data pretty well except for the wells within the low temperature zone in Olkaria Central field. To obtain a reasonable match for these wells, I reduced the upflow rate from the west and permeability in the Olkaria fault and Olkaria fracture zones and increased the permeability of the East field thus allowing more fluid to divert south through the present production field instead of moving to the Central field. Other minor adjustments in permeabilities on other elements were also necessary. Table 2 gives a summary of the main adjustments done to recalibrate the old model.

### 5.3.2 Production history matching

After performing a successful natural state simulation that matches relatively well the observed thermodynamic conditions, the model is now used as an initial state for the exploitation modelling. The main objective here is to have a model that will be able to simulate the observed data. The data to be matched are usually the production rate history and enthalpies as well as pressure drawdown. Parameters that are adjusted include porosities, permeabilities and flow rates (production indices). Other rock properties are assumed constant.

From the reservoir data, it is observed that the fluid in-place in Olkaria East field is a mixture of liquid water and steam. We therefore have to employ Darcy's equation for two-phase flow as discussed earlier. This implies that relative permeabilities have to be introduced. In the previous simulation by Bodvarsson and Pruess (1984), relative permeabilities were assumed to be linear functions of saturation as indicated in Table 1 and the same will be employed in this work.

Wells in Olkaria have multiple feed points. The best way to model this would be to allow fluid to flow into the well by assigning a productivity index and fluid mobility and pressure in the feed zone. There are very few data regarding productivity indices of Olkaria wells so to do this would require parameter adjustment during simulation. Due to limited time available, this could not be done for this study. The production rates from different layers were therefore specified and varied in different proportions of the total rate so as to be capable of maintaining reasonable enthalpies and pressures (forced flow).

In this work, production was assumed to come from one well each located in block A8, B7, B8, B9, and C9 (Figure 22) and each producing out of 3 feed zones, one in each model layer. Injection history described in the next chapter was also implemented. Percentage of flow rates extracted from layers in the producing blocks are shown in Table 3.

Best model

Appendix B2 has the graphs of production history matching. The graphs give relatively good match to production data. Cases where there exists a drastic decline in enthalpy as in element B8 could not be avoided due to the fact that cold water is injected into the same element that is being produced from. However, the low enthalpies calculated due to injection still agree quite well with the measured in the wells that were affected by cold injection such as well OW-16 and OW-19 (Appendix C). The high extreme in the enthalpy happening in 1985 to 1986 is due to over production that occurred when turbine number 3 was added to the system. Thereafter, a drastic decline in reservoir pressure followed as the reservoir was adjusting to the high load. The high extreme starting in 1998 is due to connection of the deepened well OW-5 which now produces from deeper aquifers that are not included in the grid.

Pressures obtained also agree quite well with the measured data (Chapter 6 and Appendix A). For example the calculated pressure data for elements B7 and B8 (where most production has taken place) are quite comparable with the measured data. The calculated pressure in layer 3 of element B 8 is 58 bars in July 2000 and is equal to with the measured pressure at 1300 m in well OW-8 in October 2001 (58 bars).

## 6.0 OLKARIA EAST FIELD RESPONSE TO PRODUCTION

### 6.1 Production history

Olkaria East geothermal field has been under commercial exploitation since July 1981 when the first 15 MWe generation unit was commissioned. Additional two 15 MWe units were put on line in December 1982 and April 1985. Since then the field has been generating 45 MWe of electricity. Initially, 23 wells (OW-2, 4, 5, 6, 7, 8, 10, 11, 12, 13, 14, 15, 16, 17, 18, 19, 20, 21, 22, 23, 24, 25, and 26) supplied steam for the three units but as time progressed, some wells declined in output and had to be isolated. New make-up wells were drilled to restore the generating capacity, which had declined to 31 MWe by 1994 (Mwangi, 2000). Four make-up wells (OW-27, 28, 29 and 30) were connected in 1995 and two more (31 and 33) in 1996. Figure 23 shows the field production history, the values of mass rates are yearly averages and the enthalpies are weighted averages. Mass production during well testing has been neglected.

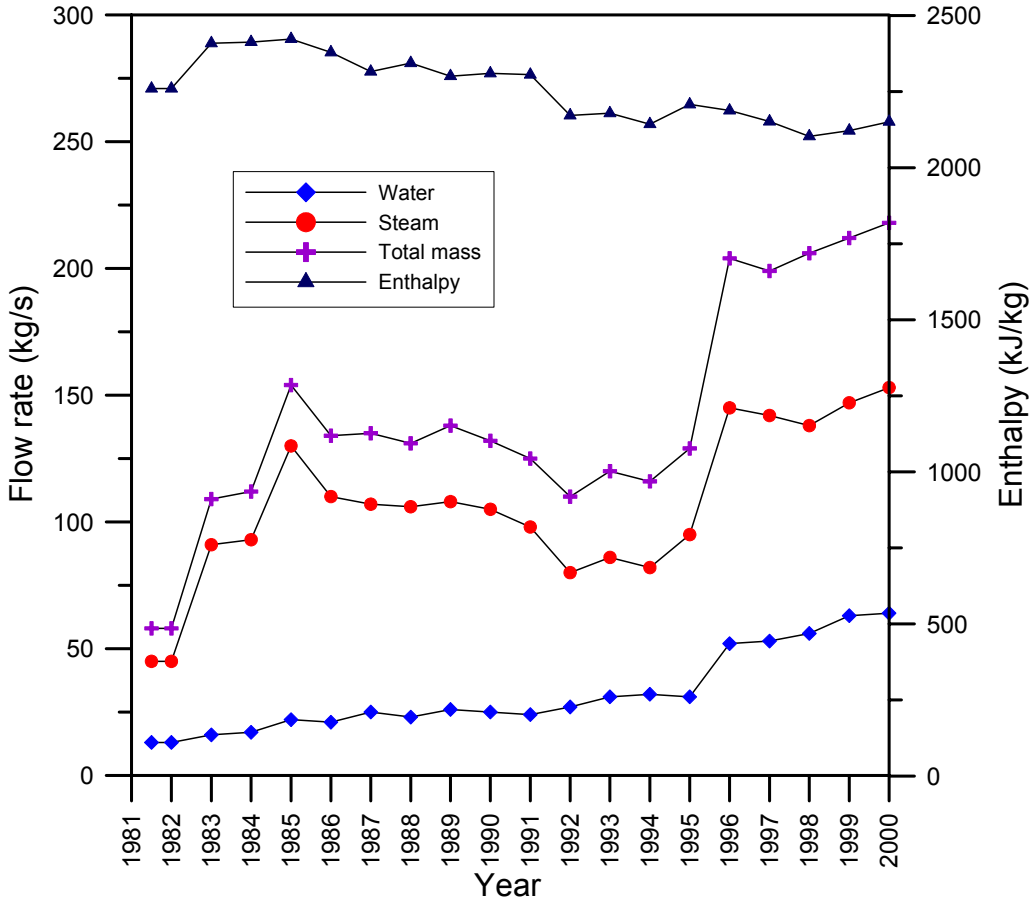


Figure 23: Production history

### 6.2 Re-injection/Injection history

Well OW-3

A tracer and injection test experiment was done in well OW-3 from April to September 1993 (Ambusso, 1994). Cold fresh water at 18°C from Lake Naivasha was injected in this well continuously for 172 days at an average rate of 100 t/hr (27.78 kg/s). 125 kg of Sodium

fluorescein dye was introduced as a slug after 45 days of injection. Production and chemical changes were observed in wells OW-2, 4, 7, 8, 10 and 11. Chloride decline occurred in wells OW-2 and 4 during the injection period and tracer returns were observed in wells OW-4, 2 and 7 with OW-4 registering the highest recovered mass of about 38 %, well OW-2, 0.1 % and well OW-7, 0.07 % (Ofwona, 1996). Hot re-injection of separated brine from wells OW-27, 31 and 33 has been going on in this well (OW-3) since May 1995 at approximately 13 t/hr (3.6 kg/s).

Well OW-12

Tracer/injection test experiment was done in this well from 12.7.96 to 1.9.97. Cold fresh water from Lake Naivasha was injected continuously at an average rate of 100 t/hr (27.78 kg/s) for 416 days. 500 kg of Sodium fluorescein tracer was introduced as a slug after 20 days of injection. Wells around OW-12 were monitored for chemical and output changes. High tracer returns were obtained from wells OW-15, OW-16 and OW-19. The same wells also experienced drastic decline in chloride concentration and enthalpies with big increase in water flow.

Well OW-R3

Tracer/injection test experiment was done in this well from May 1995 to July 1.9.96. Cold fresh water from Lake Naivasha was injected continuously at an average rate of 100 t/hr (27.78 kg/s) over the duration of the experiment. 500 kg of Sodium fluorescein tracer was introduced as a slug after 27 days of injection. Wells close to OW-R3 were monitored for chemical and output changes. Very little tracer returns were obtained from wells OW-25, OW-29 and OW-30 and none from the closest wells OW-32 and 34. There was also very little or no change at all in the fluid chemistry as well as production output from the neighbouring wells.

Other tracer and injection experiments have been done in wells OW-R2 and OW-704 (Karingithi, 1995) in Olkaria Northeast field.

### 6.3 Changes due to exploitation

Appendix C shows production history of some selected wells in the producing field and Figures 24 to 27 show changes in reservoir chloride and enthalpies. The field response can be summarized as increased boiling in the centrally located wells giving rise to dry steam and high chloride concentration and induced recharge in the wells located at the periphery resulting in modest decline in chloride concentration and enthalpies. The recharging of these wells is also supported by the slow pressure depletion rates depicted in their downhole data (Figure 21 and Appendix A).

### 6.4 Pressure drawdown

Due to high demand of steam, no wells within the production field were available specifically for monitoring pressure response due to production. Only well OW-3 and well OW-9 were considered unsuitable for production and could have been used for this purpose but well OW-3 was used for field injection experiments and well OW-9 had internal flow and was also later on plugged due to its close proximity to the project offices. However, well OW-8 offered some good pressure decline history. This well was first drilled to 1080 m in November 1978 and intercepted permeable zones at 600 - 700 m and 900 - 1080 m depth. It was then

deepened to 1600 m in 1983 intercepting more permeable zones at 1300 – 1400 m. It remained shut-in from 1979 to 1983 and again to September 1985 when it was connected to the steam supply system. Production from this well continued until October 2000 when it was shut-in. Pressure and temperature measurements were done in October 2001 and the pressure data can be seen in Figure 28.

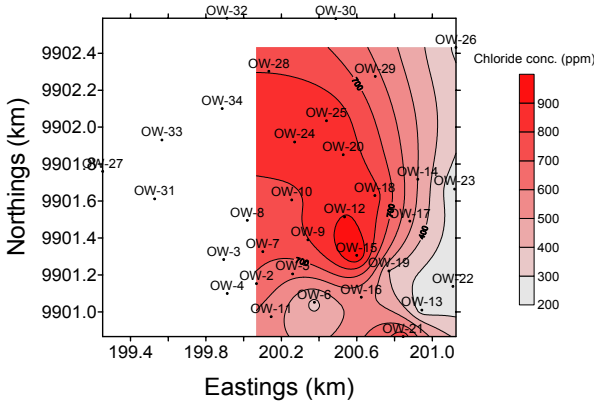


Figure 24: Chloride concentrations in 1986

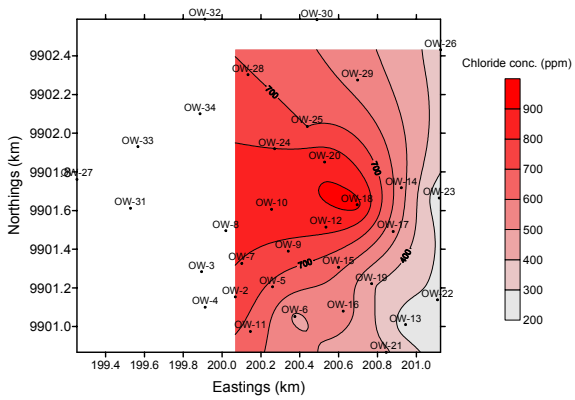


Figure 26: Chloride concentrations in 2000

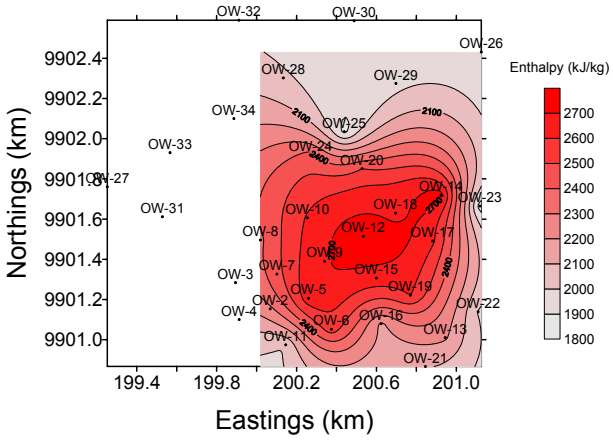


Figure 25**:** Enthalpies in 1986

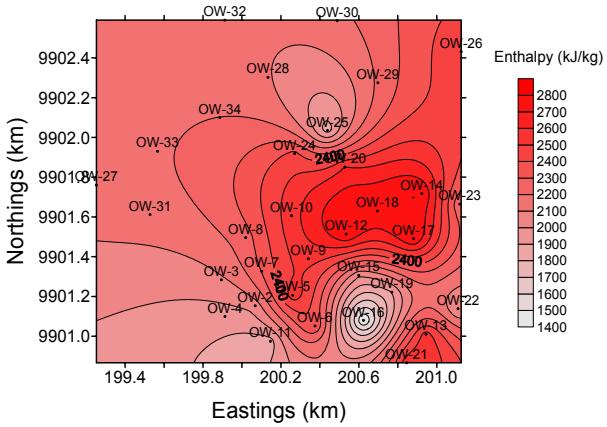


Figure 27**:** Enthalpies in 2000

Another well that could offer a good indication of pressure decline history is well OW-5. This well was drilled to 910 m in 1978 and produced from 1981 to 1996 during which its total mass flow declined from 9 kg/s to 2.6 kg/s. It was then deepened to 2200 m in November 1997. Its pressure data is shown in Figure 29.

Well OW-3 (Figure 30) was never connected to the production system and has been used for re-injection experiments. It was shut in for a long period of time before 1992 and can offer some good pressure drawdown data up to 1992. Other producing wells have been logged at different times when opportunity arises during wellhead equipment servicing and unit shut downs during maintenance (See Appendix A).

Well OW-21 (Figure 31) represents one of the wells at the periphery that seems to have had pressure decline only up to 1997 and thereafter has been stable suggesting a good pressure support boundary. However, the measurement is done only when the well is temporarily isolated from the system and has not been shut long enough to attain stable pressure. Its data and the rest from the other wells are therefore not included in the analysis in the next section.

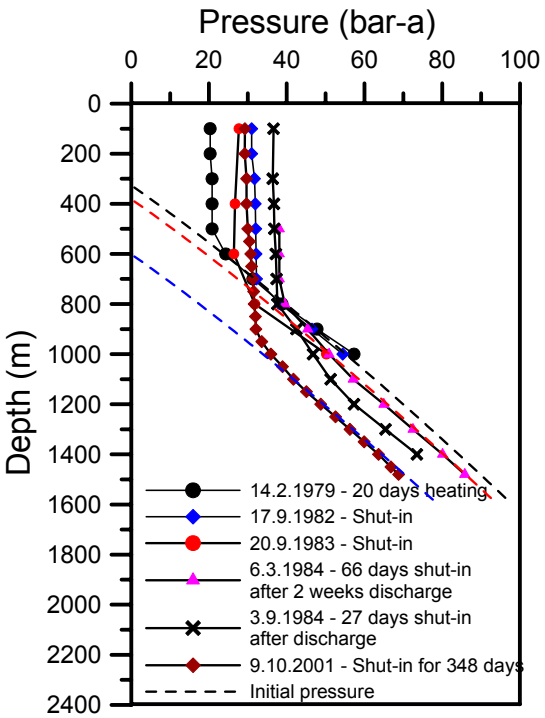


Figure 28: Pressure decline in well OW-8

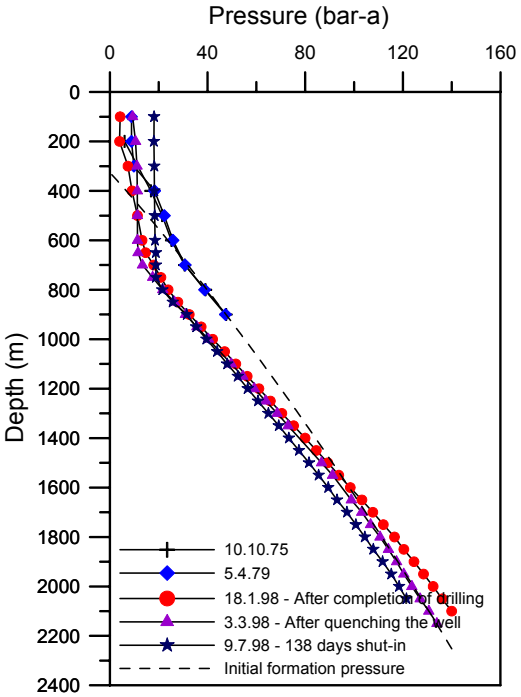


Figure 29: Pressures in well OW-5

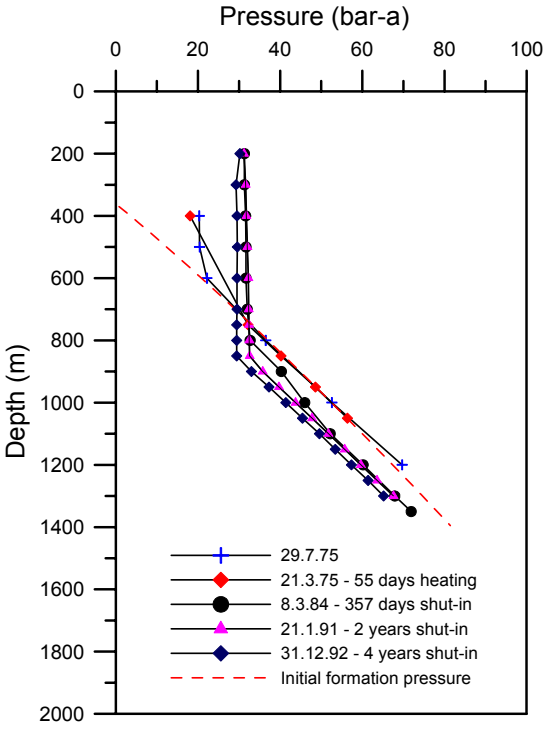


Figure 30: Pressure decline in well OW-3

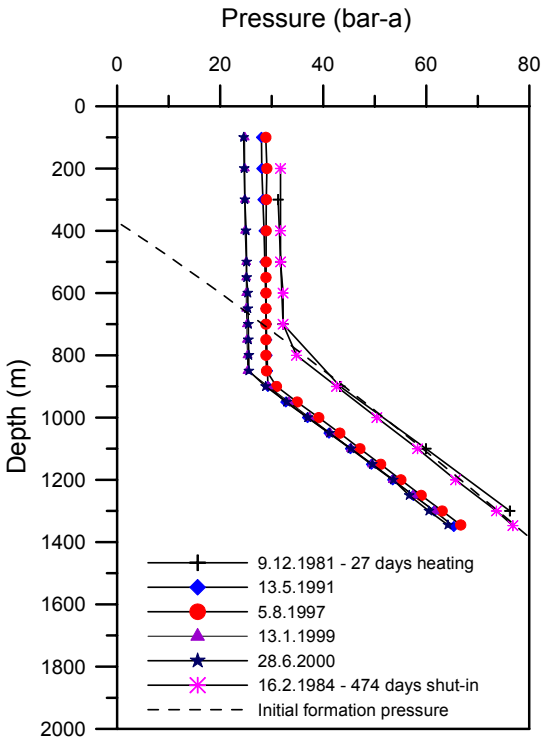


Figure 31: Pressure decline in well OW-21

From the pressure logs, it is observed that the steam zone is expanding down into the liquid reservoir as exploitation time increases resulting in lowering of the boiling level. This decline in boiling level with time can be quantified to represent drawdown. Data for wells OW-8, 5

and 3, which I think, gives a good representation of field drawdown have been combined and plotted in Figure 32 below together with the net mass production rate.

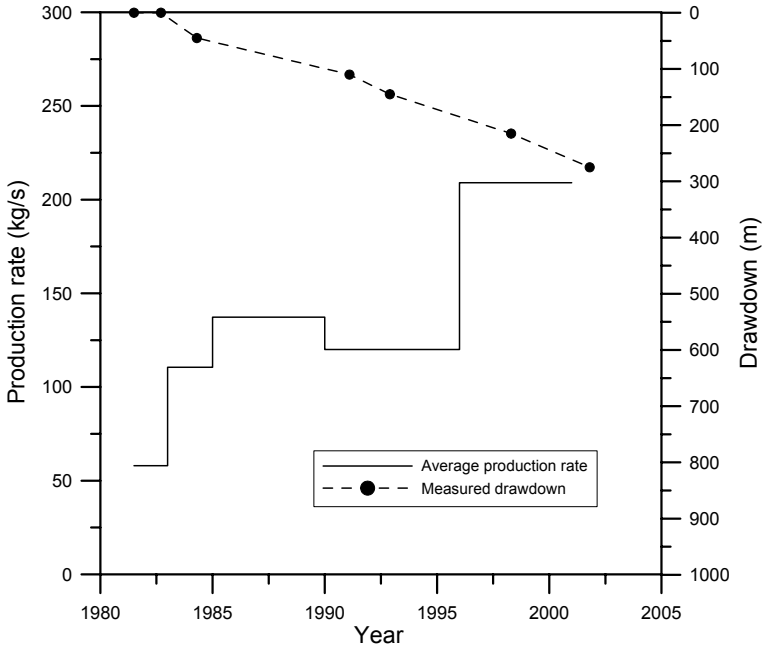


Figure 32**:** Average production rate and drawdown history

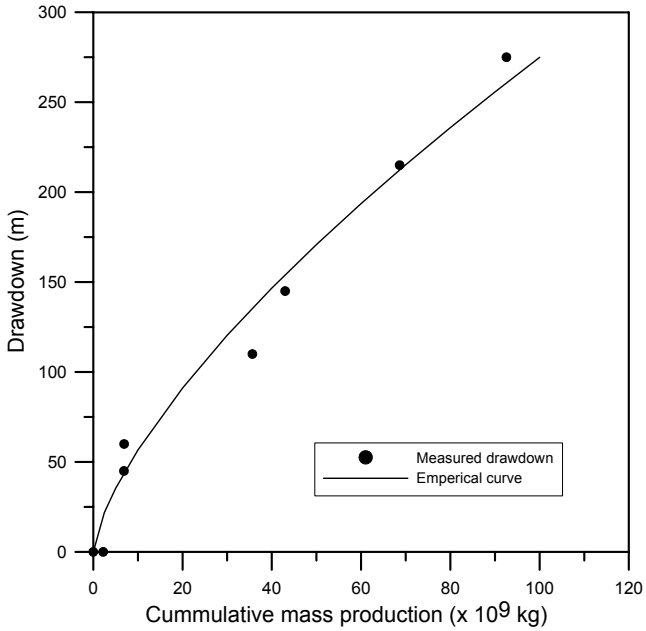


Figure 33: Drawdown with cumulative production

### 6.5 Analysis of pressure drawdown

We now apply Equations from section 4 to analyse the available drawdown data. It is justified to consider this pressure response as the same as that in a free surface reservoir as evident by the stability of steam zone pressure. Figure 33 shows a graph of drawdown $\Delta h$ (m) with cumulative mass production $M$ (kg).

An empirical curve fit through the data points is given by

$$\Delta h = 7.82x10^{-6} M^{0.686} \qquad (7.1)$$

This empirical match may not apply well when there is a significant change in production. However, the graph shows that the relation between drawdown and cumulative mass production is not linear and so Equation 4.22 cannot be applied. The rate of drawdown decreases with increase in cumulative mass production indicating recharge. For this reason, it is most appropriate to analyse the drawdown data with a water recharge model.

Applying unit response function analysis of section 4.2 to the drawdown and production data we obtain the following function:

$$F(t) = \frac{1}{0.58}\left[1 - e^{-t/7.7}\right] \qquad (7.2)$$

where $t$ is in years and $F(t)$ in meters.

Figure 34 below shows how this unit response function fits the drawdown data and what future predictions can be expected for different production scenarios beginning the year 2010. The match is relatively good except for the two middle points that were measured in well OW-3. These data points could be lower than expected due to the fact that well OW-3 had been used for several injection experiments and the formation pressure around it could somehow been modified.

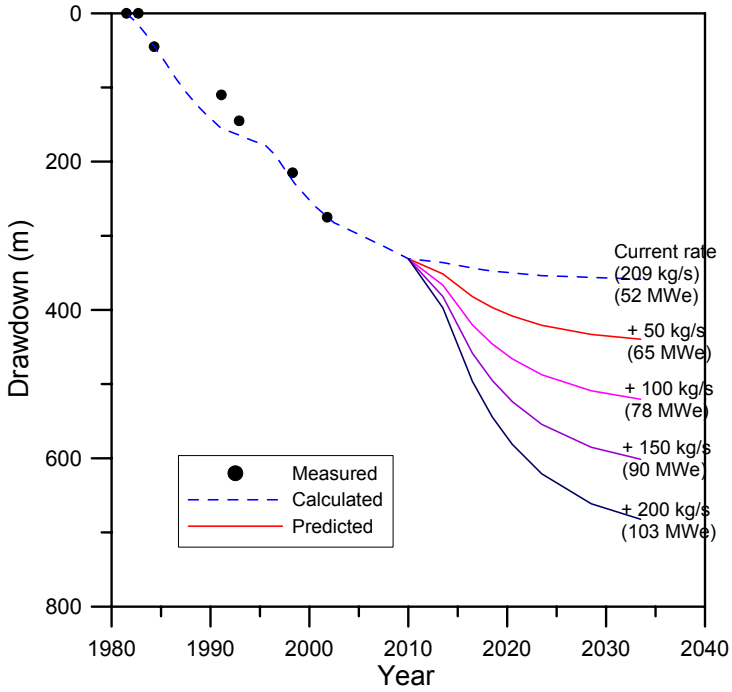


Figure 34: Unit response function fitted to drawdown data

From equation 7.2, we have the reservoir parameters as $\alpha_r$ = 0.58 kg/s.m and $\xi$ = 7.7 years. Assuming that the reservoir fluid density = 730 kg/m$^3$ (which corresponds to the density of saturated water at 290°C), then $S_m$ = 20000 kg/Pa and $\alpha_r$ = 80 kg/MPa.s. From Equation 4.10, if we use a production area of 4 km$^2$, then the overall effective formation porosity is calculated to be 0.05. If we compare the recharge coefficient and mass storage coefficient with those calculated for the Wairakei field (Grant et al., 1982), we find the Olkaria parameters to be almost ten (10) times lower. This could possibly be due to the lower formation permeabilities in Olkaria.

## 7.0 DISCUSSIONS AND CONCLUSIONS

A simple first order differential equation has proved quite satisfactory in modelling drawdown of the deep, water dominated reservoir in the Olkaria East field due to long time exploitation. The porosity of 5% obtained assuming an area of 4 $km^2$ and unconfined (free surface) reservoir, compares quite well with that obtained by the numerical simulation (6%). This implies that effective rock porosity in the present production field is within this range. Pressure data analysis has shown that Olkaria East reservoir fits well when an open system model is applied and this is supported by the observations so far made from the behaviour of producing wells in the periphery of the East field where some wells like OW-16, OW-19, OW-22 and OW-23 have continued to discharge increasing water output and have had quite stable total mass flow, indicating connection with good pressure support from recharging aquifers. However, due to the low bulk formation permeability within the field, the recharge rates are low and to some extent, has very little effect on the centrally located wells, which have continued to show more boiling effects.

Conceptually speaking, Olkaria reservoir seems to possess discrete convective cells that are possibly associated with zones of magma intrusions providing local heating. These zones manifest themselves as hot spots surrounded by cold downflow zones implying that there is good recharge to maintain the convective processes. To maintain cold temperatures in the vicinity of a huge thermal gradient, the cooled water movement in the downflow zones have to be very rapid implying that the permeability in these zones are relatively high and could be related to young faults.

From the updated 3-D natural state model, about 320 kg/s of 1290 kJ/kg of water recharge the eastern part of the geothermal system and 245 kg/s recharge the western part. Steam loss amounting to 128 kg/s equivalent to 358 MWt is lost mainly along the Ololbutot fault zone. This steam loss is what cools this zone to make it have uncharacteristic cold zone between hot zones in the east and west. A part of the water (134.4 kg/s) flows to the north and a part (304.3 kg/s/) flows to the south. Permeability values within the major structures in the geothermal system can be approximated to be 500 milli-darcy in the Ololbutot fault zone, 250 milli-darcy in the Olkaria fracture zone and 230 milli-darcy in the Olkaria fault zone.

Values obtained from lumped convective model of the Northeast field agree reasonably well with those from the distributed (numerical) models and indicates that lumped models can be used as a first approximation or as a check to the results of distributed parameter models.

In summary, this study has provided the following:

1. That Olkaria East reservoir is an open system with a good pressure support and can be approximated by a simple first order differential equation whereby the recharge can be modelled as a direct proportion of pressure drawdown. In the natural state, the hydrology is controlled by convection.

2. Three upflow zones seem to exist in the Eastern Olkaria geothermal system with two in the Northeast field and one in the East field.

3. In the natural state, the Eastern system can be simulated by a recharge of 320 kg/s of 1290 kJ/kg water and the Western system by 245 kg/s of 1200 kJ/kg water. Steam amounting to 128 kg/s is lost along the Ololbutot fault and Olkaria Central zones resulting in cold temperatures deep down in the wells.

4. Pressure drawdown in the Olkaria East field is localised within the producing zones. The deep reservoir appears to be still intact and can be exploited further to boost up the generating capacity of the field.

5. A reasonable match to the history data has been achieved from a coarse grid by lumping together many wells within a specified grid block and producing the sum out of one well. With this match, it is predicted that mean enthalpies will fall to about 1700 kJ/kg – 1800 kJ/kg in the next 20 years if production is maintained at the same rate. However, a better prediction would be obtained from an extended grid producing from deeper aquifers.

6. Pressure drawdown will eventually stabilize as the fluid recharge rates equalize the production rates.

Recommendations for further work

Because of limited time, it was not possible to investigate the effect of production from deeper aquifers than the specified in the vertical grid. It is therefore recommended that the numerical grid be expanded to include the possibility of producing from deeper aquifers. With the expanded grid, performance predictions should then be done to re-asses the power potential of the Olkaria East system.

## Nomenclature

Variables

| | |
|---|---|
| C | Specific heat capacity, kJ/kg |
| $D_{ij}$ | Interblock distance ($d_i + d_j$), m |
| $t$ | Time, s |
| $P$ | Pressure, $N/m^2$, Bar, Pa |
| $\rho$ | Density, $kg/m^3$ |
| $S$ | Saturation |
| $S_m$ | Mass storage coefficient, kg/Pa |
| $T$ | Temperature,°C |
| $k$ | Permeability, $m^2$ |
| $K$ | Hydraulic conductivity, m/s |
| $k$ | Absolute permeability tensor, darcy |
| $k_{rw}$ | Relative permeability of water phase |
| $k_{rs}$ | Relative permeability of steam phase |
| $K_{ij}$ | Weighted interface permeability |
| $\phi$ | Effective porosity of the formation |
| $q$ | Discharge rate or volume flux, $m^3/s$ |
| $Q$ | Source/sink term |
| $z$ | Depth, m |
| $h$ | Enthalpy, kJ/kg |
| $u$ | Internal energy, kJ/kg |
| $U$ | Mass flux vector, $kg/s/m^2$ |
| $Aij$ | Interface area between ith block and jth block |
| $Vi$ | Volume of the ith block, $m^3$ |
| $F_{mij}^{n+1}$ | Mass flux from block i to block j evaluated at the end of the (n + 1)th time step |
| $F_{eij}^{n+1}$ | Energy flux from block i to block j evaluated at the end of the (n + 1)th time step |
| $Q_{mi}^{n+1}$ | Mass production from block i evaluated at the end of the (n + 1)th time step |
| $Q_{ei}^{n+1}$ | Energy production from block i to block j evaluated at the end of (n + 1)th time step |
| $M_{mi}^{n+1}$ | = Mass accumulation term |
| $M_{ei}^{n+1}$ | Energy accumulation term |
| $l$ | Horizontal distance, m |
| $v$ | Velocity, m/s |
| $W$ | Mass flow, kg/s |
| $M$ | Mass (kg) |
| $\alpha_r$ | Recharge coefficient |
| $\beta$ | Volume coefficient of thermal expansion |
| $\lambda$ | Rock matrix thermal conductivity, J/m°Cs |
| $\varepsilon$ | Energy dissipation factor |
| $\xi$ | Time constant, years |
| Ra | Raleigh number |
| $\Phi$ | Pressure potential |
| $\nu$ | Kinematic viscosity, $m^2/s$ |
| $\mu$ | Dynamic viscosity, Pa.s |

Subscripts

| | |
|---|---|
| w | water |
| s | steam |
| r | rock |
| E | energy |
| M | mass |
| cap | capillarity |
| sat | saturation |

## References


Ambusso, W.J., 1994: Results of injection and tracer tests in Olkaria-East geothermal field. *Proceedings of the 19th Workshop on Geothermal Reservoir Engineering, Stanford University, California*, 155-160.

Arason, P., and Björnsson, G., 1994: *ICEBOX*. 2nd edition, Orkustofnun, Reykjavík, 38 pp.

Bear, J., 1979: *Hydraulics of groundwater*. McGraw-Hill Inc.

Bodvarsson, G. S., 1980: *Olkaria geothermal field – Preliminary studies of the reservoir behaviour under exploitation*. Kenya Electricity Generating Co. Ltd., internal report.

Bodvarsson, G. S., and Pruess K., 1981: *Olkaria geothermal field – Numerical studies of the generating capacity of the reservoir.* Kenya Electricity Generating Co. Ltd., internal report.

Bodvarsson, G. S., and Pruess K., 1984: *History match and performance predictions for the Olkaria geothermal field*. Kenya Electricity Generating Co. Ltd., internal report.

Bodvarsson, G. S., and Pruess K., 1987: *Numerical simulation studies of the Olkaria geothermal field.* Kenya Electricity Generating Co. Ltd., internal report.

Bodvarsson, G. S., Pruess K., Haukwa C., and Ojiambo S., B., 1990: Evaluation of reservoir model predictions for the Olkaria East geothermal field, Kenya. *Geothermics, 19-5*.

Bodvarson, G.S., Pruess K., Stefánson V., Björnsson S., Ojiambo S.B., 1987: East Olkaria Geothermal field, Kenya B History match with production and pressure decline data. *J. Geophys. Res., 92-B1*, 521-539.

Brown P. R. L., 1984: Subsurface stratigraphy and alteration of the Eastern section of the Olkaria geothermal field, Kenya. *Proceedings of the 6th New Zealand Geothermal Workshop, Geothermal Institute, Auckland,* 33-42.

Clarke, M.C.G., Woodhall, D.G., Allen, D., and Darling G., 1990: *Geological, volcanological and hydrogeological controls on the occurrence of geothermal activity in the area surrounding Lake Naivasha, Kenya, with coloured 1:100 000 geological maps.* Ministry of Energy, Nairobi, 138 pp.

Eliasson, J., 1973: *Convective groundwater flow*. Institute of Hydrodynamics and Hydraulic Engineering, Technical University of Denmark.

Eliasson, J., Kjaran P. S., and Gunnarsson G., 1980: Two phase flow in porous media and the concept of relative permeabilities. *Proceedings of the 6th Workshop on Geothermal Reservoir Engineering, Stanford University, Stanford, California,* 288-296.

Glover, R. I., 1972: *Chemical characteristics of water and steam discharges in the rift valley.* U. N. geothermal resources exploration project report.

Grant, M.A., Donaldson, I.G., and Bixley, P.F., 1982: *Geothermal reservoir engineering*. Academic Press, New York, 369 pp.

Gudmundsson J. S., and Thorhallsson S., 1986: The Svartsengi reservoir in Iceland. *Geothermics, 15-1,* 3-15.

Karingithi, C. W., 1995: Results of injection and tracer tests in Olkaria North East Field in Kenya. *Geothermal Resources Council, Trans., 19.*

Kenya Power Company Ltd, 1981: *Recommendations for further geothermal exploration at Olkaria*. KPC internal report.

Kjaran, S. P., and Eliasson, J., 1983: *Geothermal reservoir engineering lecture notes*. UNU Geothermal Training Programme, Iceland, report 2, 250 pp.

Kjaran, S.P., Halldórsson, G.K., Thórhallsson, S., and Elíasson, J., 1979: Reservoir engineering aspects of Svartsengi geothermal area. *Geothermal Resources Council, Trans., 3,* 337-339.

Leach, T.M., and Muchemi G.G., 1987: Geology and hydrothermal alteration of the North and West exploration wells in the Olkaria geothermal field, Kenya. *Proceedings of the 9th New Zealand Geothermal Workshop, Geothermal Institute, Auckland,* 187-192.

Moridis G. J., and Pruess K., 1998: T2SOLV: An enhanced package of solvers for the Tough2 family of reservoir simulation codes. *Geothermics, 27-4,* 415-444.

Muchemi, G. G., 1999: *Conceptualized Model of the Olkaria Geothermal field.* Kenya Electricity Generating Company Ltd., internal report.

Mwangi, M.N., 2000: Country update report for Kenya 1995-1999. *Proceedings of the World Geothermal Congress 2000, Kyoto- Tohoku, Japan,* 327-333.

Naylor, W.I., 1972: *Geology of the Eburru and Olkaria prospects.* U.N. Geothermal Exploration Project, report.

Odongo, M.E.O., 1993: A geological review of Olkaria geothermal reservoir based on structure. *Proceedings of the 15th New Zealand Geothermal Workshop, Geothermal Institute, Auckland,* 169-173.

Ofwona, C.O., 1996: Analysis of injection and tracer tests data from the Olkaria-East geothermal field, Kenya. Report 10 in: *Geothermal Training in Iceland 1996*. UNU G.T.P., Iceland, 197-218.

Ofwona, C.O., 2000: Recent reservoir studies of the Olkaria geothermal field, Kenya. *Proceedings of the World Geothermal Congress 2000, Kyoto- Tohoku, Japan,* 2767-2772.

Ogoso-Odongo, M. E., 1986: Geology of the Olkaria geothermal field. *Geothermics, 15-6, 741-748.*

Pruess, K., Oldenburg, C., and Moridis, G., 1999: *TOUGH2 user=s guide version 2.0,* Lawrence Berkeley National Laboratory, 197 pp.

Simiyu, S. M., and Malin, P. E., 2000: A "volcano seismic" approach to geothermal exploration and reservoir monitoring: Olkaria, Kenya and Casa Diablo, USA. *Proceedings of the World Geothermal Congress 2000, Kyoto- Tohoku, Japan,* 1759-1763.

Svanbjörnsson, A., Matthiasson, J., Frimannsson, H., Arnorsson, S., Björnsson, S., Stefansson, V., and Saemundsson, K., 1983: Overview of geothermal development at Olkaria in Kenya. *Proceedings of the 9th Workshop on Geothermal Reservoir Engineering, Stanford University, Stanford California*, 65-72.

Wambugu, J. M., 1996: Assessment of Olkaria-Northeast geothermal reservoir, Kenya based on well discharge chemistry. Report 20 in: *Geothermal Training in Iceland 1996.* UNU Geothermal Training Programme, Iceland, 481-509.

White, S. P., and Kissling, W. M., 1992: Modelling geothermal Reservoirs – recent developments. *Proceedings of the 14th New Zealand Geothermal Workshop, Geothermal Institute, Auckland,* 99-104.

Yang, Z., Bullivant, D. P., Zyvoloski, G. A., and O´Sullivan, M. J., 1991: Numerical experiments with the simulation of natural states of geothermal reservoirs. *Proceedings of the 13th New Zealand Geothermal Workshop, Geothermal Institute, Auckland,* 161-166.

## Tables

Table 1: Parameters for the natural state model (Bodvarsson and Pruess, 1987)

| **Rock properties** | **Fluid properties** | **Permeabilities, $m^2$ (x $10^{-15}$)** | | | **Flow rates (kg/s) and Enthalpies (kJ/kg)** | | | | | | |
|---|---|---|---|---|---|---|---|---|---|---|---|
| Density: 2650 $kg/m^3$ | Approximated as pure water and all properties based on steam tables | | Vertical | Horizontal | | A | B | C | D | E | Steam |
| Heat capacity: 1000 J/kg°C | | Olkaria Fault | 240 | 240 x 240 | Inflow | | 250 | | | 350 | |
| Thermal conductivity: 2.0 W/m °C | | Olkaria Fracture | 500 | 500 x 500 | Outflow | 175.2 | | 107.6 | 152.9 | | 126 |
| Relative Permeabilities: | | | | | | | | | | | |
| $k_{rs}(S_s) = (S_s - 0.05)/0.55$ | | Ololbutot Fault | 500 | 500 x 500 | Enthalpy | | 1290 | | | 1090 | 2800 |
| $k_{rw}(S_w) = (S_w - 0.40)/0.60$ | | | | | Element | | 2E 9 & 2E 10 | | | 311 C | |

Table 2: Parameters for the natural state model (this work)

| **Rock properties** | **Fluid properties** | **Permeabilities, $m^2$ (x $10^{-15}$)** | | | **Flow rates (kg/s) and Enthalpies (kJ/kg)** | | | | | | |
|---|---|---|---|---|---|---|---|---|---|---|---|
| Density: 2650 $kg/m^3$ | Approximated as pure water and all properties based on steam tables | | Vertical | Horizontal | | A | B | C | D | E | Steam |
| Heat capacity: 1000 J/kg °C | | Olkaria Fault | 230 | 230 x 230 | Inflow | | 320 | | | 245 | |
| Thermal conductivity: 2.0 W/m°C | | Olkaria Fracture | 250 | 250 x 250 | Outflow | 134.4 | | 137.8 | 166.5 | | 128 |
| Relative Permeabilities: | | | | | | | | | | | |
| $k_{rs}(S_s) = (S_s - 0.05)/0.55$ | | Ololbutot Fault | 500 | 500 x 500 | Enthalpy | | 1290 | | | 1200 | 2800 |
| $k_{rw}(S_w) = (S_w - 0.40)/0.60$ | | | | | Element | | 2E 8, 1E 9, 2D 6 & C 8 | | | 311 C | |

Table 3: Parameters for the exploitation model (best model)

| **Block** | **Flow rates (%)** | | | **Porosity** |
|---|---|---|---|---|
| | **Layer 1** | **Layer 2** | **Layer 3** | |
| A 8 | 5 | 40 | 55 | 0.06 |
| B 7 | 30 | 30 | 40 | 0.06 |
| B 8 | 35 | 35 | 30 | 0.06 |
| B 9 | 20 | 30 | 50 | 0.06 |
| C 8 | 20 | 30 | 50 | 0.06 |
| C 9 | 5 | 25 | 70 | 0.06 |
| Average permeability in the well field: $15 \times 10^{-15}$ $m^2$ | | | | |

# APPENDIX A

## Formation temperature and pressures in the Olkaria reservoir

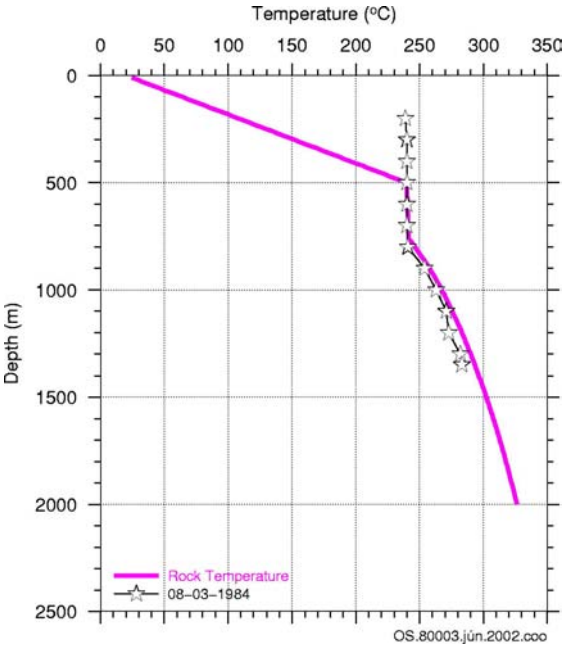


Figure A 1: Well OW-3 temperature

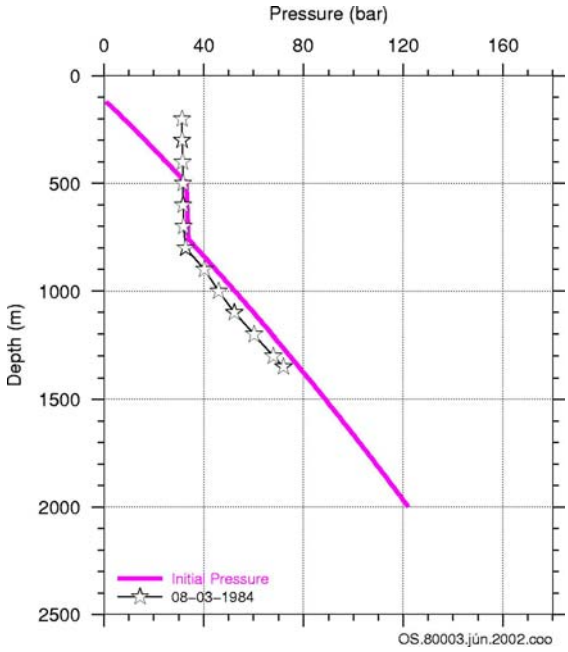


Figure A 3: Well OW-3 pressure

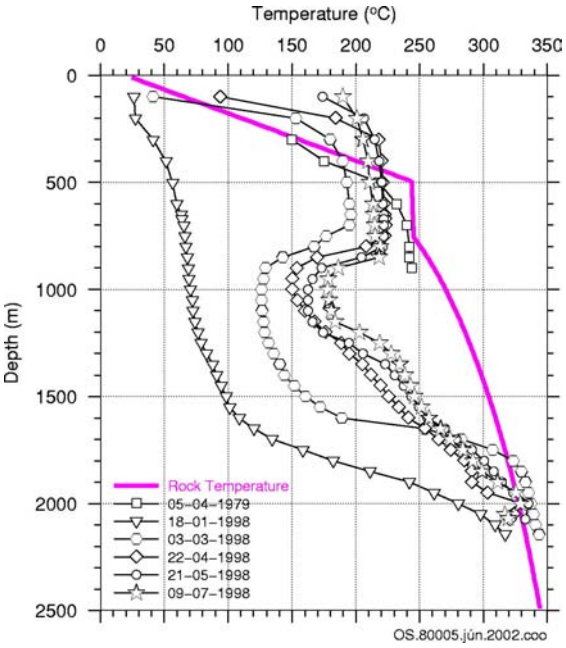


Figure A 2: Well OW-5 temperature

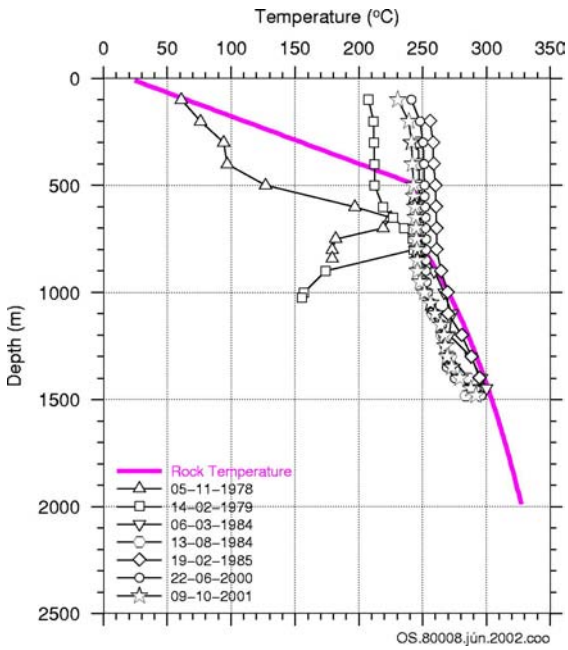


Figure A 4: Well OW-8 temperature

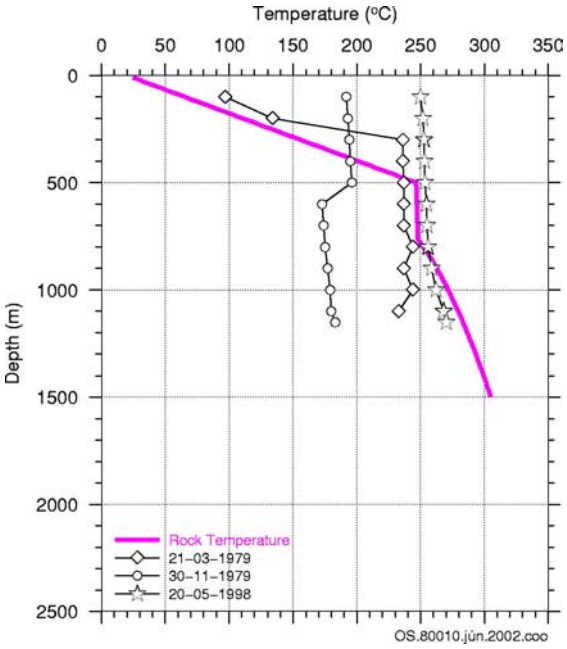


Figure A 5: Well OW-10 temperature

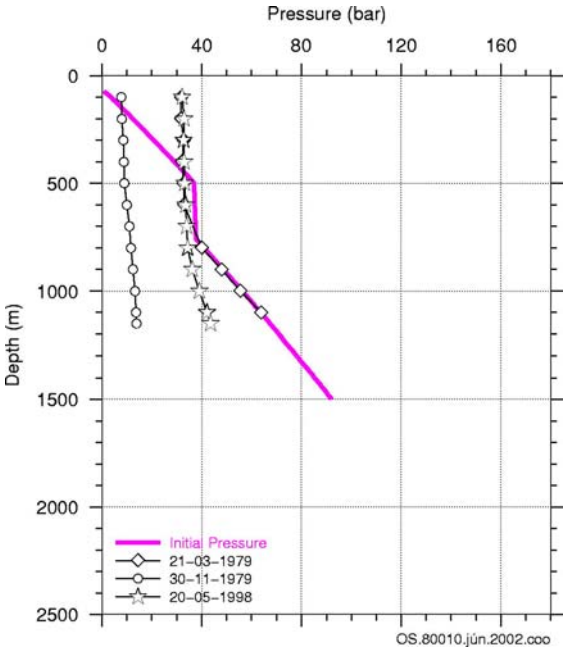


Figure A 7: Well OW-10 pressure

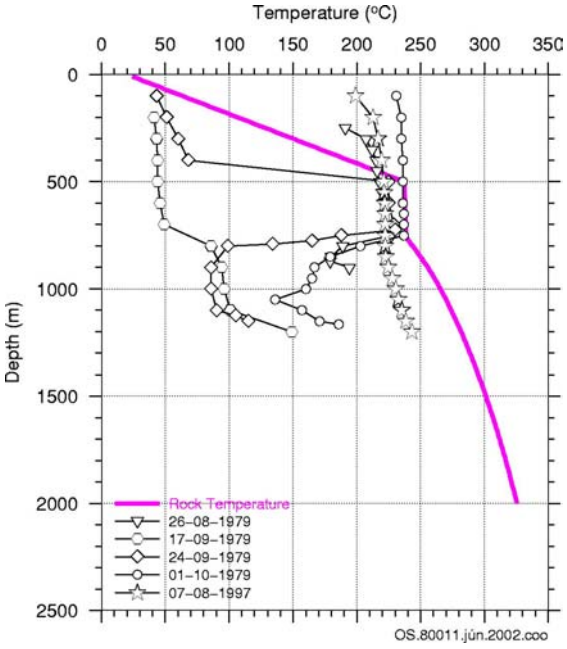


Figure A 6: Well OW-11 pressure

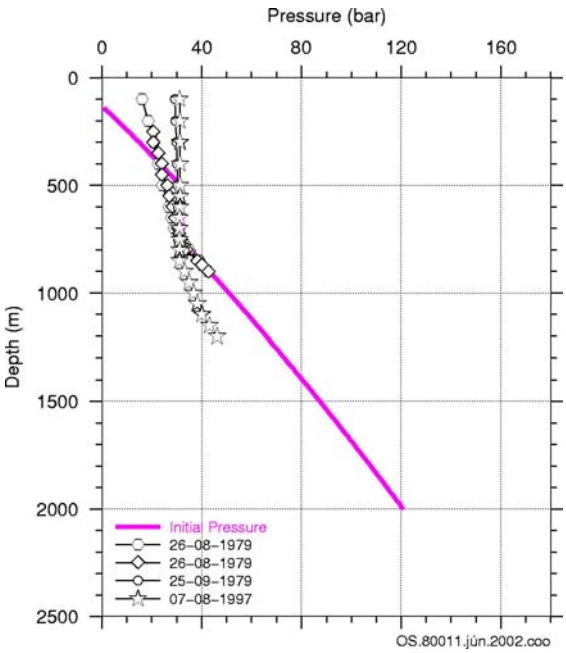


Figure A 8: Well OW-11 pressure

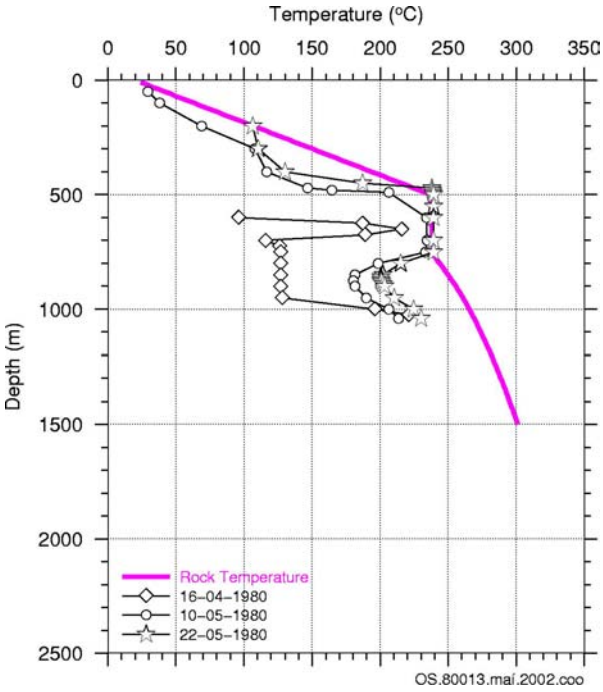


Figure A 9: Well OW-13 temperature

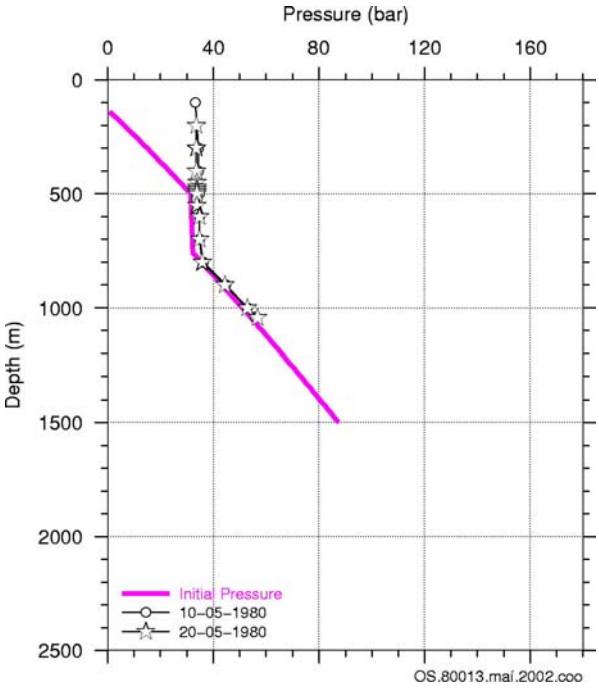


Figure A 11: Well OW-13 pressure

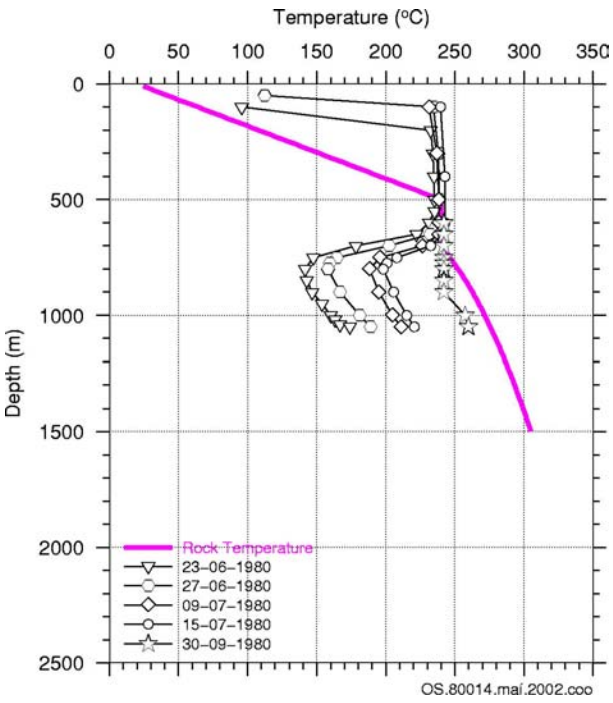


Figure A 10: Well OW-14 temperature

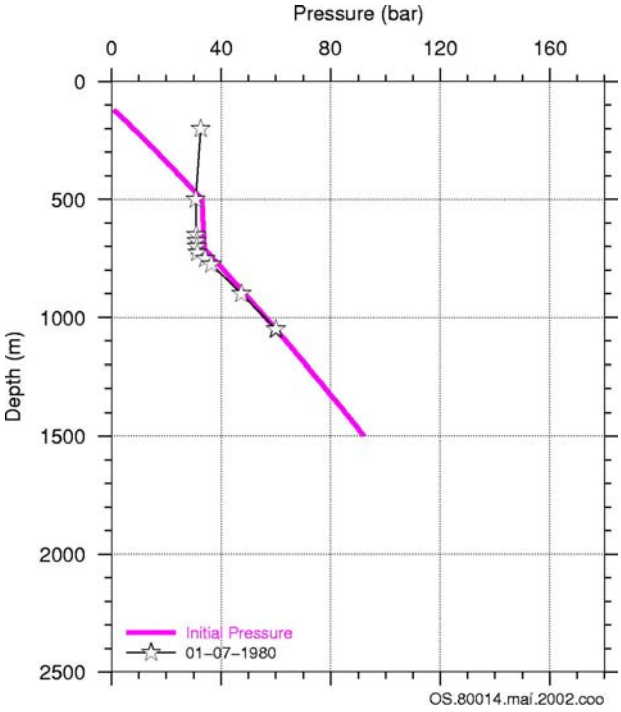


Figure A 12: Well OW-14 pressure

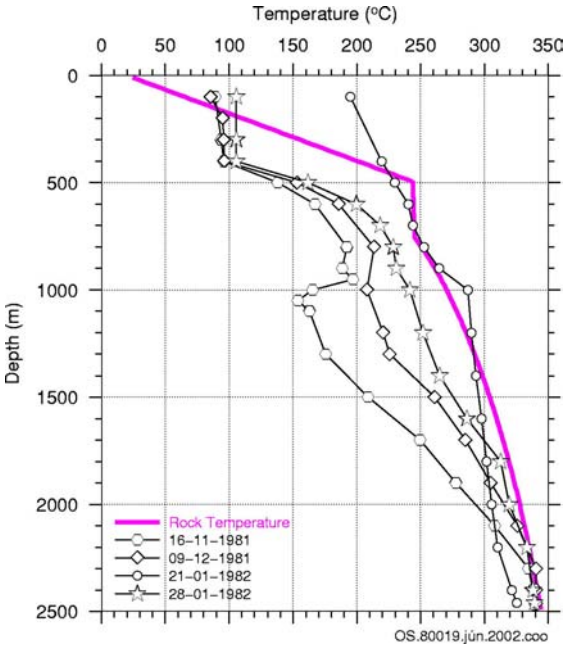


Figure A 13**:** Well OW-19 temperature

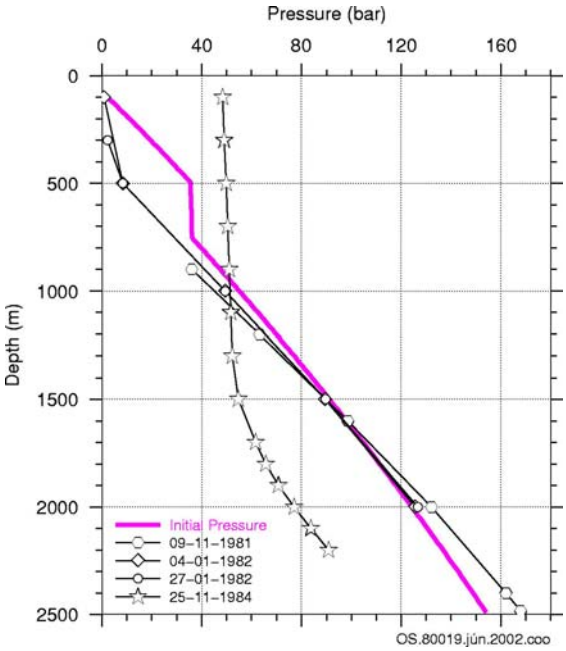


Figure A 15: Well OW-19 pressure

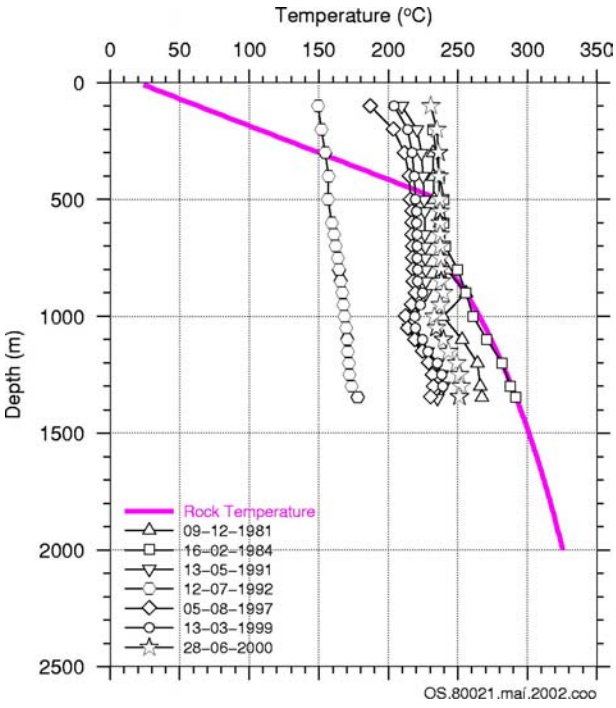


Figure A 14: Well OW-21 temperature

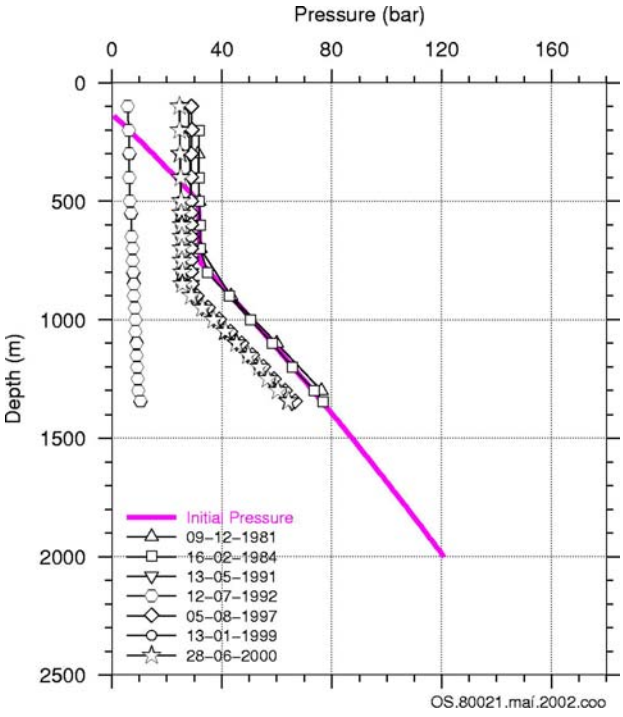


Figure A 16: Well OW-21 pressure

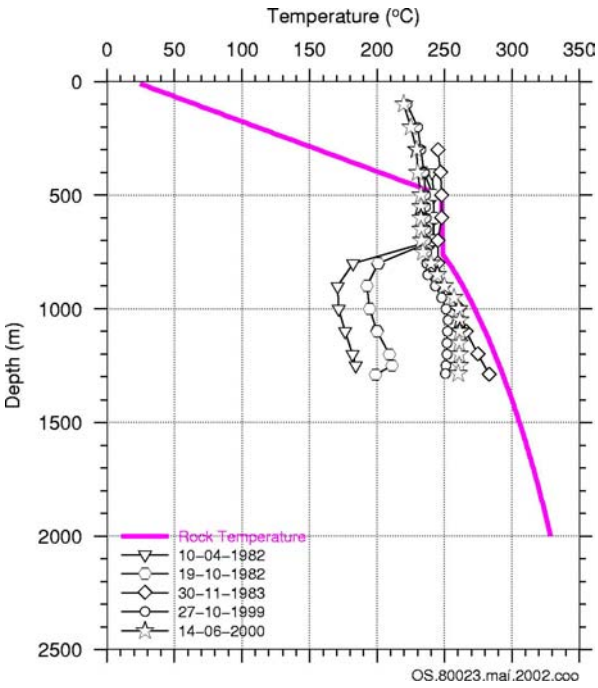


Figure A 17: Well OW-23 temperature

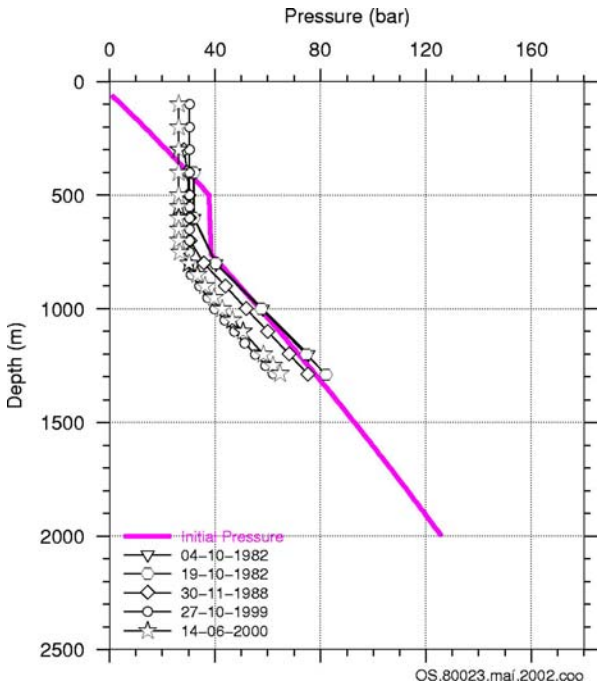


Figure A 19: Well OW-23 Pressure

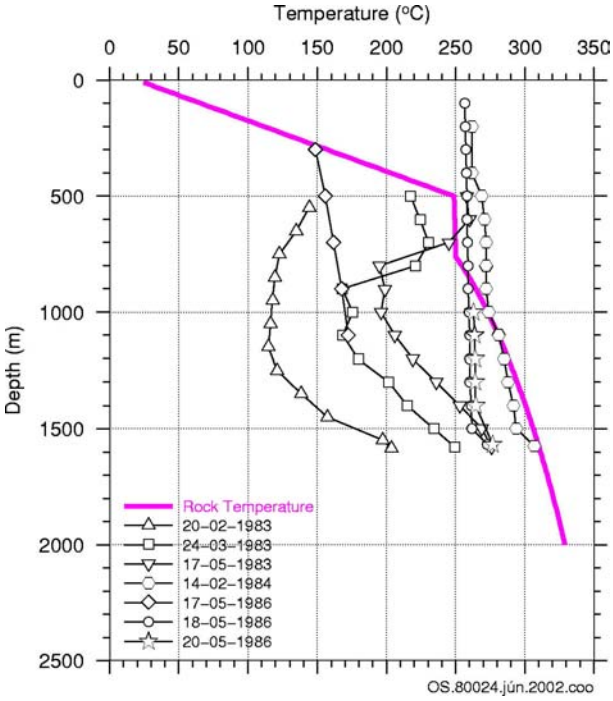


Figure A 18: Well OW-24 temperature

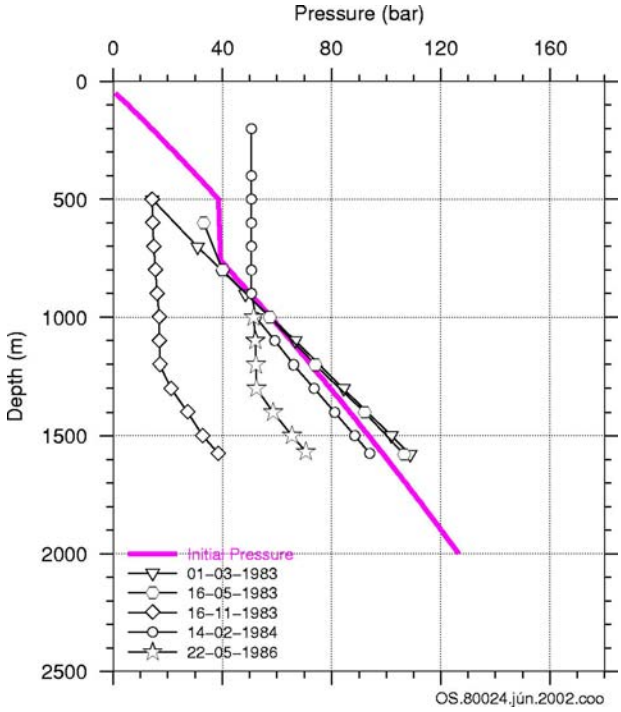


Figure A 20: Well OW-24 pressure

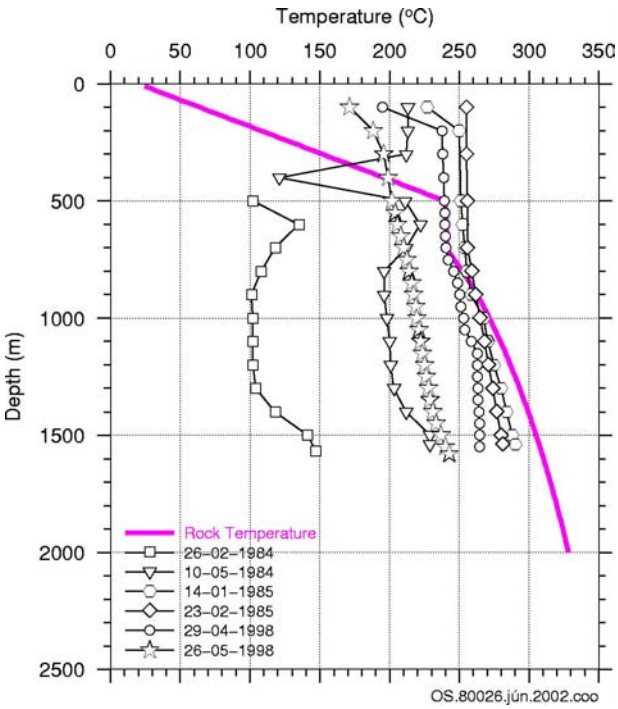


Figure A 21: Well OW-26 temperature

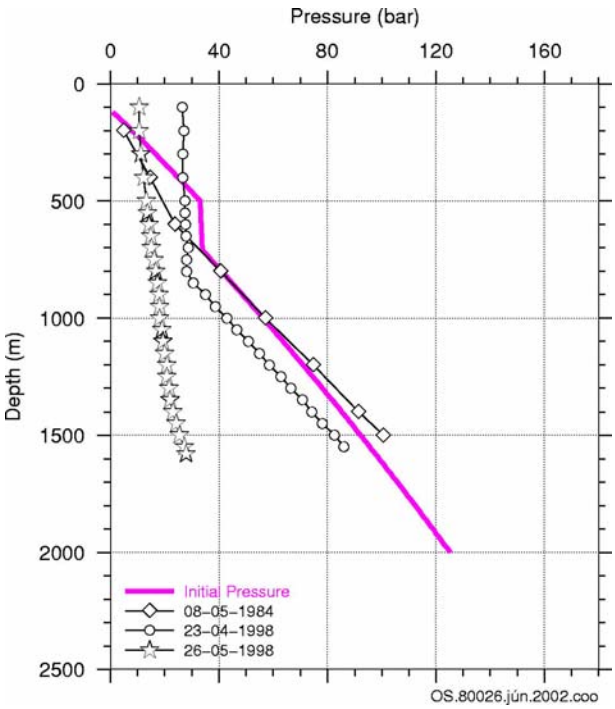


Figure A 23: Well OW-26 temperature

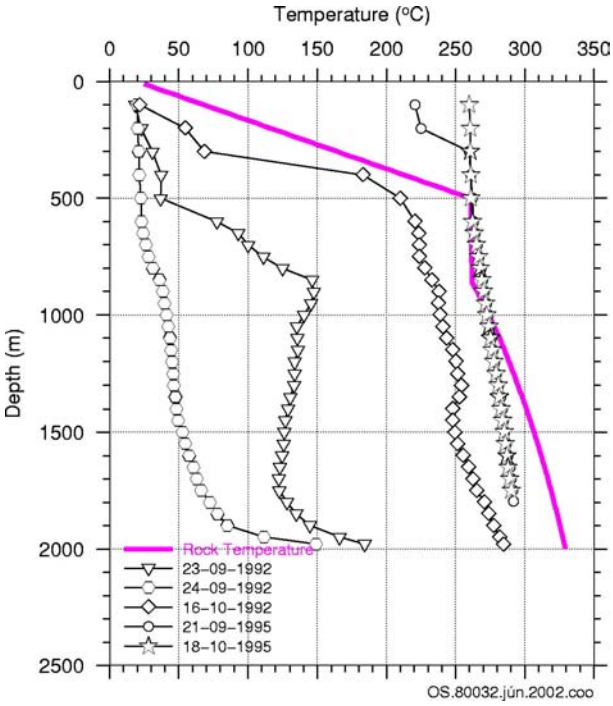


Figure A 22: Well OW-32 temperature

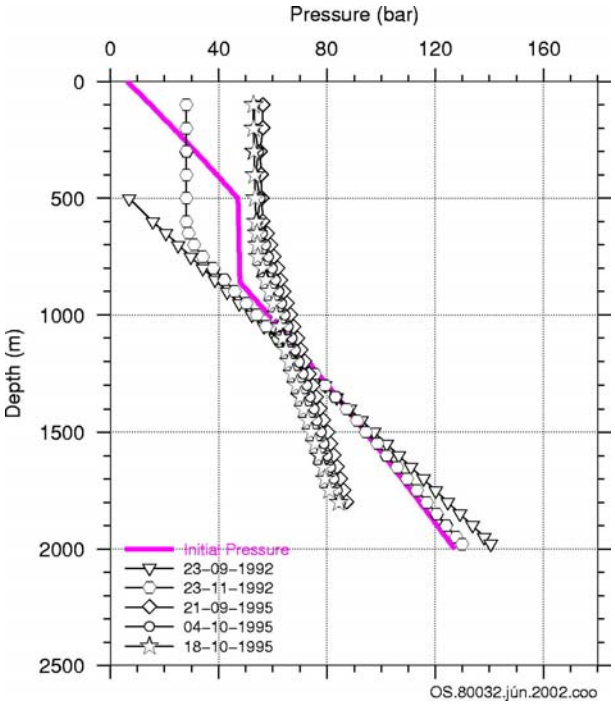


Figure A 24: Well OW-32 pressure

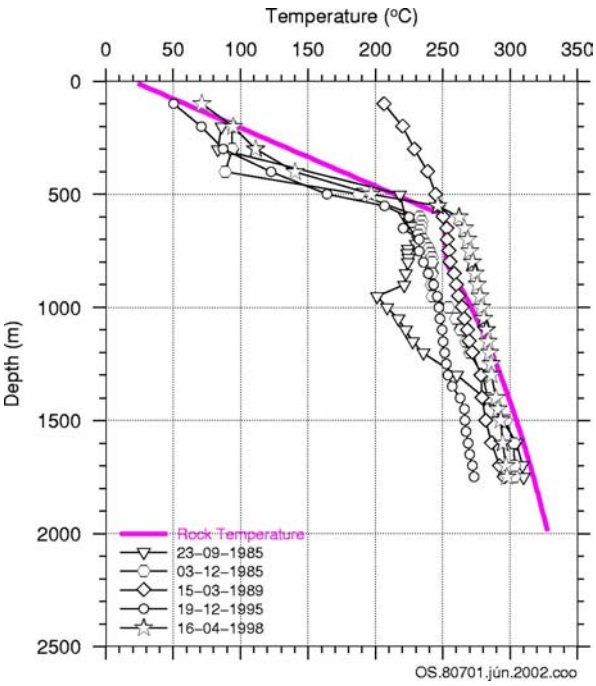


Figure A 25: Well OW-701 temperature

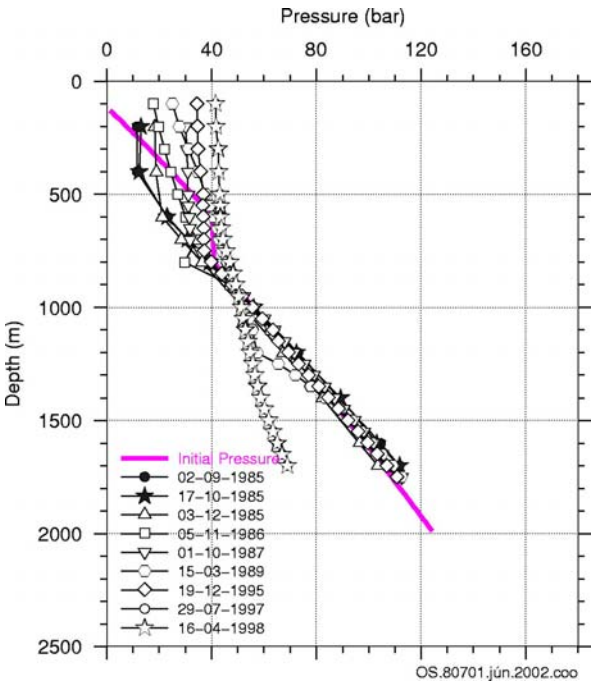


Figure A 27: Well OW-701 pressure

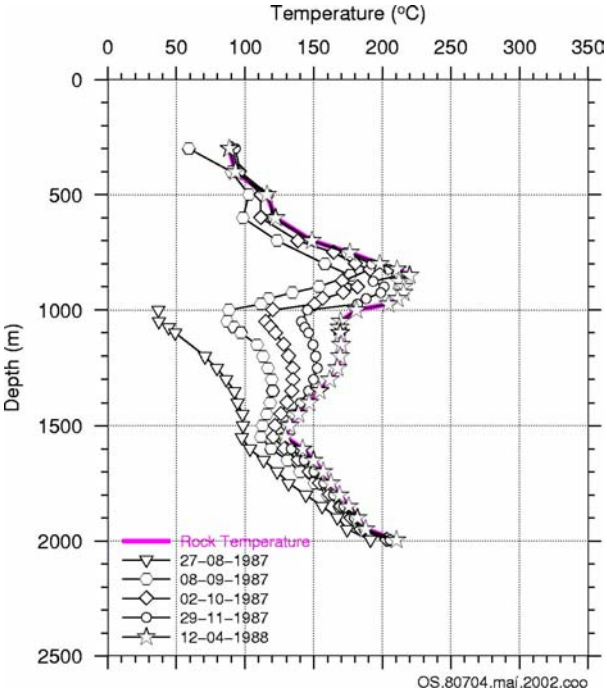


Figure A 26: Well OW-704 temperature

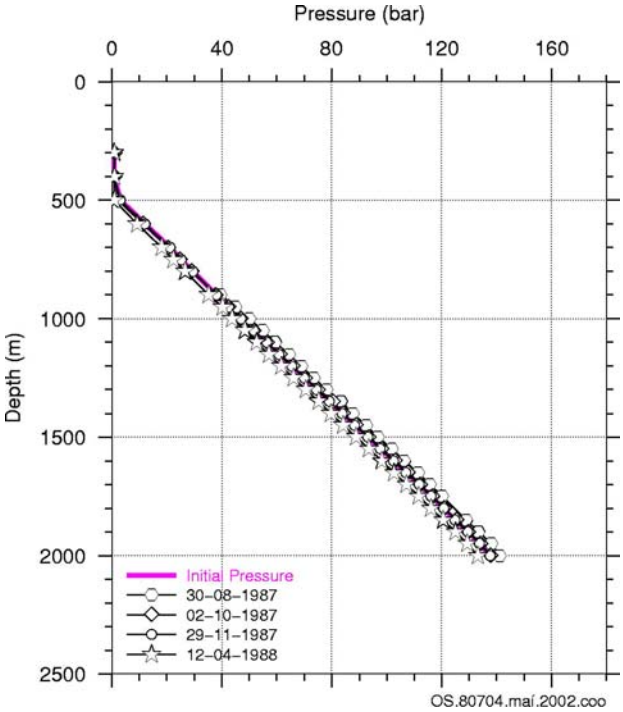


Figure A 28: well OW-704 pressure

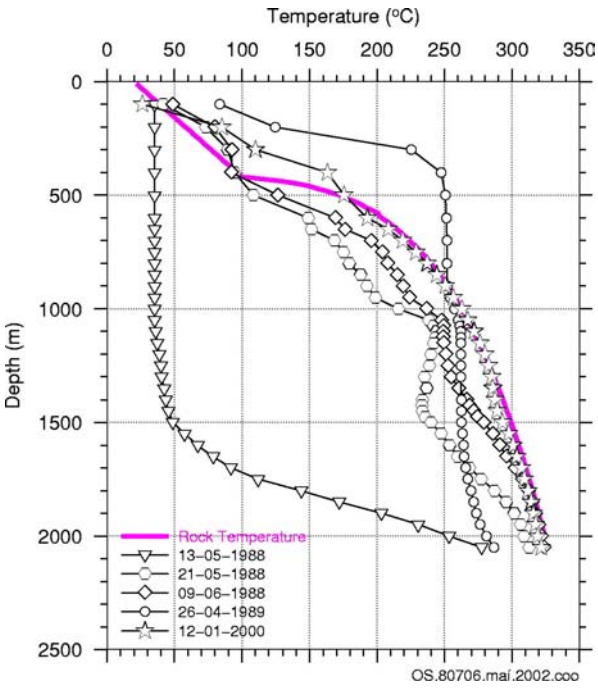


Figure A 29: Well OW-706 temperature

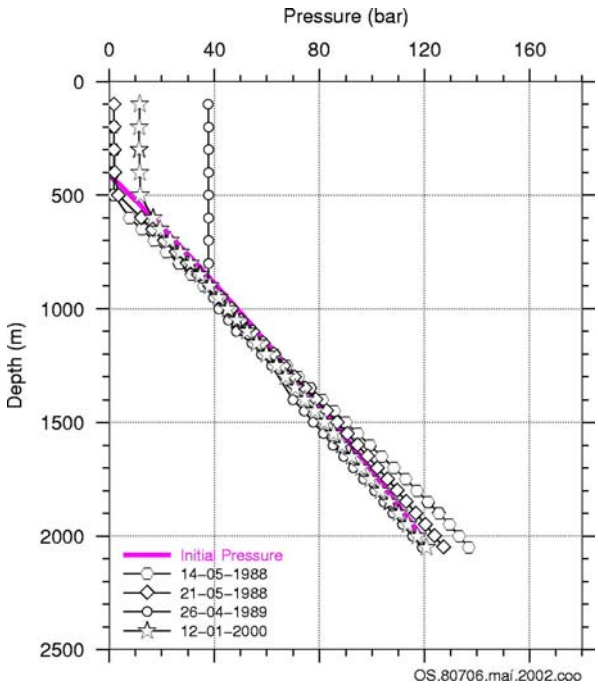


Figure A 31: Well OW-706 pressure

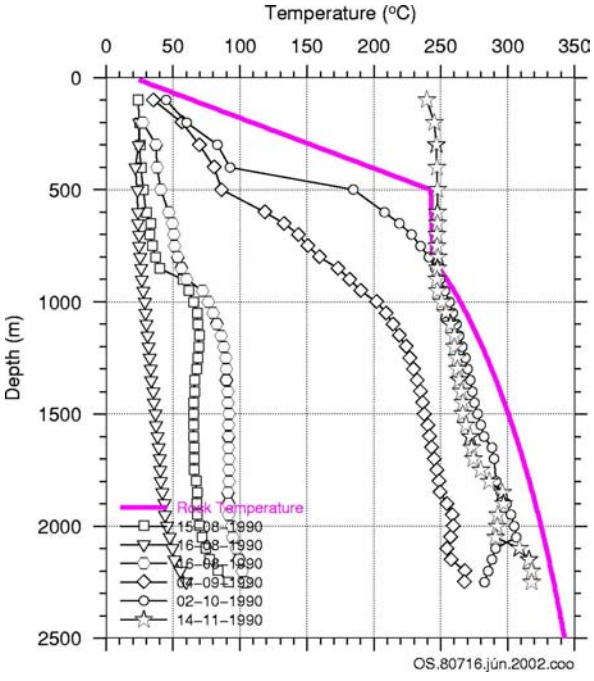


Figure A 30: Well OW-716 temperature

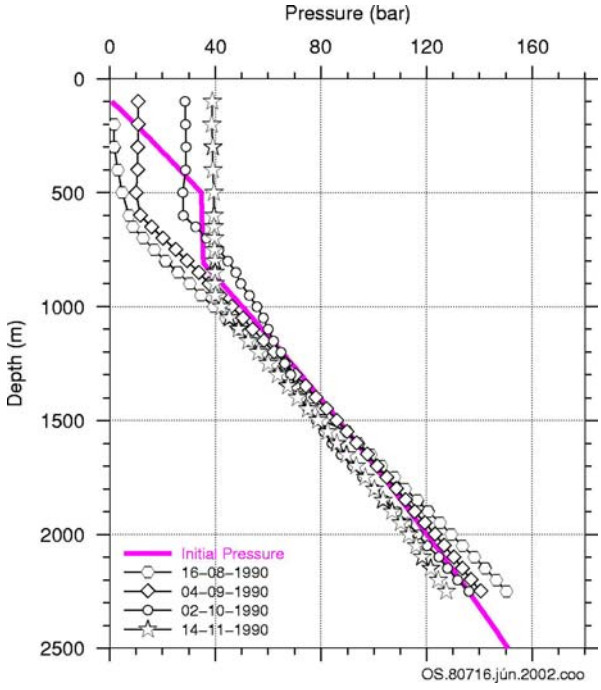


Figure A 32: Well OW-716 pressure

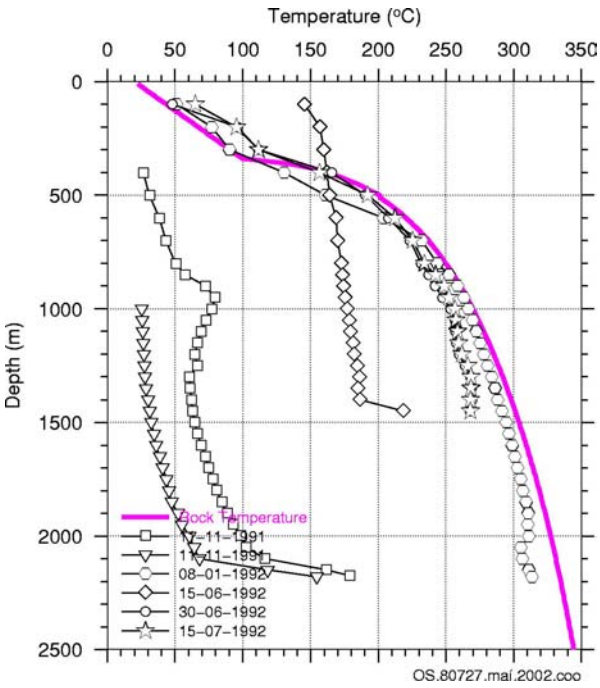


Figure A 33: Well OW-727 temperature

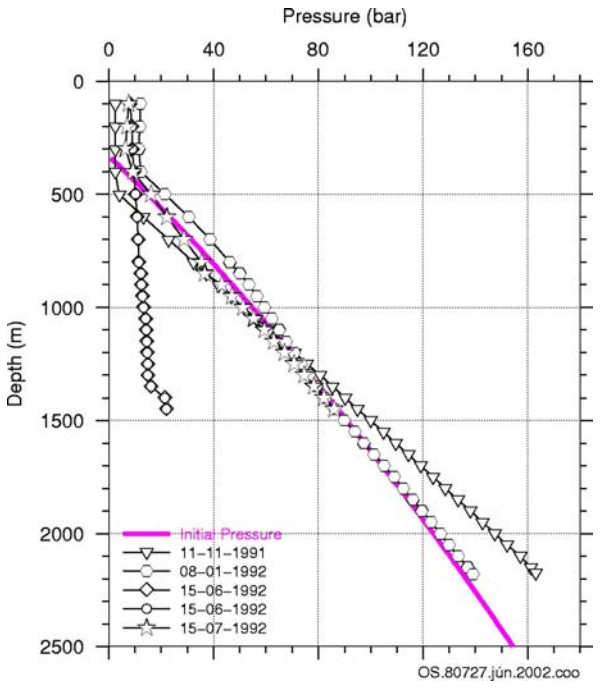


Figure A 35: Well OW-727 pressure

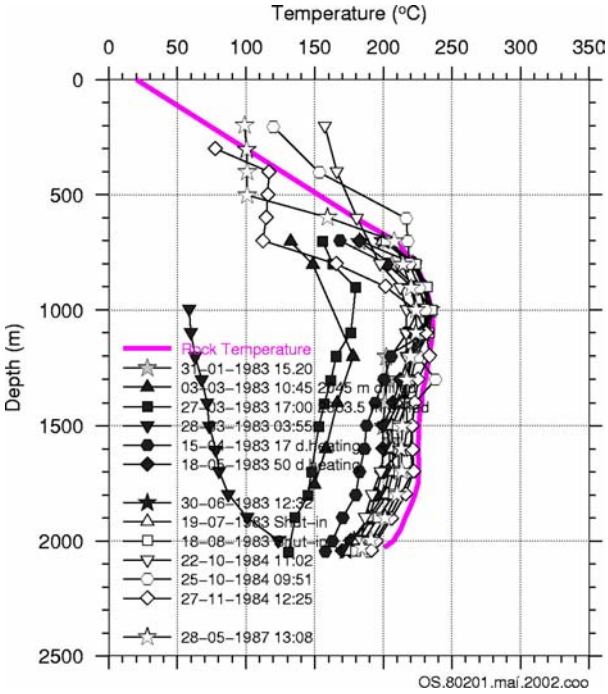


Figure A 34: Well OW-201 temperature

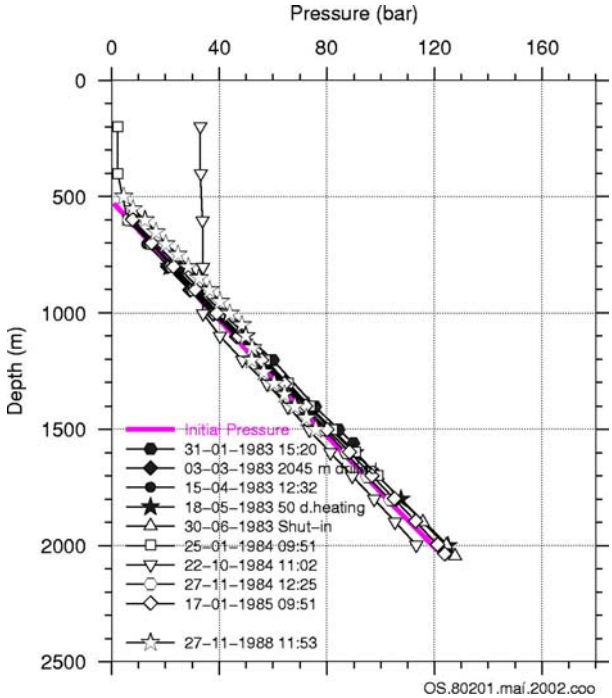


Figure A 36: Well OW-201 pressure

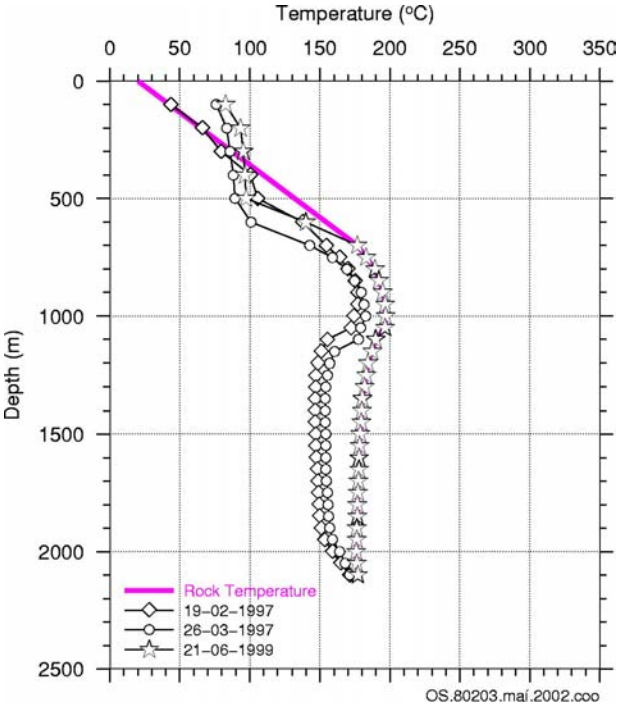


Figure A 37: Well OW-203 temperature

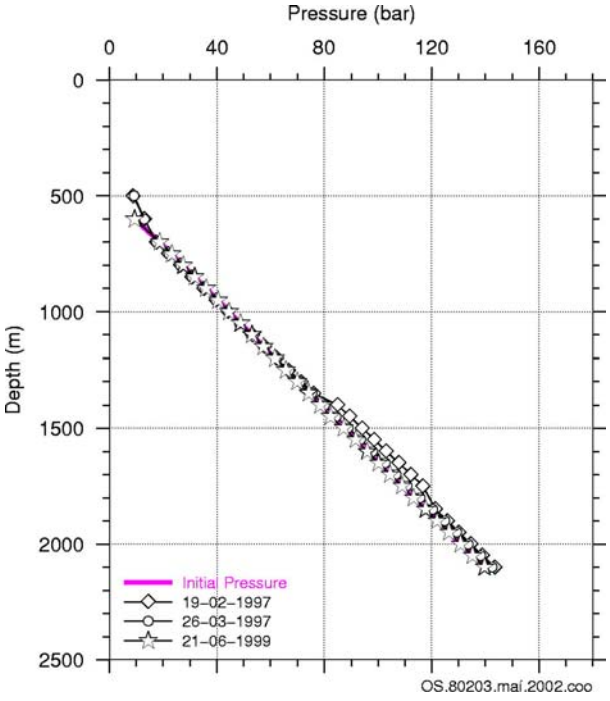


Figure A 39: Well OW-203 pressure

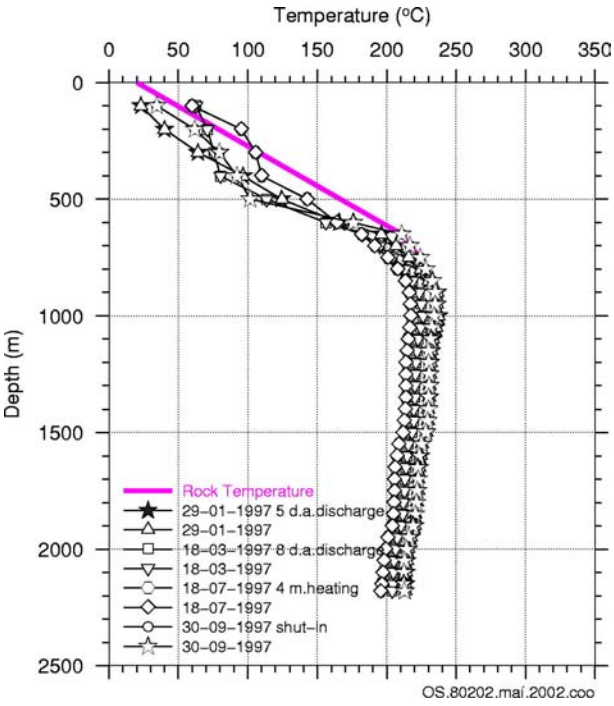


Figure A 38: Well OW-202 temperature

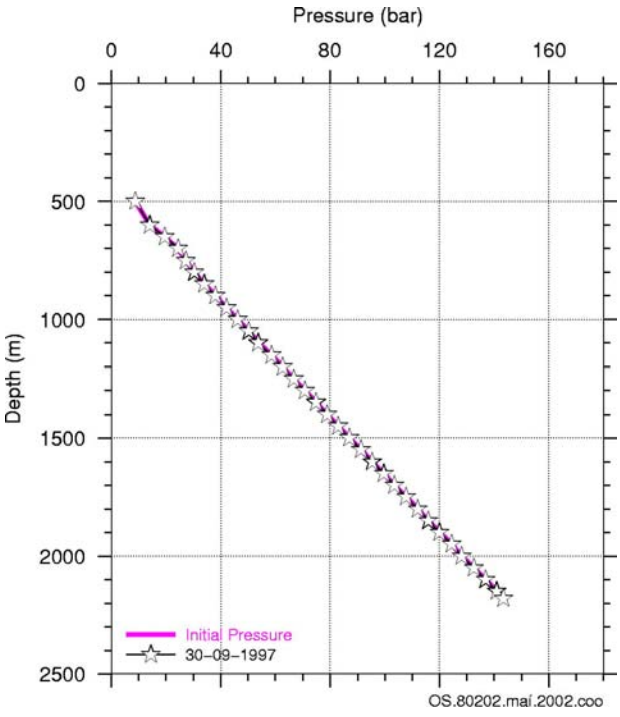


Figure A 40: Well OW-202 pressure

## APPENDIX B1

### Results of the update of 3-D natural state model

(In the Figures below, the dashed lines represent estimated formation temperature and pressure, filled black stars are values obtained from Bodvarsson and Pruess, (1987), and the open squares connected with lines are the model update from this work. The label on top of the pressure data refer to the element from which the well is located)

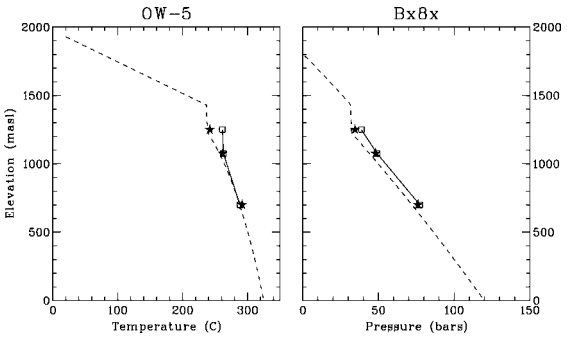


Figure B1 1: Calculated temperature and pressure for well OW-5

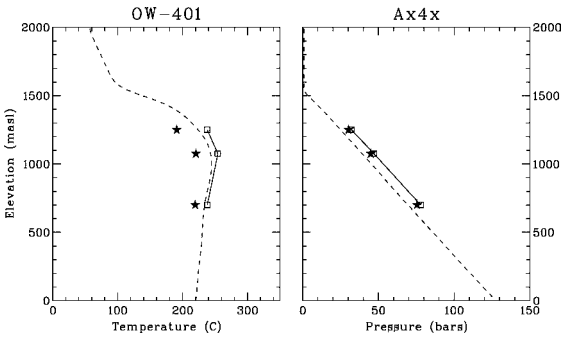


Figure B1 4: Calculated temperature and pressure for well OW-401

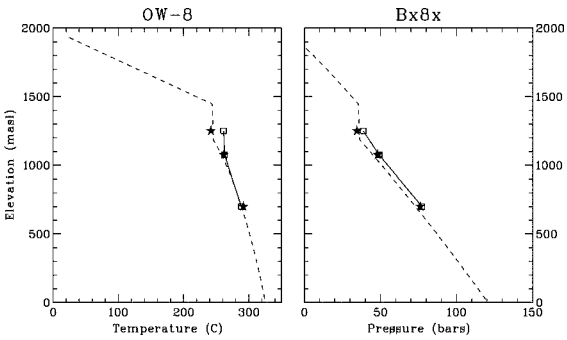


Figure B1 2: Calculated temperature and pressure for well OW-8

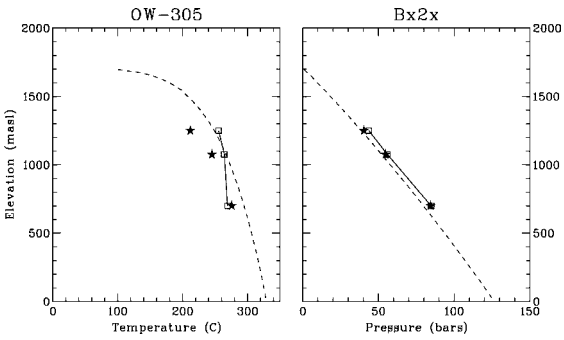


Figure B1 5: Calculated temperature and pressure for well OW-305

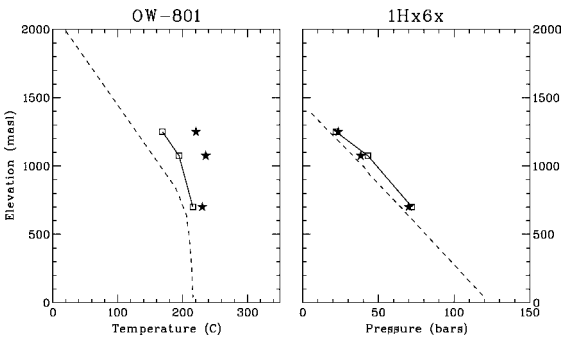


Figure B1 3: Calculated temperature and pressure for well OW-801

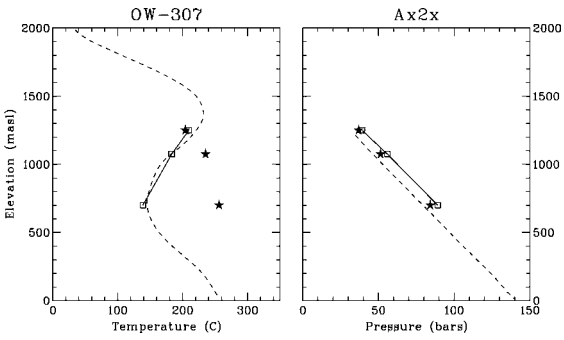


Figure B1 6: Calculated temperature and pressure for well OW-307

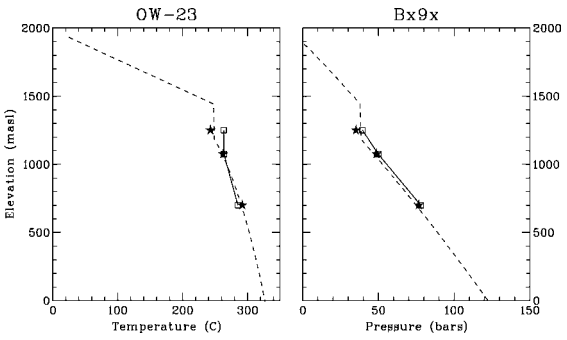


Figure B1 7: Calculated temperature and pressure for well OW-23

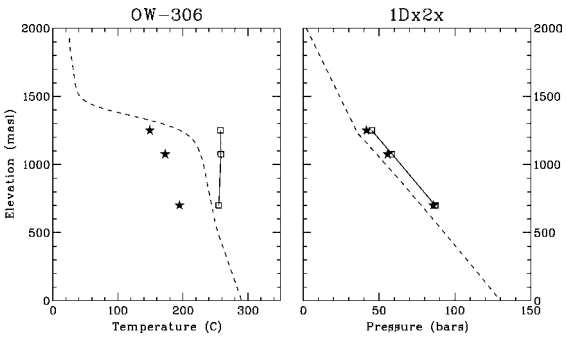


Figure B1 11: Calculated temperature and pressure for well OW-306

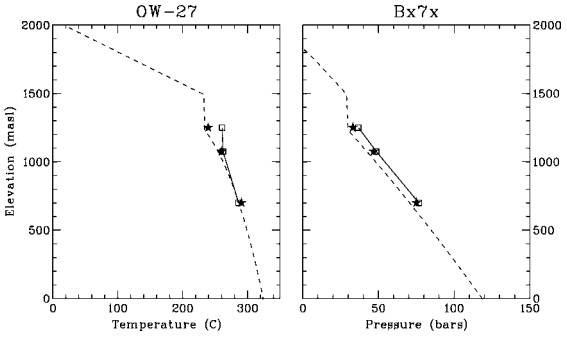


Figure B1 8: Calculated temperature and pressure for well OW-27

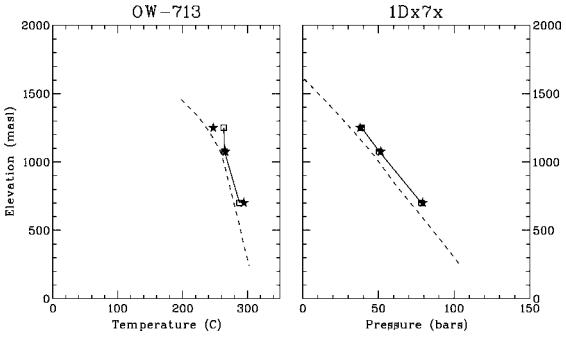


Figure B1 12: Calculated temperature and pressure for well OW-713

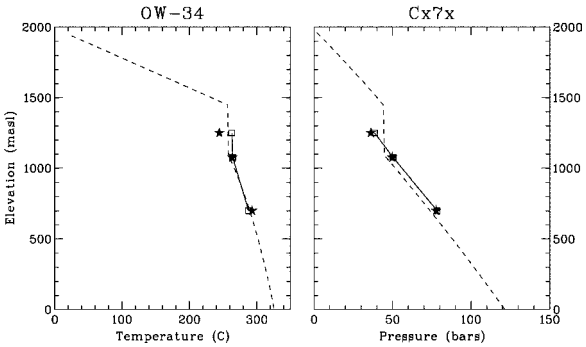


Figure B1 9: Calculated temperature and pressure for well OW-34

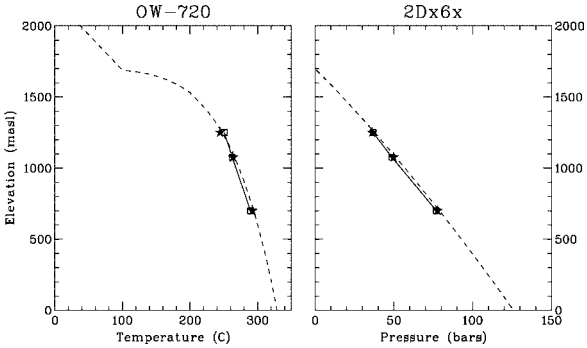


Figure B1 13: Calculated temperature and pressure for well OW-720

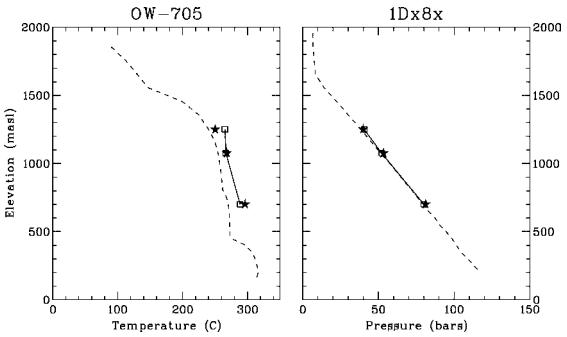


Figure B1 10: Calculated temperature and pressure for well OW-705

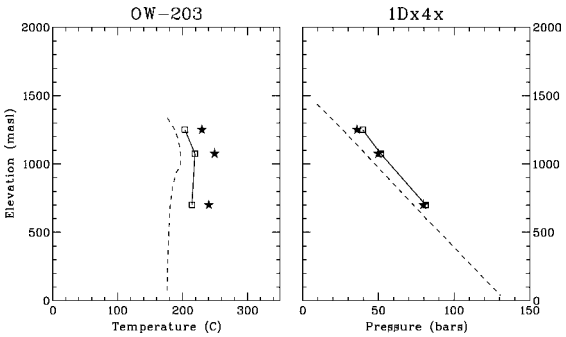


Figure B1 14: Calculated temperature and pressure for well OW-203

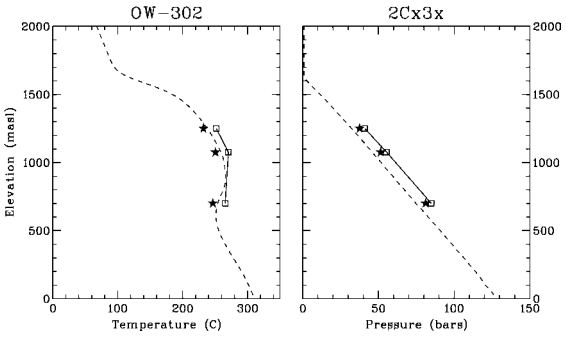


Figure B1 15: Calculated temperature and pressure for well OW-302

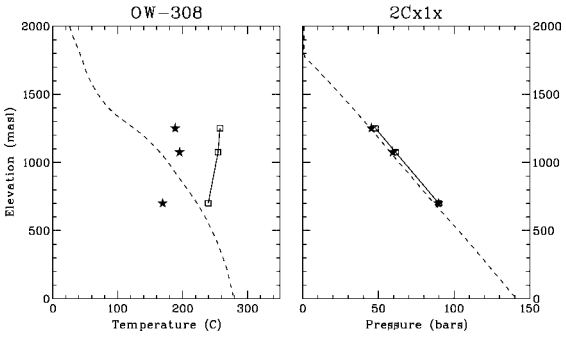


Figure B1 16: Calculated temperature and pressure for well OW-308

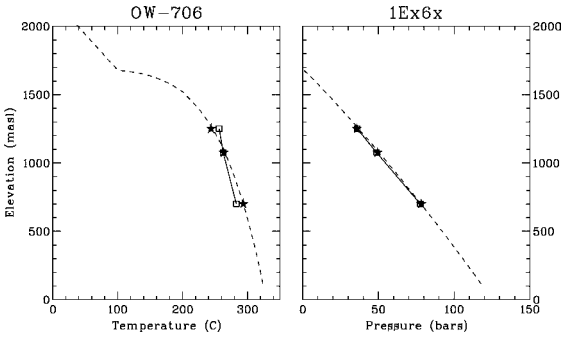


Figure B1 17: Calculated temperature and pressure for well OW-706

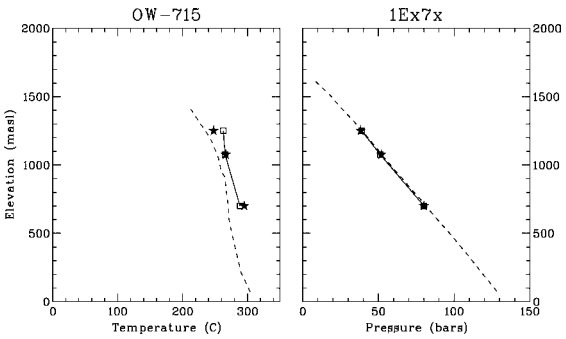


Figure B1 18: Calculated temperature and pressure for well OW-715

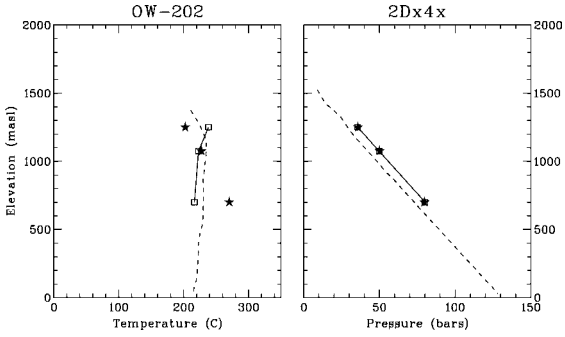


Figure B1 19: Calculated temperature and pressure for well OW-202

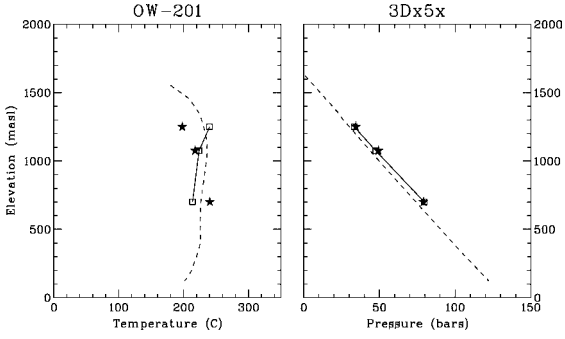


Figure B1 20: Calculated temperature and pressure for well OW-201

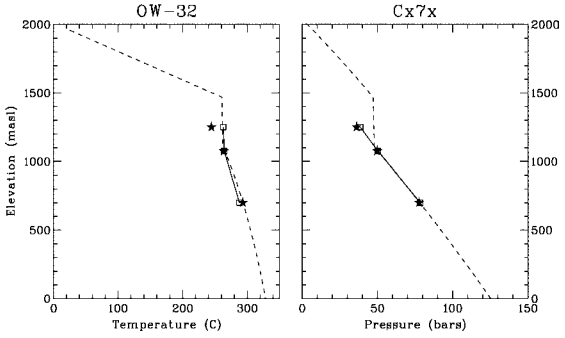


Figure B1 21: Calculated temperature and pressure for well OW-32

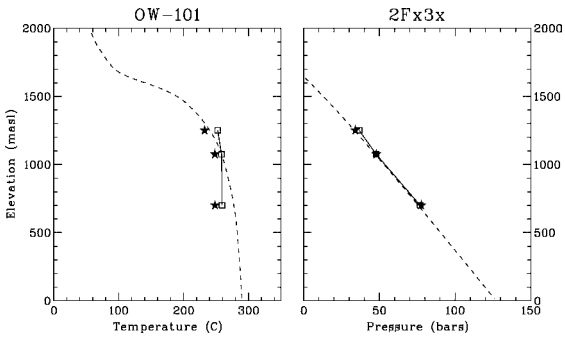


Figure B1 22: Calculated temperature and pressure for well OW-101

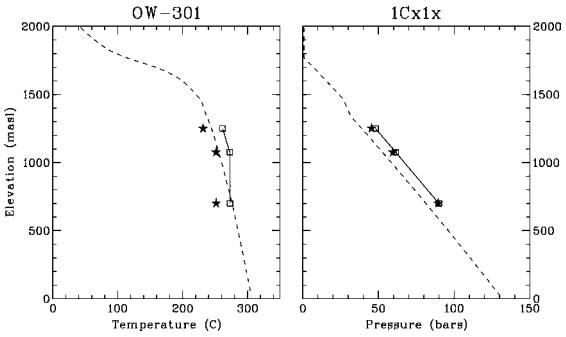


Figure B1 23: Calculated temperature and pressure for well OW-301

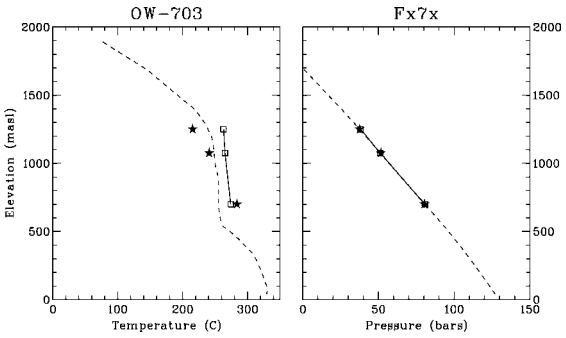


Figure B1 24: Calculated temperature and pressure for well OW-703

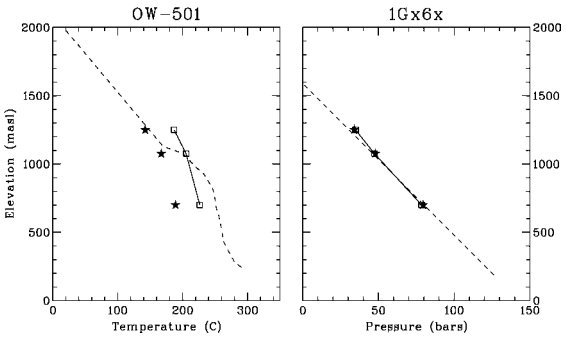


Figure B1 25: Calculated temperature and pressure for well OW-501

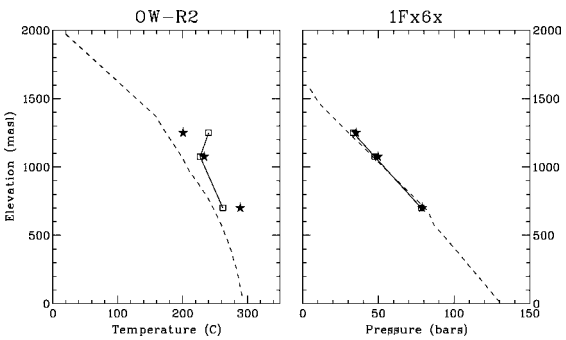


Figure B1 26: Calculated temperature and pressure for well OW-R2

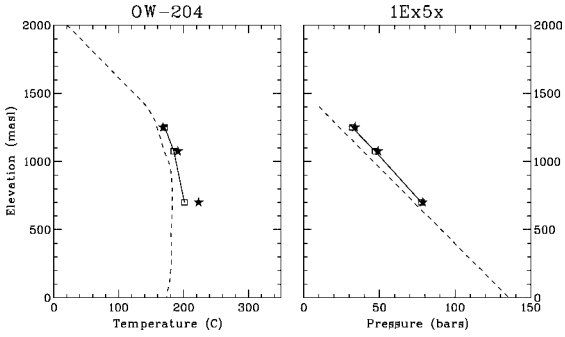


Figure B1 27: Calculated temperature and pressure for well OW-204

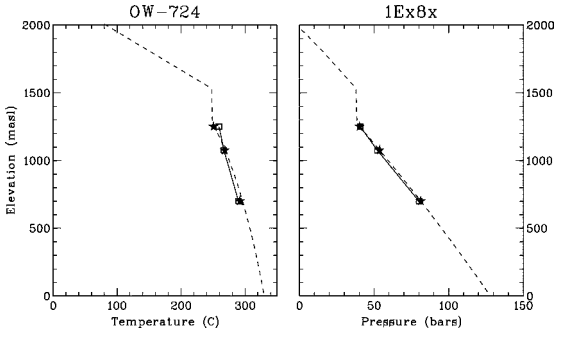


Figure B1 28: Calculated temperature and pressure for well OW-724

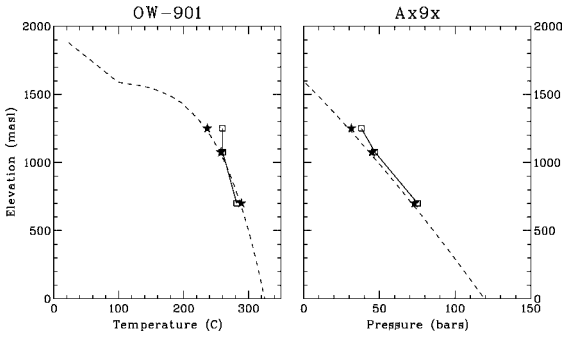


Figure B1 29: Calculated temperature and pressure for well OW-901

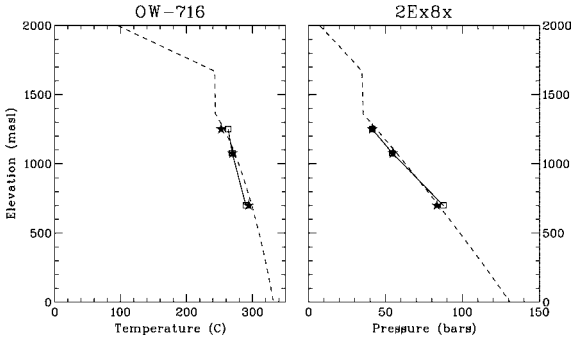


Figure B1 30: Calculated temperature and pressure for well OW-716

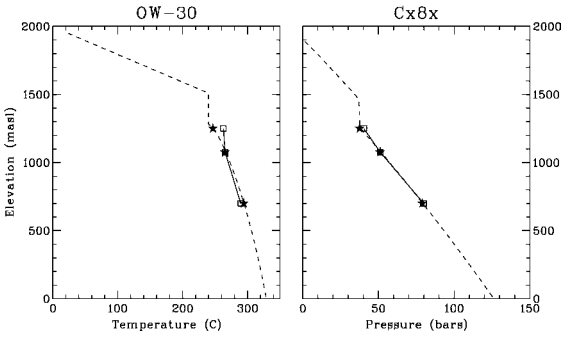


Figure B1 31: Calculated temperature and pressure for well OW-30

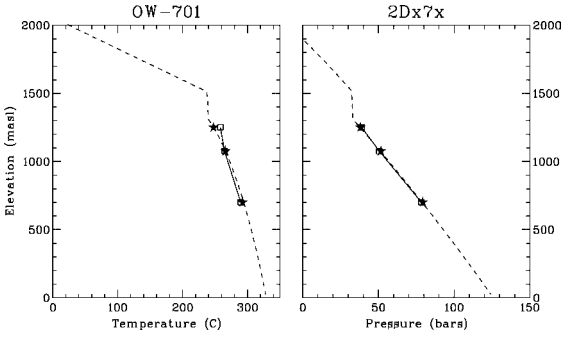


Figure B1 33: Calculated temperature and pressure for well OW-701

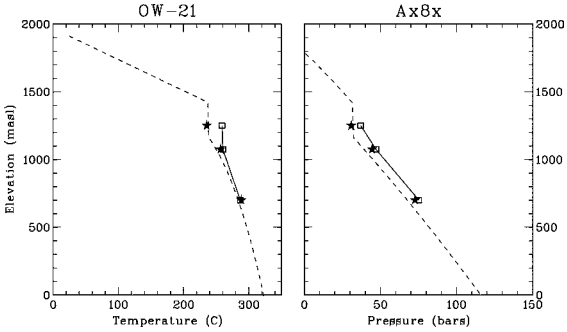


Figure B1 32: Calculated temperature and pressure for well OW-21

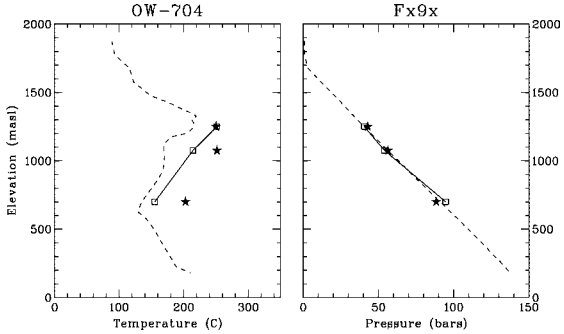


Figure B1 34: Calculated temperature and pressure for well OW-704

## APPENDIX B2

### Production history matching of the "best" exploitation model

(The Figures below show the model match of the production history. The lines are the computed and the dots are measured)

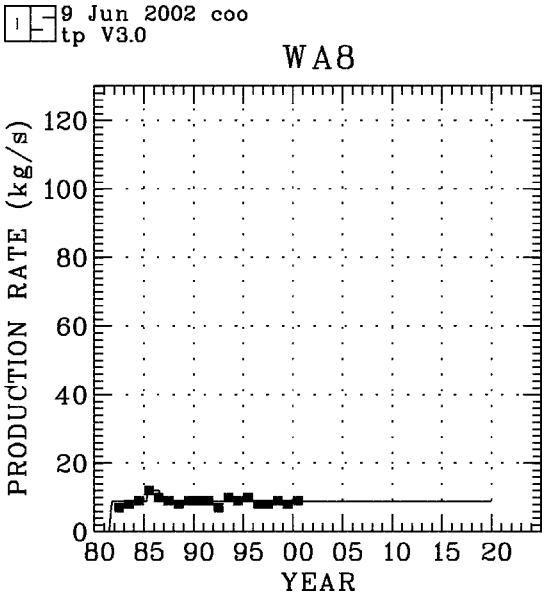


Figure B2 1: Production from block A8

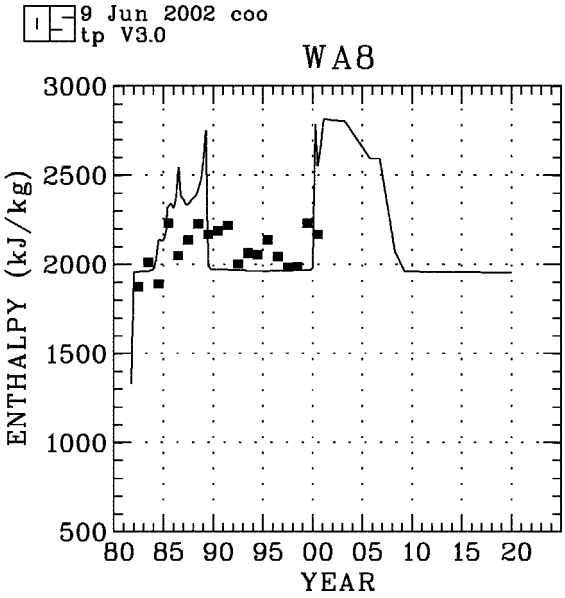


Figure B2 3: Enthalpy in block A8

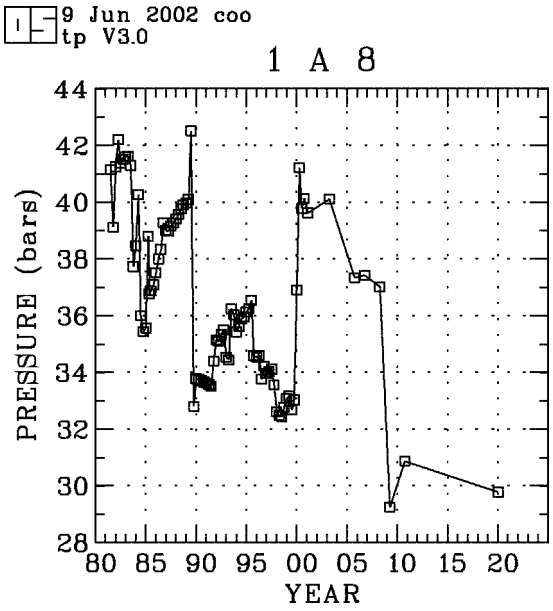


Figure B2 2: Calculated pressure in element 1A8

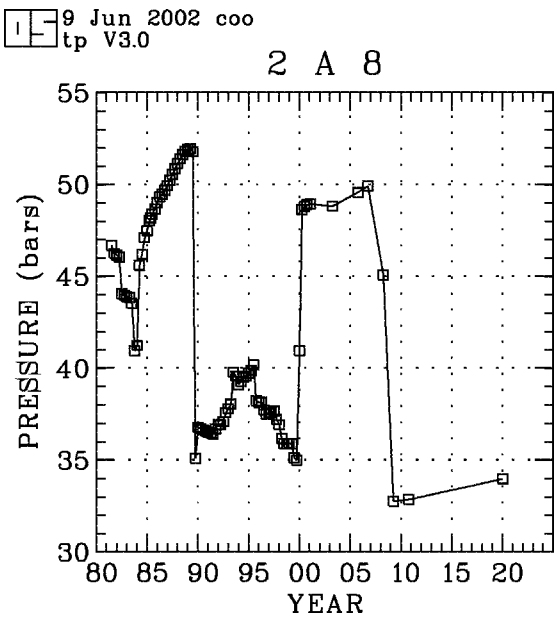


Figure B2 4: Calculated pressure in element 2A8

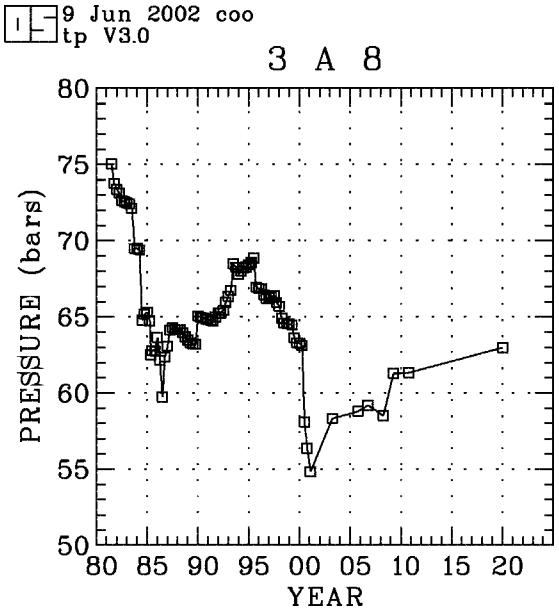


Figure B2 5: Calculated pressure in element 3A8

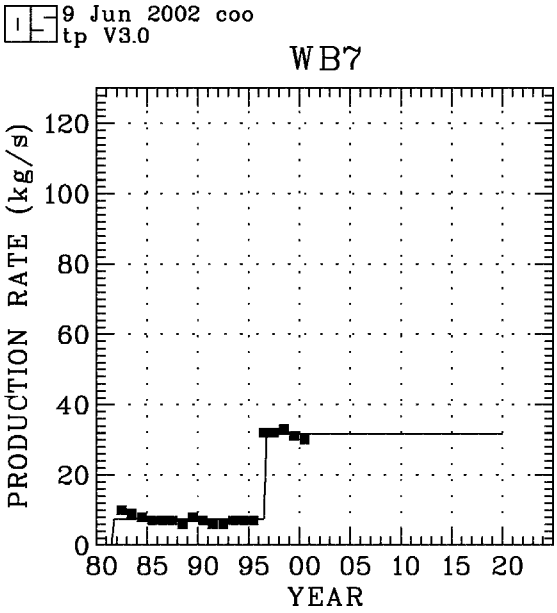


Figure B2 7: Production from block B7

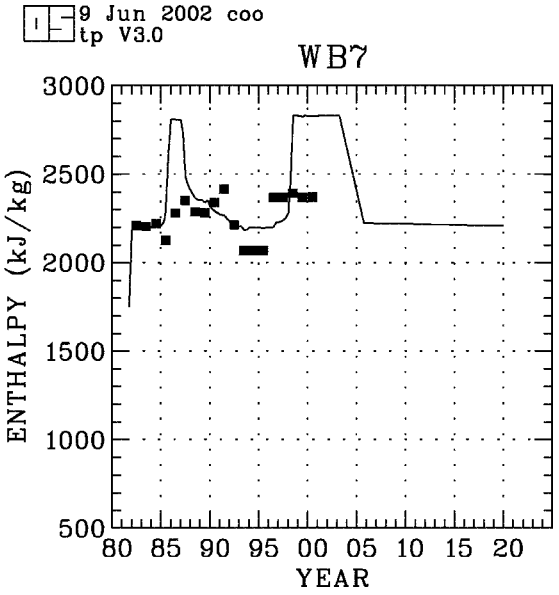


Figure B2 6: Enthalpy in block B7

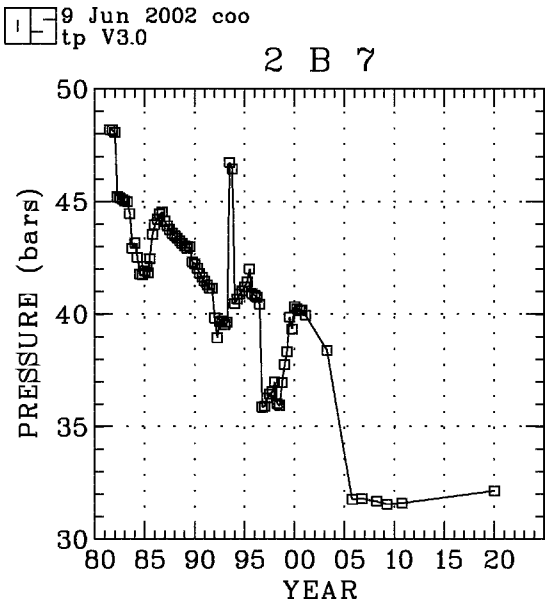


Figure B2 8: Calculated pressure in element 2B7

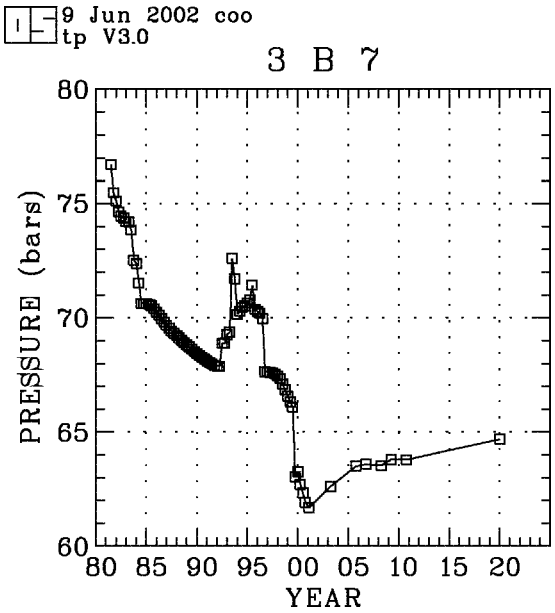


Figure B2 9: Calculated pressure in element 3B7

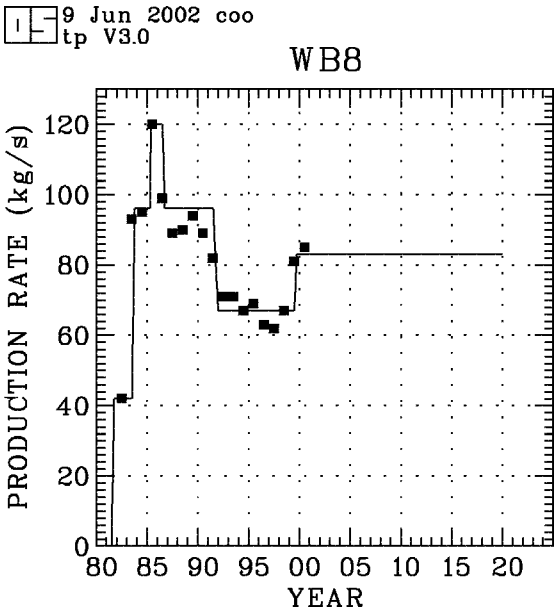


Figure B2 11: Production from block B8

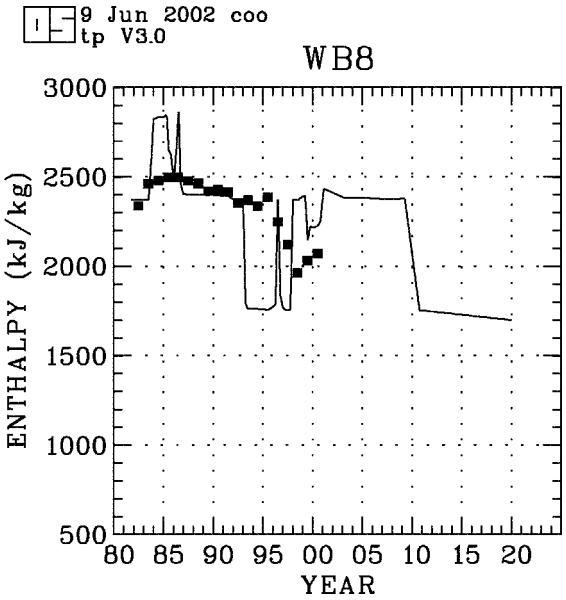


Figure B2 10: Enthalpy in block B8

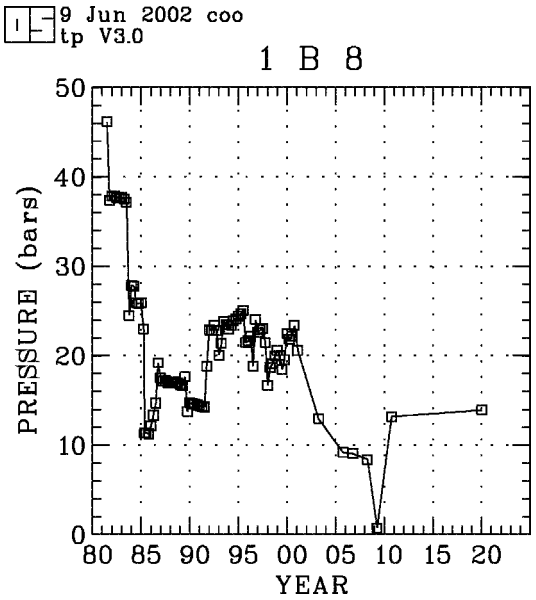


Figure B2 12: Calculated pressure in element 1B8

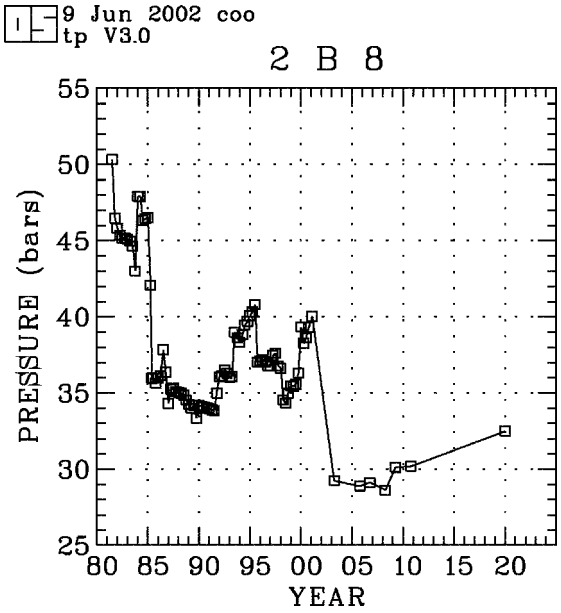


Figure B2 13: Calculated pressure in element 2B8

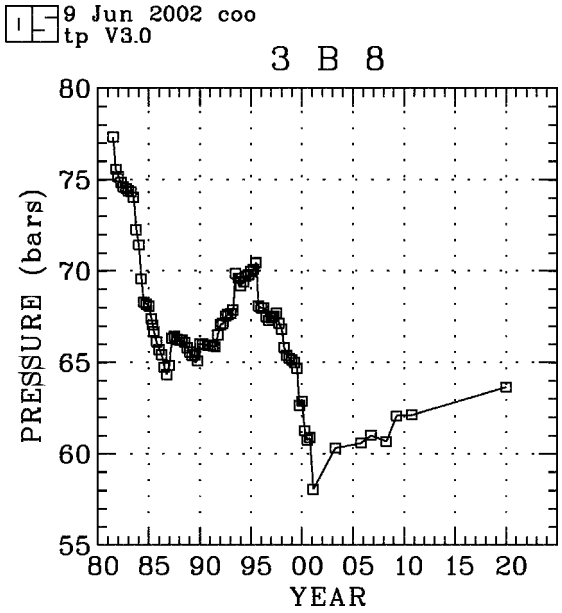


Figure B2 15: Calculated pressure in element 3B8

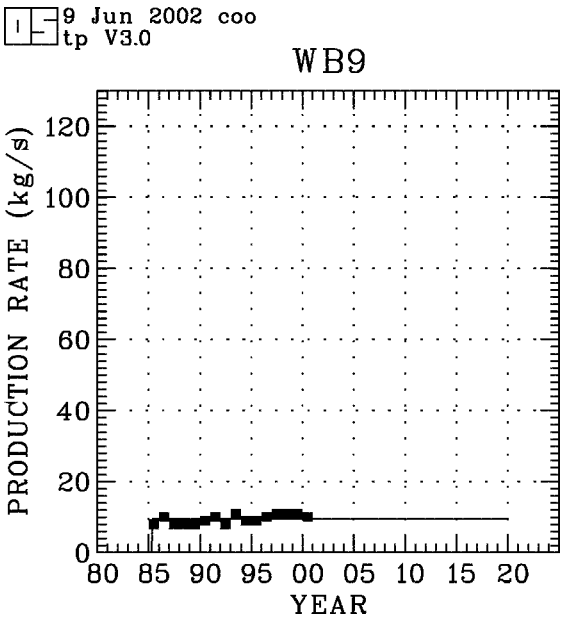


Figure B2 14: Production from block B9

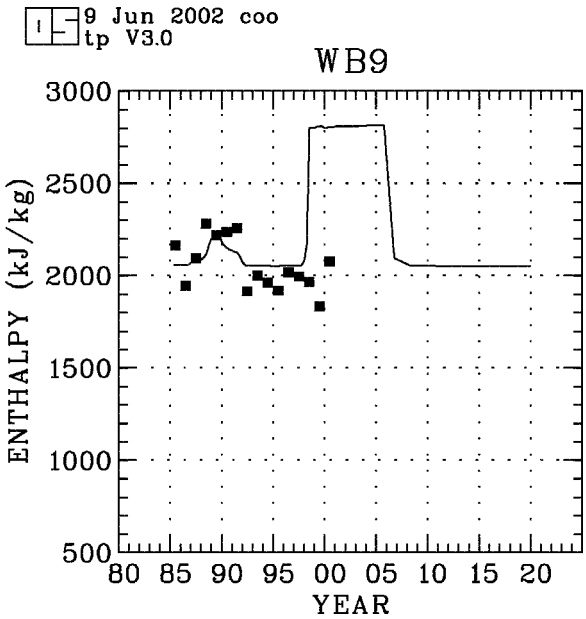


Figure B2 16: Enthalpy in block B9

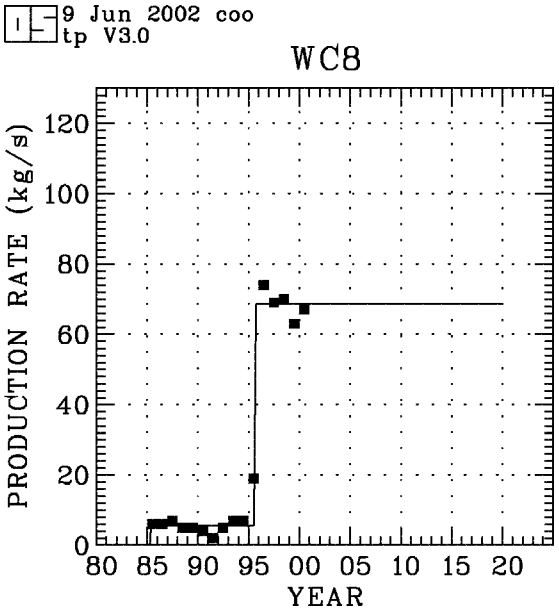


Figure B2 17: Production from block C8

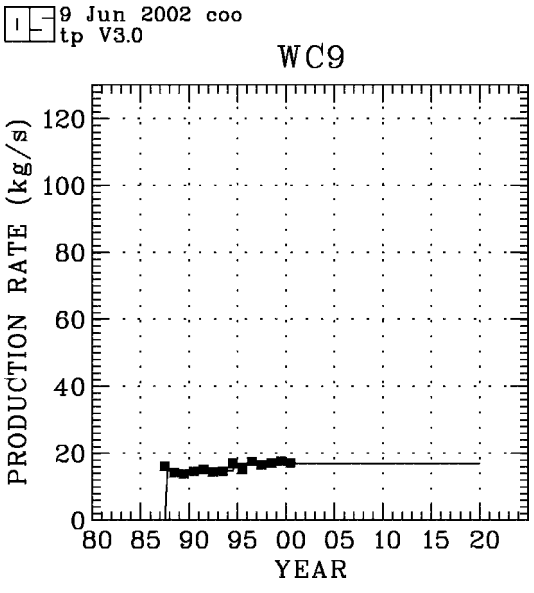


Figure B2 18: Production from block C9

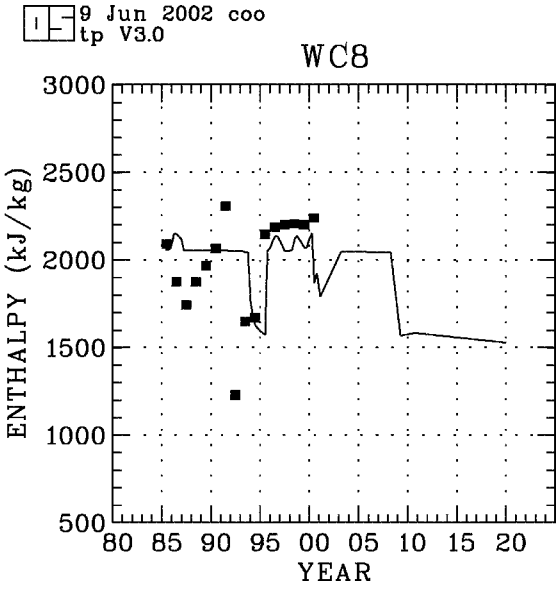


Figure B2 19: Enthalpy in block C8

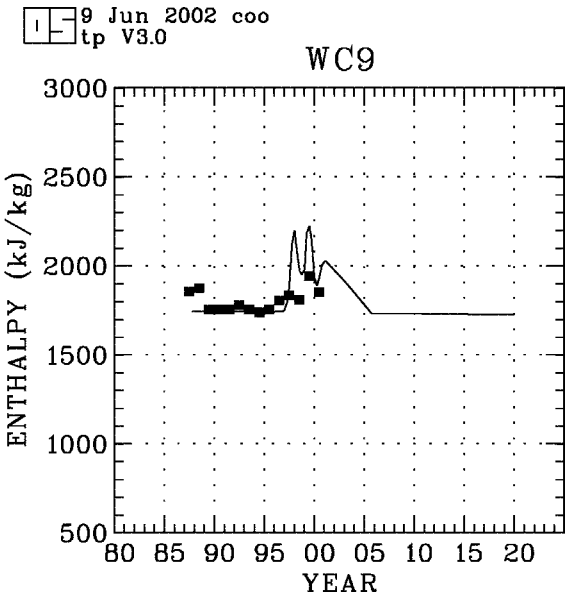


Figure B2 20: Enthalpy in block C9

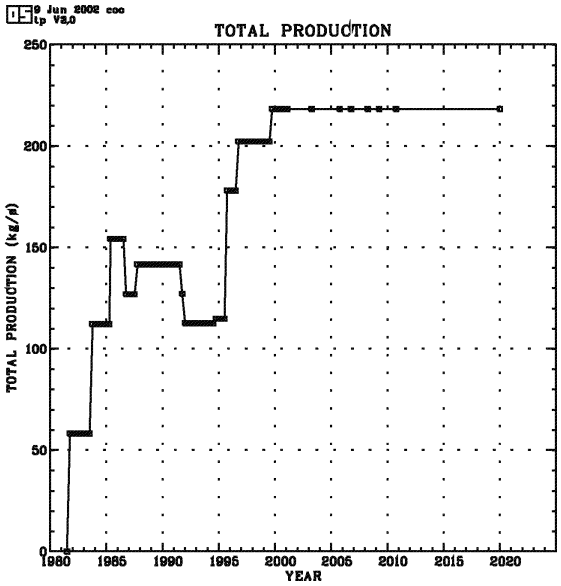


Figure B2 21: Total production from the field

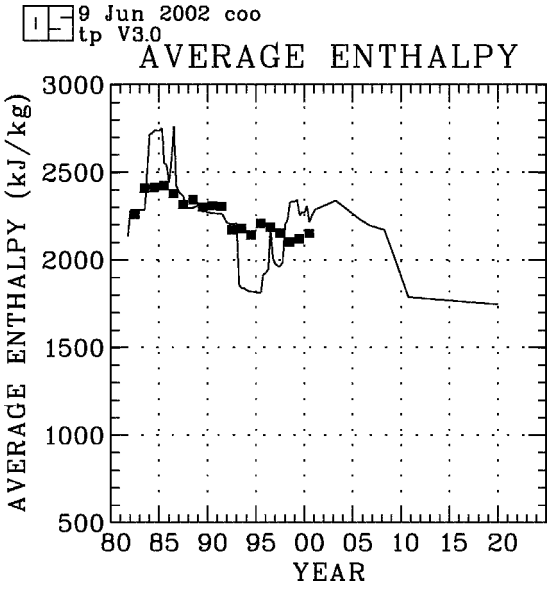


Figure B2 22: Average enthalpy in the field

# APPENDIX C

## Graphs of flow history of some wells from the Olkaria East production field

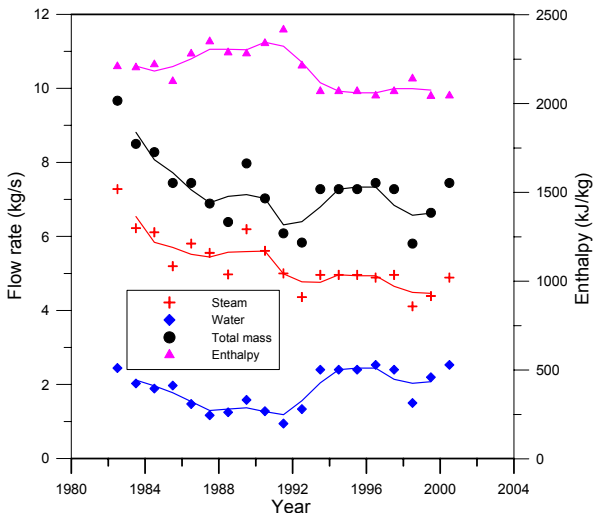


Figure C 1: Output from well OW-2

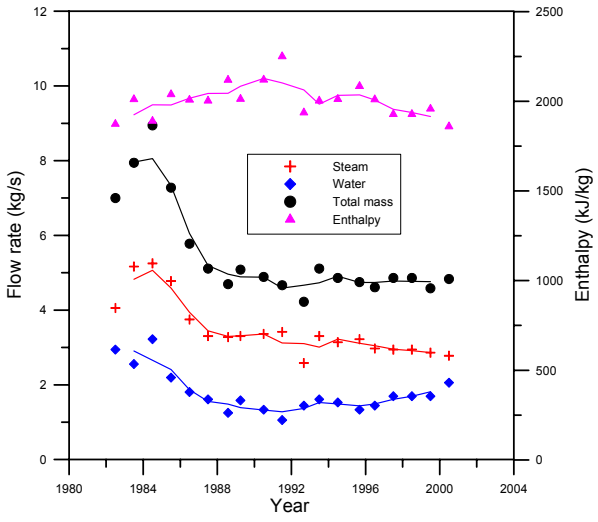


Figure C 3: Output from well OW-11

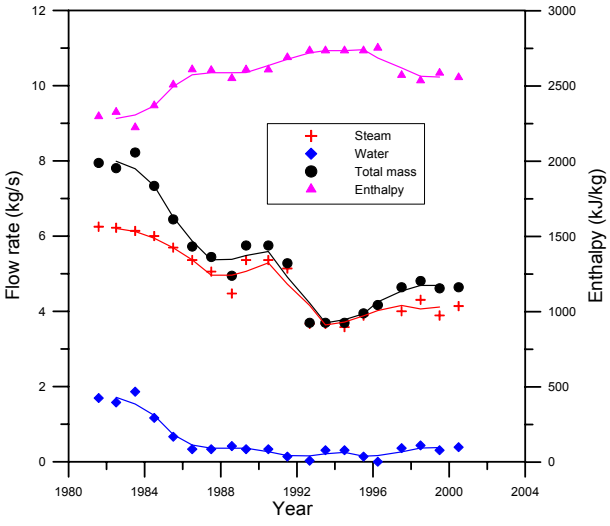


Figure C 2: Output from well OW-10

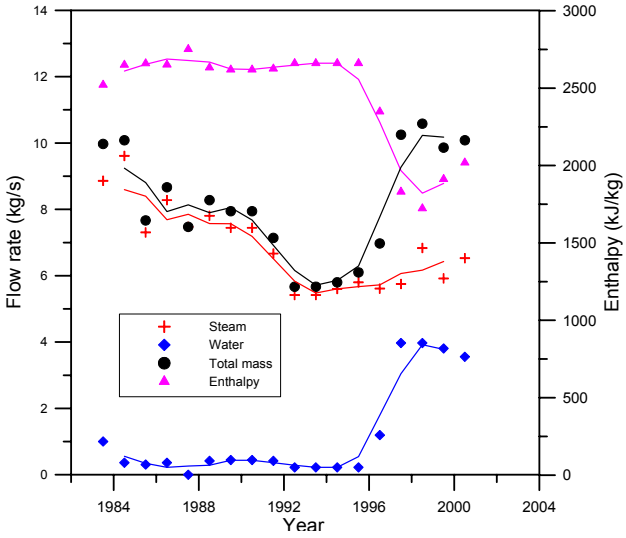


Figure C 4: Output from well OW-15

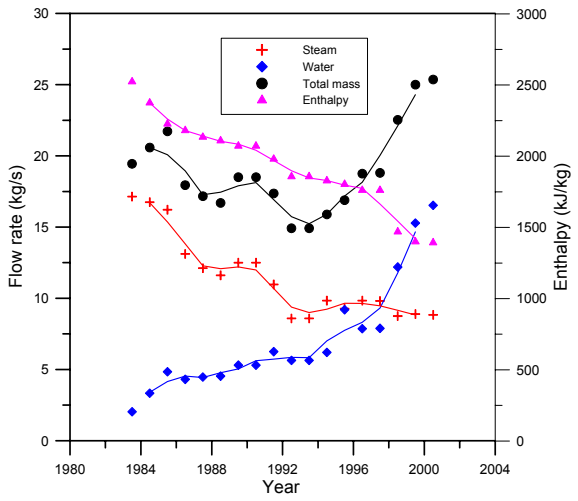


Figure C 5: Output from well OW-16

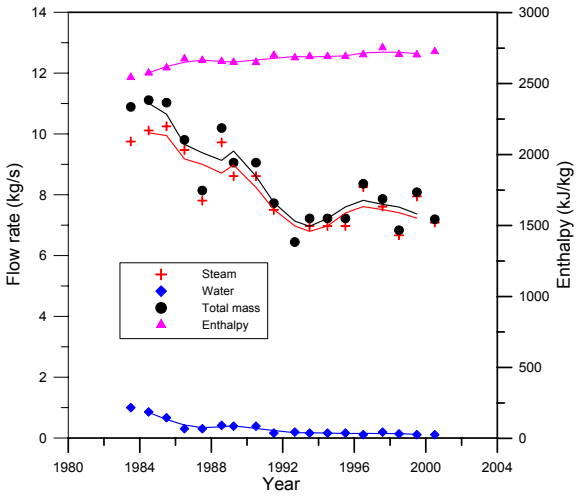


Figure C 8: Output from well OW-18

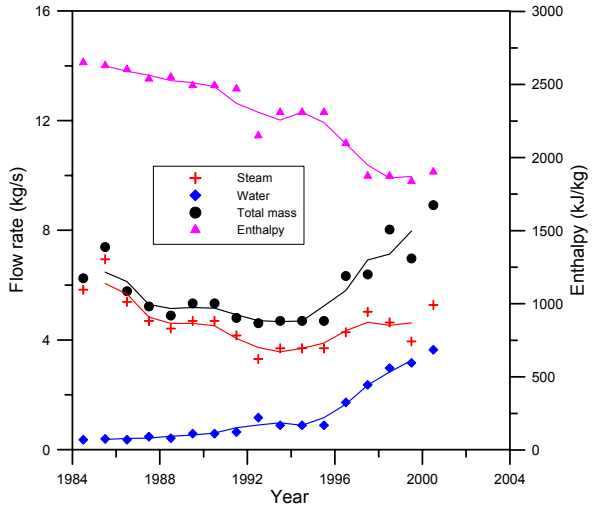


Figure C 6: Output from well OW-19

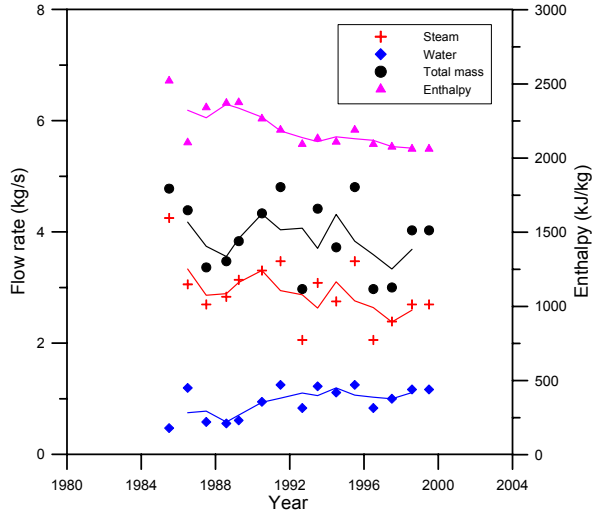


Figure C 9: Output from well OW-21

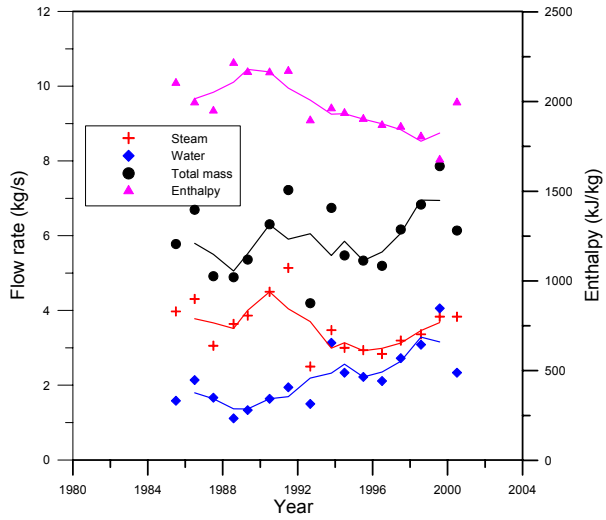


Figure C 7: Output from well OW-22

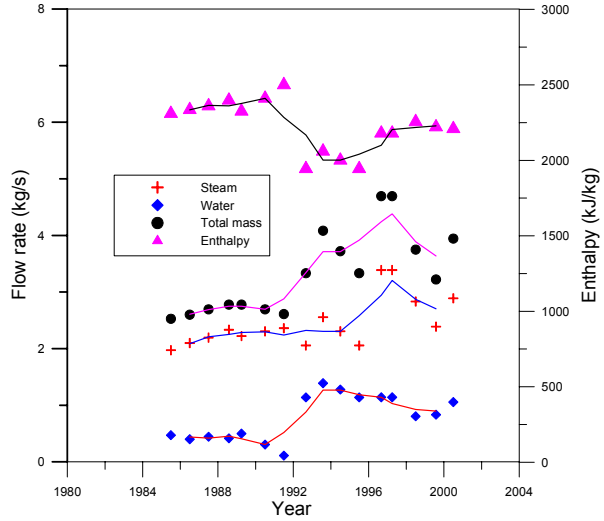


Figure C 10: Output from well OW-23

## APPENDIX D

### Solution to the discretized equations

Solution by Newton's method

Let the solution vector be defined by

$$\mathbf{x} = (x_1, x_2, ...x_{2N-1}, x_{2N})^T \quad \text{(D1)}$$

where $x_1 = P_1^{n+1}$, $x_2 = T_1^{n+1}$ (or $S_1^{n+1}$) are the primary variables at element *i*, $x_{2(j-1)+1}$, $x_{2(j-1)+2}$ at element j etc. The residual equations can then take the form

$$\mathbf{R = f(x) = 0} \quad \text{(D2)}$$

where $\mathbf{f} = (f_1, f_{2,}, ..., f_{2N})^T$. Let $\mathbf{x_{k+1}}$ be the value of **x** at the (k + 1)th iteration; then

$$\mathbf{x_{k+1} = x_k + \Delta x_k} \quad \text{for k = 0,1,2, ...} \quad \text{(D3)}$$

If $\mathbf{x_{k+1}}$ is an approved approximation to **x** then

$$\mathbf{f(x_{k+1}) = f(x_k + \Delta x_k) \approx 0}$$

Applying an n-dimensional Taylor's series expansion gives,

$$\mathbf{f(x_{k+1}) = f(x_k + \Delta x_k) = f(x_k) + \nabla\ f(x_k)\ \Delta x_k} + ...$$

neglecting higher order terms in $(\mathbf{\Delta x_k})^2$ gives

$$\mathbf{f(x_{k+1}) = f(x_k) + J(x_k)(x_{k+1} - x_k) \approx 0} \quad \text{(D4)}$$

where $\mathbf{J(x_k)}$ is the Jacobian matrix of the system given by

$$J_{ij} = \left[\frac{\partial f_i}{\partial x_j}\right] \quad \text{for } i = 1,2, ..., \text{n and } j = 1, 2, 3, ...., \text{n} \quad \text{(D5)}$$

evaluated at $\mathbf{x_k}$. If $\mathbf{x_{k+1}}$ is a solution then $\mathbf{R^{k+1} = f(x_{k+1}) = 0}$ and we obtain

$$\mathbf{x_{k+1} = x_k - J^{-1}(x_k) f(x_k)} \quad \text{(D6)}$$

If the matrix $\mathbf{J(x_k)}$ is singular, then the inverse $\mathbf{J^{-1}(x_k)}$ cannot be calculated.

This method has two major disadvantages:

(1) Convergence may not be achieved unless the initial approximation is a good one.
(2) The method requires the user to provide the derivatives of each function with respect to each variable. The user must therefore provide $n^2$ derivatives and any computer implementation must evaluate the *n* functions and the $n^2$ derivatives.

This method is therefore not appropriate for solving large problems.

Solution by conjugate gradient method

The conjugate gradient method provides a powerful means for solving linear equation systems with positive definite symmetric matrices. A matrix $\boldsymbol{A}$ is symmetric and positive-definite if $\boldsymbol{A_{ij} = A_{ji}}$ and $\boldsymbol{x^T Ax > 0}$ for any $\boldsymbol{x \neq 0}$.

Let Equation D4 be written in the form

$$\mathbf{Ax = b} \tag{D7}$$

where **A** is symmetric positive-definite (in our case, the Jacobian matrix), **x** is the solution vector ($\mathbf{x = x_{k+1} - x_k}$) and **b** is the residual.

Given an initial guess $\mathbf{x}_0$ at the solution, the conjugate gradient method generates a sequence of increasingly improved approximate solutions $\mathbf{x}_1$, $\mathbf{x}_2$, ...., residuals corresponding to the approximations and search directions. Iteration terminates when the error is deemed small enough or has reached a preset value.

Solving Equation D7 is equivalent to problem of minimizing the quadratic form

$$\mathrm{f}(\mathbf{x}) = \frac{1}{2}\mathbf{x}^{\mathrm{T}}\mathbf{Ax} - \mathbf{x}^{\mathrm{T}}\mathbf{b} \tag{D8}$$

Minimization of D8 is achieved when $\mathbf{x} = \mathbf{A}^{-1}\mathbf{b}$. That is when

$$\nabla \mathrm{f}(\mathbf{x}) = \mathbf{b} - \mathbf{Ax} = \mathbf{0} \tag{D9}$$

Writing D9 in residual form gives

$$\mathbf{r = b - Ax} \tag{D10}$$

The approximate solution $\mathbf{x}_{(i+1)}$ is computed by

$$\mathbf{x}_{(i+1)} = \mathbf{x}_{(i)} + \alpha_{i+1}\mathbf{p}_{(i+1)} \tag{D11}$$

where $\alpha$ is the search parameter chosen to minimise $\mathrm{f}(\mathbf{x}_{(i+1)})$ along the direction vector $\mathbf{p}_{(i+1)}$. The new residual form of equation D10 gives

$$\mathbf{r}_{(i+1)} = \mathbf{b} - \mathbf{Ax}_{(i+1)} \tag{D12}$$

and substituting D11 in D12 and solving, we obtain

$$\alpha_{i+1} = (\mathbf{r}_i^T \mathbf{r}_i)/(\mathbf{p}_{i+1}^T \mathbf{Ap}_{i+1}) \tag{D13}$$

The vector $\mathbf{p}_{(i+1)}$ is determined from the criterion that successive directions of search should be A-conjugate (orthogonal). This implies that

$$\mathbf{p}_i^T \mathbf{Ap}_j = 0 \text{ for } i \neq j \tag{D14}$$

Also, **P** has to be orthogonal to **r**. The vector $\mathbf{p}_{(i+1)}$ therefore relates with $\mathbf{r}_i$ by

$$\mathbf{p}_{(i+1)} = \mathbf{r}_i + \beta_{i+1} \mathbf{P}_i \tag{D15}$$

where

$$\beta_{i+1} = (\mathbf{r}_i^T \mathbf{r}_i)/(\mathbf{r}_{i-1}^T \mathbf{r}_{i-1}) \tag{D16}$$